Modelling for Ecosystem Restoration

Hydrodynamic Modelling of the Yolo Bypass Using HEC-RAS

By

Laila Kasuri

A.B. (Harvard University) 2013

THESIS

Submitted in partial satisfaction of the requirements for the degree of

MASTER OF SCIENCE

in

Civil Engineering

in the

OFFICE OF GRADUATE STUDIES

of the

UNIVERSITY OF CALIFORNIA

DAVIS

Approved:

____

Jay Lund

____

Bassam Younis

____

Fabian Bombardelli

Committee in Charge

2014

Contents

Abstract

The Yolo Bypass is an engineered flood bypass that provides significant benefits to native fish and bird species, while serving as a central component of the Sacramento Valley's flood control system. The bypass provides opportunities for managing various land uses and sustaining much of Yolo County's agricultural economy. Growing concerns over the dwindling numbers of native fish in the valley have prompted for the push for environmental management actions that maximize ecosystem benefits and preserve native fish species while maintaining economically-driven objectives. The success of these ecosystem management projects can be evaluated through a model that simulates the existing conditions and various alternatives from any proposed changes.

This thesis develops a tested, two-dimensional hydraulic model for the Yolo and Sutter Bypass to investigate flooding extents, depths and duration in the Yolo Bypass for various alternatives. It also presents smaller case-study applications to investigate the effects of structural and operational modifications on the Bypass, and corroborates the value of using hydrodynamic models in simulating and testing different scenarios.

Keywords: *Yolo Bypass, hydrodynamic model, HEC-RAS, ecosystem management*

Acknowledgements

I am deeply indebted to my thesis advisor, Jay Lund for letting me be a part of his research group. Jay is an incredible professor, researcher and practitioner who knows the multiple facets of water resources in California and around the world, but most importantly, he wants his students to succeed. Through his support and advice, I have been able to breeze through my Master's program. Jay, you are truly an exceptional and generous advisor.

I would also like to express my utmost gratitude to my project advisor, William Fleenor. Bill has been the one to guide me throughout my research and without his help, I would not have been able to complete my thesis in time. I have learned so much from him and throughout my time as a student, he has always been extremely patient with me. He is always available for his students and I am humbled to have learned so much from him. He is an amazing and kind person to work with and is a great mentor. Thank you Bill!

I would also like to thank other members of my thesis committee, Dr. Bassam Younis and Fabian Bombardelli. Professor Younis is an exceptional teacher and makes hydrodynamics quite fun! Professor Bombardelli really provided useful comments for my thesis.

Thank you to all the people at the Center for Watershed Sciences, Chris, Barbara, and Paula for always greeting us in the morning. To my office mates, Ben Lord, Lauren Adams, Jenny Ta, Mustafa Dogan and Steve Micko for always being willing to chat with me.

Lastly, thanks to my lovely Davis friends who have helped me out in every possible way. Ben Lord, Heather Sprague, Sara Miler, Leah Zivalic, Jenny Mital, Reed Thayer, Jeff Navarrete, Eze and Sol, Mustafa, Karandev, Ian, Molly, Emily and so many other amazing friends. Thank you for being gems, offering me help when moving, being there for me through thick and thin, and always be willing to lend me a ride!

And to Liv, Quetzal, Jan and Fania, along with the international group for hosting the best potlucks and lending me a couch to sleep on when I was transitioning from one apartment to another!

Abbreviations

ASCE	American Society of Civil Engineers
BDCP	Bay Delta Conservation Plan
Cal/EPA	Cal/EPA California Environmental Protection Agency
CALFED	State (CAL) and federal (FED) agencies participating in Bay-Delta Accord
CDEC	California Data Exchange Center
CEQA	California Environmental Quality Act
CESA	California Endangered species Act
CVFED	Central Valley Floodplain Evaluation and Delineation
CVFPP	Central Valley Flood Protection Plan
CVP	Central Valley Project
CWA	Clean Water Act
DEM	Digital Elevation Model
Delta	Sacramento–San Joaquin Delta
DWR	California Department of Water Resources
DWSA	Drinking Water Source Assessment and Protection
DWSR	Drinking Water State Revolving Fund
EDA	U.S. Economic Development Administration
DFG	California Department of Fish and Game
DWR	California Department of Water Resources
ESA	Endangered Species Act
GIS	Geographic Information Systems
HEC	Hydrological Engineering Center, Davis, CA
HEC-RAS	Hydrological Engineering Center, River Analysis System
IRWM	Integrated Regional Water Management
LiDAR	Light Detection and Ranging
NAVD	North American Vertical Datum of 1988
NGVD	National Geodetic Vertical Datum of 1929
NHC	Northwest Hydraulic Consultants
NMFS	National Marine Fisheries Service
NOAA	National Oceanic and Atmospheric Administration
USBR	Bureau of Reclamation
RMA	Resource Management Associates
RPA	Reasonable and Prudent Alternative
SWP	State Water Project
USACE	U.S. Army Corps of Engineers
USFWS	United States Fish and Wildlife Service
USGS	U.S. Geological Survey

List of Tables

List of Figures

1 Chapter 1: Background and Research Motivation

1.1 A Brief History of Flood Control

The Sacramento Valley is historically prone to seasonal flooding in winter and spring, with occasional major floods. In the early 1850's, as settlements increased along the river, so did the need to control floods *(Kelley, 1998; Singer et al., 2008)*. Early flood management efforts were localized, where private landowners sought to protect their own land by building embankments. However, the advent of hydraulic mining further reduced the water-carrying capacity of the valley's river, resulting in increased flood risk. This risk was realized in 1862, when destructive flooding created an 'Inland Sea' within the Central Valley and exposed the inadequacy of the embankments (*Kelley, 1998).* This eventually led to increased State involvement in flood management. In 1861, the State of California created the State Reclamation Board to oversee land reclamation and organize reclamation districts *(CA DWR, 1951)*. By 1868, this responsibility was transferred to the counties and the State Reclamation Board was dissolved. After a series of destructive floods, in 1911, the California Legislature re-instated the State Reclamation Board, and by 1917 following the Flood Control Act, the Board was authorized to spend $33 million on a flood control project in the Central Valley *(US Congress, 1917; CA DWR, 1951; James & Singer, 2008).* This project, known as the Sacramento River Flood Control Project, was designed to allow the Sacramento River to overflow its banks at select locations, allowing winter and spring flows to be conveyed through the Sutter and Yolo Bypasses and into the Delta (*CA DWR, 2011a)*.

During this period, large-scale water supply projects also were being planned, with even greater State and Federal involvement. The Central Valley Project (CVP) began in 1938 and the State Water Project (SWP) began in 1951, as part of a larger basin-wide flood control plan *(James and Singer, 2008).* Since then, the effects of hydraulic mining, agriculture and settlement have transformed the Central Valley to what it is today. The State and Federal water projects have had major effects on the Sacramento River and the Yolo Bypass which are fundamental to urban and agricultural development and ecosystem sustainability in the Sacramento Valley and the Delta *(James and Singer, 2008).*

1.2 The Yolo Bypass in the context of Delta Restoration

Classical, highly-engineered flood control systems often disconnect rivers from the floodplain, resulting in loss of ecologically essential habitats *(Tockner and Schiemer, 2002).* In that regard, the Yolo Bypass is an excellent example of a "reconciled" system, since it allows the river to remain connected to the habitats it sustains *(Salcido, 2012; Moyle, 2013*). Furthermore, by directing up to 80% of Sacramento River flood flows, it has been a successful flood control structure. The Bypass supports more than 42 fish species, including spittail and Chinook salmon *(Sommer et al., 2001, Sommer et al., 2006).* In addition, it may also be an important source to the downstream food web of the Delta and San Francisco Estuary (*Schemel, 2004).*

In recent years, concerns have arisen over the dwindling numbers of native fish, such as delta smelt, Chinook salmon and many others. Due to this, recent state water plans are proposing to modify portions of this Bypass system to reconcile ecosystems in the Sacramento/San Joaquin Delta. More specifically, these proposals call for various conservation measures for maximizing ecosystem benefits and preserving native fish species while maintaining economically-driven objectives (*BDCP, 2012*). The California Natural Resources Agency and the U.S. Department of the Interior have, for example, proposed increasing the frequency and duration of flooding in the Yolo Bypass to improve fish passage, increase floodplain rearing and spawning habitat and also maintain flood control and agricultural functions (*BDCP, 2012; Howitt et al., 2013*). These proposals, among others, are components of the Bay Delta Conservation Plan (BDCP), a habitat conservation plan intended to support the U.S. Fish and Wildlife Service and the National Marine Fisheries Service under the federal Endangered Species Act (*BDCP, 2012).*

Such proposals generally include construction of a notch in the Fremont Weir and the installation of operable gates to lower the height at which Sacramento River water can flow into the Bypass. This would increase the frequency and duration of Yolo Bypass flooding to improve native fish habitat *(BDCP, 2012***)**. Any operational or structural change in the bypass system would change the extents and depths of flooding, something of particular interest to various stakeholders. Evaluating the success of these conservation projects and modifications to operations of existing structures in the Bypass requires a model to estimate flooding durations, extents, and frequencies from any proposed changes *(Suddeth, 2014)*. The major aim of this thesis was to construct a hydraulic model and investigate flooding extents, depths and durations in the Yolo Bypass for various alternatives.

1.3 Thesis Objectives

This study investigates the impacts of proposed diversions and distributary modifications on the discharge and stage along the Sacramento River and the resulting flooding extents and depths in the Yolo and Sutter Bypasses. Specific objectives are:

- Establishing two working hydrodynamic models, one for the larger Sacramento Valley Bypass system comprising of the Yolo and Sutter Bypasses, and a second, smaller one for the Yolo Bypass. Both models must be calibrated and validated to ensure that they can reliably predict current water stage and discharge dynamics, particularly for low bypass flows. Figure 1 shows the extents of the larger hydraulic model developed in this study.
- Developing a Digital Elevation Model (DEM) that includes the Yolo and Sutter Bypasses and conduct a sensitivity analysis on the effects of spatial resolution and grid spacing on model results.

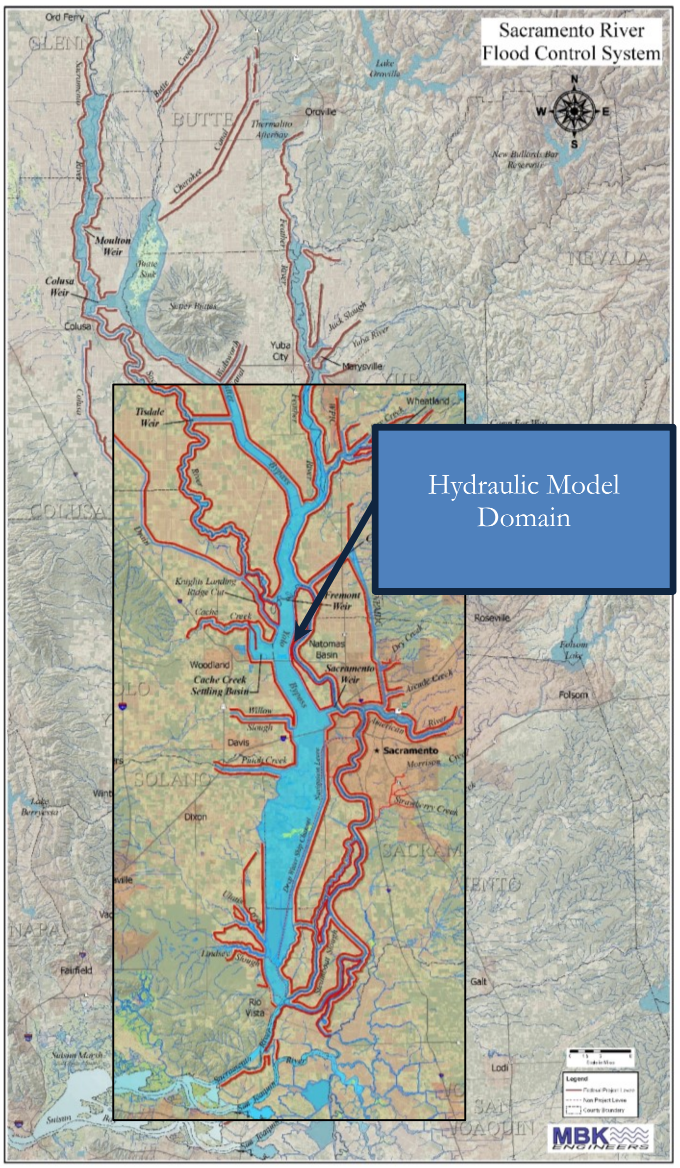

Figure 1: Study area scope within the Sacramento Flood Control Project. (Source: California, Division Water Resources, 1951)

The tested model for the smaller Yolo Bypass will be used to investigate the effects of structural and operational modifications on the Bypass. These include: a) the effects of controlled flows of 2,000 cfs, 4,000 cfs and 6,000 cfs through the Fremont Weir, b) the extents and depths within particular land uses that can be expected for use with economic and optimization models (*Suddeth, 2014*) and c) the effects of introducing gates and berms to go with optimization analysis (*Suddeth, 2014*).

The thesis outlines the methodology behind the construction of both the models and presents applications of a smaller model to restoration projects in the Yolo Bypass. The Yolo Bypass is a particularly good case-study. It already provides significant benefits to native fish and bird species, while serving as a central component of the Sacramento area's flood control system. Furthermore, it is a large engineered area that provides opportunities for managing various land uses and sustaining much of Yolo County's agricultural economy *(Howitt et al., 2013*). Lastly, lessons learned on the Bypass are applicable to similar flood bypasses elsewhere.

1.4 Thesis Structure

The thesis has eight chapters. **Chapter 2** gives a thorough description of the study area, within the context of the larger Sacramento Valley, including the various structures within the area. The next two chapters are part of the literature review. **Chapter 3** reviews numerical hydraulic models and the underlying equations. Previous modelling efforts in the Yolo Bypass and their limitations are also discussed. Finally an overview of the software used is presented. **Chapter 4** reviews the main inputs required for a hydraulic model, and the role of GIS in developing these inputs. It also reviews methods used in generating terrains used in hydraulic models.

Chapter 5 discusses the development of the smaller Yolo Bypass model and detailed description of the larger model development, including data collection, pre-processing, geometry, boundary conditions and calibration. **Chapter 6** presents a sensitivity analysis of the effects of DEM accuracy, spatial resolution and different solution schemes on model results.

Chapter 7 presents some case study applications of the model to demonstrate its usefulness. One particular application is to Suddeth's (2014) study that prescribes the most economically profitable flood footprint (*Suddeth, 2014*). The hydraulic model is used to mirror this footprint by testing what modifications to the Bypass would give the optimized footprint. **Chapter 8** draws insights from model results, applications and sensitivity analysis to give overall conclusions.

2 Chapter 2: Overview of the Study Area

The Sacramento River Flood Control Project was built because the Valley's runoff could not be reliably contained within the banks of the Sacramento River, especially during major floods (*James and Singer, 2008; Singer et al., 2008; Kelley, 1998*). This meant that adjacent low-value land would have to be reserved for occasional flooding, sometimes now popularly called "making room for the river", much like in the Mississippi River (*Kelley, 1998; James and Singer, 2008*). The Bypass system was designed to work in conjunction with the 980 miles of levees along the Sacramento, Feather, and American Rivers (*Kelley, 1998; James and Singer, 2008*). The operation of these bypasses is controlled by overflow weirs, namely the Moulton, Colusa, Tisdale, Fremont, and Sacramento weirs. These weirs act like relief valves, diverting excess flows to the adjacent bypasses, eventually reaching the Delta (*Kelley, 1998; James and Singer, 2008; Russo, 2010*).

For this study, the larger hydraulic model extends from south of the Tisdale weir downstream to Rio Vista, so only three of the five weirs are included in the hydraulic model. The main hydraulic structures, including weirs and bypasses are described below, and mapped in Figure 2.

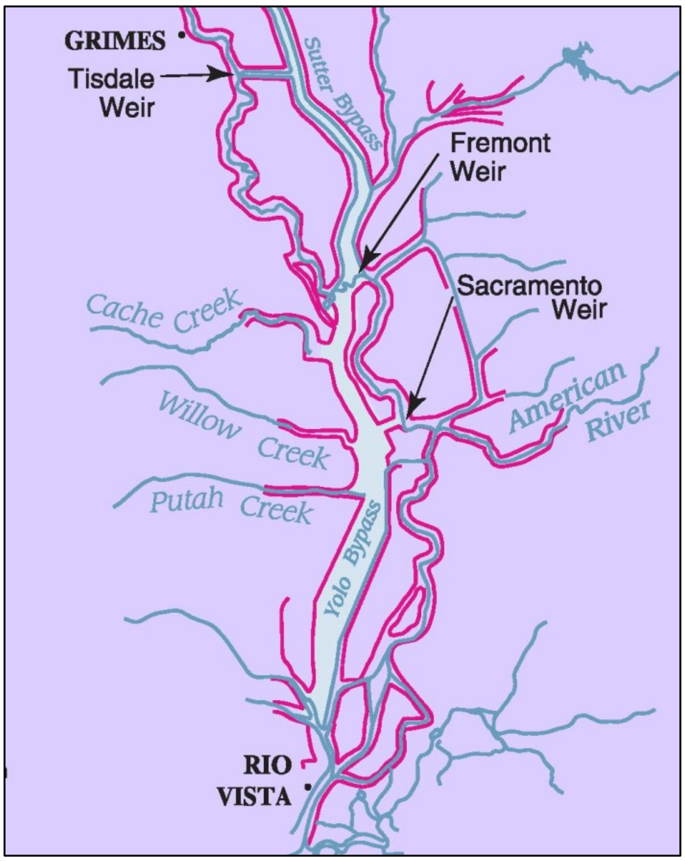

Figure 2: Model Extents with main weirs and bypasses (Source: Adapted from CA DWR)

2.1 Bypasses in the model

2.1.1 Sutter Bypass

At the southern end of the Sutter Buttes, between the Feather and Sacramento Rivers is the Sutter Bypass, a 22,000 acre[1] flood channel running parallel to the Feather River down to where it meets the Sacramento River (*CA DWR, 1951*). The Bypass lies to the west of the Sutter-Butte basins, conveying floodwaters from Butte Basin and additional floodwaters from the Sacramento River during high floods, through the Tisdale Bypass.

[1] Figures vary. This number is taken from California, Division of Water Resources, Report to the State Reclamation Board on Authorization, Construction, Maintenance and Operation of Sacramento River Flood Control Project, 1951.

It eventually conveys water back to the Sacramento River above the Yolo Bypass *(Russo, 2010).* Figure 3 shows the Sutter Bypass, highlighted in red within the larger context of the Sutter-Butte Basin.

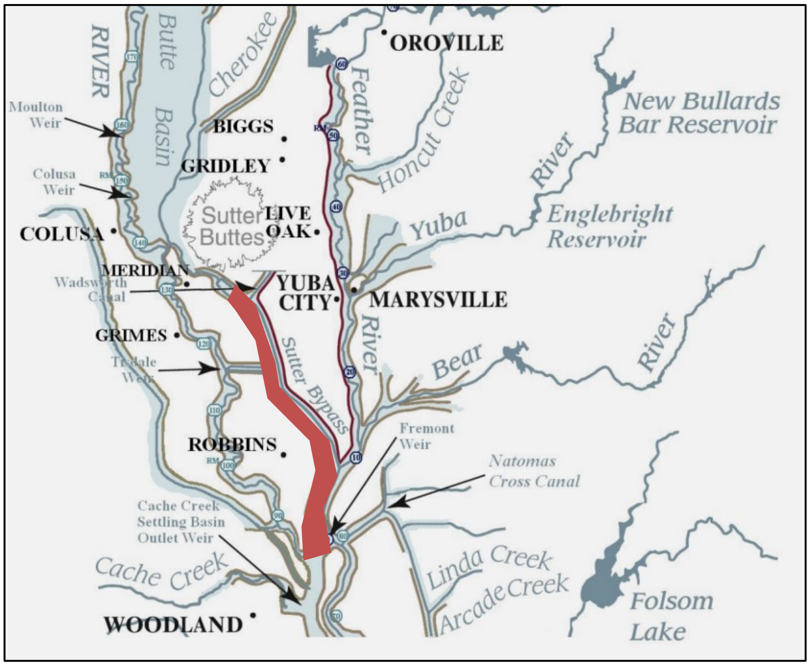

Figure 3: Sutter Bypass (highlighted in red) and Sutter Basin (Adapted from Sutter Basin Pilot Feasibility Study, USACE 2013)

2.1.2 Yolo Bypass

The 59,000 acre Yolo Bypass is a leveed floodplain in Yolo and Solano counties designed to protect the City of Sacramento and the lower Sacramento Valley (*Jones and Stokes, 2001*). The northern part of the Bypass extends from the Fremont Weir, where the Sacramento and Feather rivers meet to Interstate 80 (I-80) and is leveed on both sides by the East Bypass Levee and the West Bypass Levee. On the east, running parallel to the Bypass is the Tule Canal, a perennial channel that carries local drainage and floodwater that has spilled over the Fremont Weir. Although the channel design capacity is 3,530 cfs, it spills into the adjacent floodplain by 2,000 cfs (*Natural Heritage Institute et al., 2002*). The northern part of the Bypass is non-tidal.

The southern part of the Bypass extends from 1-80 south to Rio Vista. It has levees on both sides, except for an 8-mile unleveed western section on the Bypass, near the South Fork of Putah Creek. The Tule Canal here extends into the Toe Drain which runs parallel to the Deep Water Ship Channel. The Toe Drain ends into Prospect Slough, which lies within Liberty Island. Prospect Slough is joined by Cache Slough and Lindsey Slough, which enter from the West. Slightly upstream of this junction, the Sacramento River and Steamboat Slough enter from the East. This lower tip of the Bypass lies within the Delta and is tidally influenced (*Jones and Stokes, 2001*).

The main inflows to the Bypass are the Fremont Weir, which spills roughly twice every 3 years (*Sommer et al., 2003*), as well as much smaller western tributary inflows and local drainage. In major floods, the Sacramento River also spills into the Bypass through the Sacramento Weir, as last happened in 2006. However, in low flow conditions, water does not spill through these weirs, and the Bypass receives most of its inflows from west side tributaries. These include from north to south, Knights Landing Ridge Cut, Cache Creek, Willow Slough, and Putah Creek (*Jones and Stokes, 2001*). Base flows from these tributaries might be important for the health of aquatic and riparian habitats supported along these tributaries (*Schemel et al., 2002*). With high or moderate flows, these tributaries can cause localized flooding and could potentially help create floodplain habitat in years when weirs do not overtop. (*Jones and Stokes, 2001; BDCP, 2012*). So there is an interest to better monitor these tributaries.

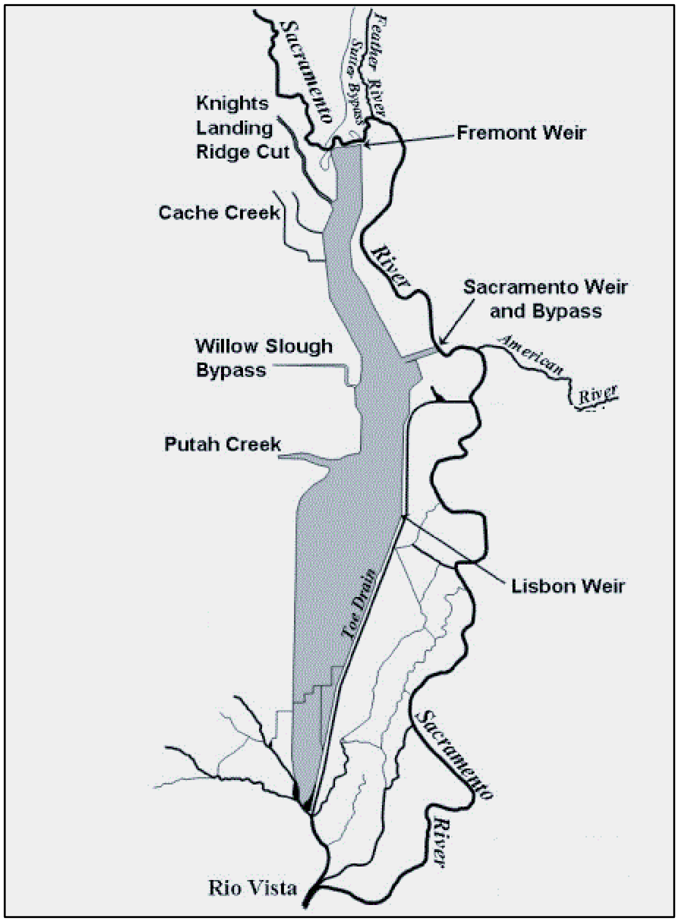

Figure 4: Yolo Bypass from the Fremont Weir to Rio Vista (Source: CA DWR, Yolo Bypass http://www.water.ca.gov/aes/Yolo/)

2.2 Weirs and Overflow structures in the model

Weirs are barriers either across or along a river designed to divert overtopping flow. In most cases, weirs act like lowered levees or obstructions, causing water to pool behind them while also allowing it to overtop when the water surface elevation reaches the weir's height. The Sacramento Valley has five concrete overflow weirs, Moulton, Colusa, Tisdale, Fremont and Sacramento, created as part of the Sacramento Flood Control Project (*CA DWR 1951; James and Singer, 2008*). Of these, only the Sacramento Weir can be manually operated. (*Russo, 2010*).

2.2.1 Tisdale Weir

The Tisdale weir is along the left bank of the Sacramento River about 56 miles north of Sacramento and near the town of Meridian, CA. When the weir is overtopped, the Sacramento River spills into a 4 mile, channel known as the Tisdale Bypass, which has a capacity of 38,000 cfs. The Tisdale Bypass then connects to the Sutter Bypass, which runs parallel to the Feather River. Typically, the Tisdale Weir is the first of the five weirs in the Sacramento River Flood Control System to overtop, and continues to spill for the longest duration (*Russo, 2010)*.

2.2.2 Fremont Weir

At the southern tip of the Sutter Bypass, just before the confluence of the Sacramento and Feather rivers is the Fremont Weir. The weir's primary purpose is to release combined flows from the Sacramento River, Sutter Bypass, and the Feather River into the Yolo Bypass (*CA DWR 1951; Jones and Stokes 2001; James and*

Singer 2008). The nearly 2-mile long weir has a crest elevation (the height at which water will start overtopping) of 33.5 feet (datum: 0=0 feet USED) and the project design capacity of the weir is 343,000 cfs, although based on surveys, this crest elevation varies between 32.1 and 32.9 feet NAVD 88 (*cbec, 2012*). The Fremont Weir appears extensively in the BDCP and other proposals to modify it, for example introducing a notch to increase flows in the Bypass or operable gates to control the timing and duration of flows (*BDCP, 2012*).

2.2.3 Sacramento Weir and Bypass

The Sacramento Weir is on the right bank of the Sacramento River, north of West Sacramento. At this point, the Sacramento River has been joined by the American and Feather Rivers. The weir's main purpose is to protect the Sacramento urban areas from high stages, with a project design capacity of 112, 000 cfs and is manually opened when the Sacramento River is at 27.5 feet stage at the I Street Bridge (*Russo, 2010*). The weir itself is a complicated structure; it is 1,920 feet long, consisting of 48 gates each with 38 vertical wooden planks that have to be manually opened to allow water to flow through them. The weir diverts the flows of Sacramento into what is called the 'Sacramento Bypass', an eastern extension of the Yolo Bypass (*Russo, 2012*). For this study, the Sacramento weir is never operated, since the interest is in looking at the flood footprint in lower flow conditions.

2.3 Inline hydraulic structures

2.3.1 Lisbon Weir

The Lisbon Weir is an inline irrigation structure along the Toe Drain, just north of the southern end of the Yolo Bypass Wildlife Area. The purpose of this weir is to impound water, so that it can be drawn off for agricultural use. Based on site visits, the weir consists of a 100-foot wide, rocky weir on the eastern end, which is at an elevation of around 6 feet and a gated weir with three flap gates on the western side, which is at an elevation of 4.5 feet. The weir dams up water for agricultural use, and also allow flood tides to surcharge the Toe Drain upstream of the weir. There are multiple gauges with different datums at Lisbon weir that record water stages and are used for model calibration. Flow downstream of the Lisbon weir is tidally influenced, and therefore the water stage shows an oscillatory movement. (*Natural Heritage Institute et al., 2002; cbec, 2012*).

2.3.2 Tule Canal/Toe Drain agricultural crossings

Based on field visits, surveys and reports (*cbec. 2012*), four "agricultural crossings" were identified in the Tule Canal/Toe drain. These structures store water for irrigation and allow movement of tractors and other farm machinery. Three of these crossings lie north of KLRC while the fourth one lies south of the Sacramento Bypass. The crossings north of KLRC lie close together, with the first and second one 0.5 miles apart and the third one another 0.6 miles south of the second one. The second and third crossings have 36-inch culverts that allow connectivity to the Tule Canal *(cbec, 2012*).

3 Chapter 3: Literature Review of Numerical Models

Hydrodynamic models can help explore alternative decisions and various conditions to inform flood and environmental restoration decisions. By providing inundation extents, durations and depths within multiple land uses, such models can simulate the effects of planned restoration projects and proposed project designs and operations. For this thesis, a numerical model is used to solve the underlying hydrodynamic equations for two-dimensional and one-dimensional flow. The basic equations for two-dimensional flow are the depth-averaged "shallow water equations" (also known as the "Saint Venant" Equations in their one-dimensional form). This chapter provides a brief literature review of the models, their types and their basic assumptions.

3.1 Introduction to numerical hydraulic models

Numerical models are mathematical models employing an algorithm or scheme to solve equations numerically that cannot be solved analytically. A hydraulic model is one kind of numerical model that solves the equations that govern flow through numerical means (*Chow, 1959*). Such models are widely used, for example in flood management studies (*Stoker, 1957; HEC, 2001*), but for their applications in restoration projects, it is important to understand some simplifications and assumptions in these models and their variants. Often these simplifications involve ignoring variations of some flow parameters over time or space, or both (*Stoker, 1957)*. A common simplification in hydraulic models for flood management is dimensionality reduction, where the model solves less than three spatial dimensions, making it less computationally burdensome (*Horritt and Bates, 2002*). To reduce dimensionality from say 2-D to 1-D, the underlying assumption would be that at a given point in time, the variations in flows and velocities are significant only in a predominant flow direction, i.e. upstream and downstream and those in the transverse are negligible. In a 2-D model, transverse variations in the water surface are not neglected but vertical velocities that would be captured by 3-D models are ignored (*Stoker, 1957; ASCE, 2000*). Similarly, other simplifications could involve assuming that flow does not vary in space, making it uniform. Uniform flow means that the depth of the flow at a particular instance is the same along the channel. Non-uniform flow means that flow velocity at a particular instance varies spatially within the fluid (*Stoker, 1957; Chow, 1959*).

Simplifications related to time may assume that flow becomes 'steady' where the flow velocity, pressure and cross-section may differ from point to point but do not differ with time. (*Stoker, 1957*). The term "unsteady flow" is where flow at a particular cross-section changes with time, so time is also considered as an additional variable. (*Stoker, 1957; Chow, 1959*).

3.2 Governing Equations

3.2.1 The Shallow Water Equations

The Shallow Water Equations are the equations of fluid motion often used for modelling long waves such as floods and storm surges. They assume vertically uniform horizontal velocity and negligible vertical acceleration (i.e. a hydrostatic pressure distribution), making them valid where the wave length is much greater than water depth. They are a set of non-linear partial differential equations, consisting of the Continuity equation (Eq. 1) and the Momentum equation (Eq. 2), described in the horizontal plane as follows:

Continuity-equation	$\frac{\partial h}{\partial t}+\frac{\partial hV_x}{\partial x}+\frac{\partial hV_y}{\partial y}=q$	(1)
Momentum-equations	$\begin{cases} S_{fx}=S_{0x}-\frac{\partial h}{\partial x}-\frac{V_x}{g}\cdot\frac{\partial V_x}{\partial x}-\frac{V_y}{g}\cdot\frac{\partial V_x}{\partial y}-\frac{1}{g}\cdot\frac{\partial V_x}{\partial t} \\ S_{fy}=S_{0y}-\frac{\partial h}{\partial y}-\frac{V_y}{g}\cdot\frac{\partial V_y}{\partial y}-\frac{V_x}{g}\cdot\frac{\partial V_y}{\partial x}-\frac{1}{g}\cdot\frac{\partial V_y}{\partial t} \end{cases}$	(2)

Where h: depth; V_x, V_y: flow velocities in the x and y directions; S_{fx}, S_{fy}: roughness terms; S_{0x}, S_{0y}: slope, g is acceleration due to gravity, q = lateral inflow, t = time.
The frictional slope terms capture the energy losses due to friction and are empirically established.

3.2.2 Solutions and common simplifications

The shallow water equations in their one-dimensional form, become the Saint Venant equations. They can be further simplified depending on whether they are steady or unsteady, uniform or non-uniform. These simplifications are shown in Figure 5.

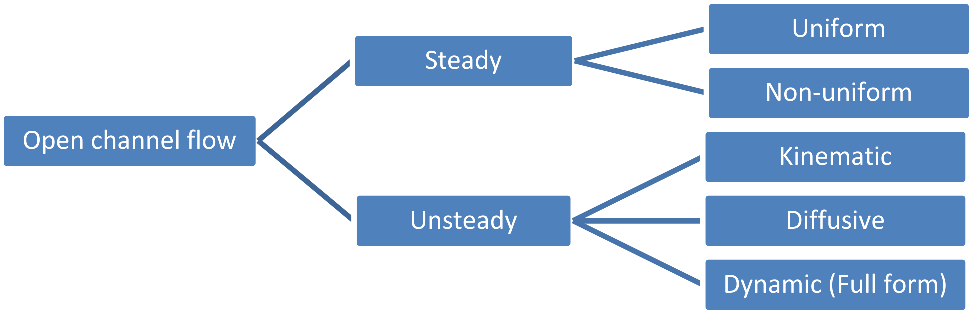

Figure 5: Common simplifications

3.2.3 Steady State

3.2.3.1 Non-uniform Flow

In steady state flow, time is not a variable that is solved for and therefore, if we take the example of 1-D non-uniform flow, the continuity and momentum equations are reduced to Eq. 3 and Eq 4:

$$\frac{\partial hV}{\partial x} = q \tag{3}$$

$$g\frac{\partial h}{\partial x} + V\frac{\partial V}{\partial x} + g\left(S_f - S_0\right) = 0 \tag{4}$$

Furthermore, since *V* and *h* are related empirically, through reorganizing to solve for *h*, we get Eq. 5 (for 1-D flow):

$$\frac{dh}{dx} = \frac{S_O - S_f}{1 - \frac{V^2}{gh}} \tag{5}$$

$\frac{V^2}{gh}$ is also the square of the Froude number, which is used to characterise flow regime.

3.2.3.2 Uniform Flow

In uniform steady flow, the bed slope is equal to the friction slope and pressure terms are ignored. The friction slope S_f is modelled with an empirical relationship, using the Manning formula when flow is uniform (Eq. 6).

$$S_f = \left(\frac{Q^2 n^2}{A^2 R^{4/3}}\right) \tag{6}$$

With n as the Manning coefficient and R the hydraulic radius, defined by R = A/P, where P is the wetted perimeter.

The flow depth can then be solved through an iterative calculation.

3.2.4 Non-steady state

In non-steady state, we have to also solve for the time derivative as well. In the one-dimensional case, the non-steady equation is shown as (Eq. 7).

$$\underbrace{\frac{\partial V}{\partial t} + V\frac{\partial V}{\partial x} + \underbrace{g\frac{\partial h}{\partial x} - \underbrace{g(S_o - S_f)}_{\text{1.Kinematic}}}_{\text{2.Diffusive}}}_{\text{3.Dynamic}} = 0 \tag{7}$$

The first term of Equation 7 describes the local acceleration, the second term describes convective acceleration while the third term describes pressure forces. Gravitational forces are represented by the bed slope (S_o) and friction forces by friction slope (S_f). The full dynamic wave equation solves for every term, while the kinematic wave and the diffusive wave solve for fewer terms, depending on the applications of the model. What must be noted however, is that in open channel flow, all waves—kinematic, diffusion and dynamic as well as their variants can exist, but it is the relative significance of these waves at a position in time that determine what simplification can be made.

3.2.4.1 Kinematic wave

Kinematic waves express the momentum equation in terms of the frictional and gravitational forces only, ignoring inertial and pressure forces. This assumption is applied in situations where the gravitational and frictional forces are much greater than the inertial and pressure forces, reducing the momentum equation so that the bed slope becomes equal to the friction slope (*Lighthill and Whitham, 1955*). Since pressure and inertia are neglected in the kinematic assumption, the main mechanism which causes the flood wave to attenuate is eliminated. Any indication of attenuation is through numerical error associated with the finite-difference scheme, not the physical mechanisms associated with the actual movement of a flood wave. Kinematic wave models have a wide range of applications from overland and channel flow, flow in furrows, erosion and sediment transport, solute transport, to name but a few (*Singh, 2001*).

3.2.4.2 Diffusive wave

The diffusive wave only ignores inertial terms but takes pressure forces, gravitational forces and friction forces into account. It is valid when the inertial acceleration is much smaller than all other forms of acceleration.

3.2.4.3 Dynamic wave

The dynamic wave solves for all terms in the full momentum equation, including inertial effects. These waves often have higher velocities and attenuate more quickly than kinematic waves. Although computationally more complex, the advent of more powerful computers has allowed the full dynamic wave equation to be solved numerically.

3.3 Previous Modelling Efforts

Many modelling efforts of the Yolo and Sutter Bypass have been made, both 1-D and 2-D, but usually, they were developed (and calibrated) for flood management studies, so they have limited value for simulating low flow scenarios for habitat restoration projects. This section discusses some of these models, although the list of models is by no means totally inconclusive. Much of the information of the previous models was obtained through literature review, and an inventory of models presented by the Yolo County Flood Control and Water Conservation District (*YCFCWC, 2002*).

In 1995, the U.S. Army Corps of Engineers developed a UNET 1-D hydraulic model of the entire Sacramento River Flood Control Project. The model, which included the Yolo and Sutter Bypass, was part of the Corps' Comp Study for the Sacramento-San Joaquin River Basin (*HEC, 1997*). The model was calibrated against data from the 1986 and later for the 1997 floods. In 2006, this model was updated for use in a newer 1-D version of HEC-RAS, calibrated against the 2006 floods and the boundary conditions were updated for use in unsteady modelling (*USACE, 2007*). While this model is suitable for analyzing flood-related issues at a system scale, it may not be appropriate for restoration projects that require analyzing shallow flooding in smaller distributary channels. This limitation is particularly relevant to cases where a restoration project might only have very localized impact on water surface levels, because this model will poorly represent shallow flows across the wide expanse of the Bypass, providing little information about localized inundation.

The U.S. Army Corps of Engineers also developed an RMA2 2-D hydraulic model for use in restoration projects, which has been applied in a number of restoration projects, for example the Yolo Wildlife Area Expansion (*YCFCWC, 2002*; *USACE, 2006*). Besides minor instability issues, the main drawback of this model was its topography and values for roughness coefficients, both of which were based on the 1997 USACE Comp Study. In 2007, although the model was updated with improved representation of bathymetry, the model has only been calibrated to the 1997 floods (*USACE, 2007*). As a result, consultants have reviewed this model to

be unsuitable for unsteady, low-flow conditions. Since this RMA2 model is steady-state, it cannot deal with tidal conditions in the lower Bypass nor can it model hydrographs. (*NHC, 2012*).
A newer 2-D model, using MIKE-21 was developed by cbec eco-engineering for Department of Water Resources (DWR) to simulate several flow alternatives past the Fremont Weir and obtain approximate flooding extents and depths. The model was reviewed by Northwest Hydraulic Consultants (NHC), who found the model limited in that it was not fully tested, the boundary conditions used were based on poor estimations and finally it was not public domain (*NHC, 2012*).

More recently, a TUFLOW model also has been under development by cbec eco-engineering but the model is yet to be reviewed. Table 1 gives a brief summary of the main modelling efforts taken.

Table 1: Previous and current modelling efforts (References: Yolo County Flood Control and Water Conservation District)

Dimension	**Software**	**Description**	**Sponsor**	**Year**
1-D	UNET	Steady state, 1-D model for the Upper and Lower Sacramento Valley	USACE	1995
	HEC-1 and HEC-2	Willow Slough, Dry Slough, Covell Drain	Yolo County Flood Control & Water Conservation District	1992
	HEC-2	Putah Creek	USACE	1995
	HEC-2	Cache Creek	USACE	1995
	HEC-RAS	Updated model for the Sacramento River.	USACE	
	HEC-RAS	Coarse-level HEC-RAS model of the Yolo Bypass from Fremont Weir to Liberty Island		2007
	HEC-RAS 4.2	As part of the CVFED effort, an unsteady model was developed for the entire Sacramento Valley using the UNET model as the basis.		
	HEC-RAS	Sutter Basin		
1-D/2-D	HEC-RAS 5.0	Coupled 1-D/2D for the Yolo Bypass and part of the Sutter Bypass south of Tisdale Weir.	This study	2013/2014
	HEC-RAS 4.2	Coupled 1-D/2D for the Yolo Bypass.	This study	2012/2013
	TUFLOW	TUFLOW is a 1-D/2-D flood modelling software – it was used to develop flooding extents in Cache Creek, Willow Slough and Putah Creek. Breach hydrographs from the HEC-RAS model were used as inputs.	Yolo County	2012
2-D	RMA2	2-D hydrodynamic model for the Yolo Bypass. Steady state. Designed for high flow scenarios.	USACE	1995 2007 (Updated)
	MIKE 21	2-D unsteady flow model for the Yolo Bypass. Boundary conditions for western tributaries based on estimates.	MWD, DWR, cbec eco-engineering	2007
	FLO2D	Model applied for two-dimension flood distribution on the floodplains for the Corp' UNET model.		

Best practices in hydraulic modelling prescribe that the boundary conditions should be a sufficient distance upstream from the area of interest (*ASCE, 2000*; *HEC, 2010*). In the case of the Bypass, this means that upstream boundaries should be considerable upstream from the Fremont Weir area, a primary interest of stakeholder groups. Currently, there is no updated, 2-D hydraulic model of such scale, which can be an impediment to restoration activities in the Bypass. As a result, the development and use of a 2-D, public domain model using a software, such as HEC-RAS that covers the Yolo and part of the Sutter Bypasses is well justified.

3.4 2-D Numerical Modelling

Two-dimensional hydraulic models are commonly used for modelling floodplains, coastal and marine environments and in flat terrains with localized flooding (*Casulli, 1990; Kodama et al., 1991; Bates and Anderson, 1993*). Two-dimensional models discretize topography to a grid, and each storage cell within the grid is assigned an average elevation based of topographic input data. Water surface depths and velocities over a surface that is often represented as a mesh or grid, can then be calculated. Older models have a fixed rectilinear mesh, and constant node spacing, and solve the underlying equations using implicit finite difference methods (*Miller and Cluer, 1998*). However, newer models allow for flexible meshes that consist of triangles or quadrilaterals giving them the ability to represent more accurate and detailed geometries. These models often use finite-element or finite-volume methods, to solve for the shallow-water equations. (*Bates and Anderson, 1993; Horritt et al., 2006*).

Two-dimensional models have advantages over one-dimensional models, of being able to represent more accurate geometries and model more complex flow conditions where the flow vectors can vary in multiple directions (*Bates and Anderson, 1993*). However, 2-D models are more computationally demanding and can become unstable if surfaces or terrains are too complex. Computational schemes have mathematical issues representing wetting and drying surfaces. Creating the terrain itself is a long and tedious process as it is interpolated from a either elevation points or lines (*Merwade 2005; Merwade et al., 2008a; 2008b*).

Given the expanding capabilities of numerical models to simulate mixed and unsteady flows, sediment transport, and dam and levee failure, their use in risk assessments, effects analysis, insurance studies and EIS reports is widespread (*HEC, 2001*). Today, many 2-D numerical models are available for use. The choice of which model to use will depend on the modelling objectives, as well as the time, data availability, expertise and money constraints. Further considerations are model scale, resolution and accuracy (*Bates et al., 1997*). For this study, since overbank flooding is being considered and since finer resolution is required to establish which land areas would be flooded, a 2-D unsteady model is the most suitable model for the hydrodynamic calculations. Furthermore, a model that is public domain is desired, as expressed by stakeholders regarding previous modelling efforts (*NHC, 2012*).

3.5 Overview of HEC-RAS modelling software

HEC-River Analysis System (RAS) is a public domain, computer software developed by the US Army Corps of Engineers' Hydrologic Engineering Center (HEC) for use in hydraulic studies. It is widely used in flood insurance studies, and has found wide acceptance among water practitioners (*HEC, 2001*). Up until 2014, HEC-RAS only had 1-D versions, but recently, HEC released a newer version capable of 2-D and coupled 1-D/2-D modelling. Although the channel can be included within the 2-D domain, it is more computationally efficient to model it as a 1-D reach while the floodplain areas are included in the 2-D domain. The computation mechanism of the 1-D component of HEC-RAS program is based on the UNET model developed by USACE, and solves the 1-D Saint Venant Equations. (*Chow, 1959*). For the 2-D areas, the model can solve the simpler Diffusion Wave equations or the full Shallow Water Equations using a finite volume scheme (*HEC, 2014*). In solving the shallow water equations, the schemes used can become unstable if the Courant condition is not met. The Courant condition, or the Courant–Friedrichs–Lewy (CFL) condition is a stability criterion for solving some partial differential equations numerically by the method of finite differences (*HEC, 2001*). It often requires the computational time step to be less than a certain number to ensure that the simulation remains stable and produces accurate results.

In HEC-RAS 5.0, the 2-D areas are discretized to a grid, based on user-assigned grid spacing. The grid can be flexible, or structured, depending on user preference. Multiple 2-D areas can be included, with varying resolution, allowing for finer resolution in the areas of interest without significantly slowing computation time. An early release limitation is that each 2-D area is assigned single roughness coefficients but has variable roughness as of October 1, 2014. The 1-D and 2-D solution is coupled on a time step basis, and each time step has multiple iterations for feedback between the 1-D and 2-D elements. As an example, the Toe Drain which is a 1-D element, is connected to the Yolo Bypass, a 2-D storage area through a lateral weir. Flow over the weir is computed with a headwater from the 1-D Toe Drain and tail water from the 2-D Bypass to which it is connected. More about the model development is explained in Chapter 5.

4 Chapter 4: Review of Data and Geoinformatics

4.1 Introduction and Applications

Greater use of two-dimensional models has increased demand for high-resolution, spatial data. Where 1-D models can often suffice with cross-sectional data to represent river geometry, 2-D models require a continuous representation of the terrain to create geometries (*Tate et al., 2002; Merwade 2005; Merwade et al., 2008a,b; Casas et al., 2010*). Other inputs, common to all hydraulic models, not just unique to 2-D models are: flow and/or stage data, roughness coefficients and data for model calibration (*Bates et al., 2004*). Need for these data has increased use of remote sensing and GIS for hydraulic modelling (*Smith et al., 2006*). These GIS linkages with 2-D or higher order models also have allowed greater complexity, by allowing the spatial variability of parameters, such as roughness to be included in the model (*Smith, 1997; Hunter et al., 2006*), as well as allowed for model calibration (*Horritt, 2006; Mason et al., 2009*) and validation (*Horritt and Bates, 2002; Horritt, 2006*). For example, remote sensing technologies are being used in various data collection efforts while newer GIS techniques are being developed to process and prepare data for use in hydraulic models.

The section presents some ways remote sensing and GIS are being used to meet data requirements for 2-D models. This includes their use in generating terrain (*Merwade 2005; Merwade et al., 2008a,b*), collecting flow and stage data in ungauged rivers (*Smith, 1997; Hirpa et al., 2006; Domeneghetti et al., 2014*), obtaining or approximating spatially distributed roughness coefficients (*Mason et al., 2003; Casas et al., 2010*) and calibration (*Mason et al., 2003*). This thesis however, mainly uses GIS and remote sensing for terrain generation, so some techniques for doing this also are discussed.

4.1.1 Topographic Data

In 2-D models or coupled 1-D/2-D models, a continuous surface of the floodplain is needed to generate elevation data for use in the mesh (*Tate et al., 2002; Merwade et al., 2008b*). Often, this surface comes as a Digital Elevation Model (DEM). DEMs are extensively used in hydrological models (*Jenson, 1991*) but their application to hydraulic models is much more recent (*Tate et al., 2002; Merwade et al., 2008a*). Furthermore, the kind of treatment that a DEM used in a hydraulic model requires can be quite different. Tate et al. (*2002*) and Merwade et al. (*2008a, b*) discuss different GIS methods to create a DEM, from multiple sources, including contours, LiDAR and GPS. Some of these are discussed later in this section.

4.1.2 Bathymetric data

Generating bathymetry often involves surveying cross-sections along the river channel and then interpolating between the cross-sections (*Merwade, 2009*). There are often two methods of obtaining bathymetry data, one is through ground surveys and the other is echo soundings, a type of sonar (*Lui, 2008*). Although both methods are well-established, there is still the problem of using such data to create a bathymetric grid (*Merwade et al., 2008a*). Elevation data for the channel are either available as point data, which must be interpolated to create a continuous surface, or they are available as linear cross-sectional data, which will require different interpolation techniques. There are a great many challenges in interpolating these data to create a surface that is representative of the channel, and some of these challenges and limitations have been discussed by Merwade et al. (*2008a*). Often these challenges remain, irrespective of how detailed the bathymetric data source is, i.e. whether it is cross-sections or echo sounding measurements (*Merwade et al., 2008a*).

4.1.3 Stage/Flow Data

Hydraulic models require boundary conditions to be specified at upstream and downstream ends of the modelled region. Often, discharge and stage data are used to provide these boundary conditions (*HEC, 2001*). Flow and stage data are usually measured at gauging stations, and in California are maintained by either the Department of Water Resources or USGS. However, in the absence of gauges, boundary flow rates are often established by results from a hydrologic model. Other methods of estimating flow and stage data use satellite imagery to estimate water surface elevations, and developing relationships based on this imagery and actual gauge data (*Bates et al., 1997; Pappenberger et al., 2006*). Applications in Bangladesh and India have employed linear relationships between satellite images of inundated area and gauged water levels for monsoon floods (*Ramamoorthi, 1990*). Pelletier (*1988*) provides an extensive review of uncertainties from each of these options, from parallax error, to miscalculated location of stage. However, applications of remote sensing to flow and stage data estimation are still not widespread and usually limited to comparison and validation purposes (*Domeneghetti et al., 2014*).

4.1.4 Bottom Roughness

Roughness coefficients are important hydraulic model inputs, as they are used to calculate frictional losses between cross-sections (*Chow, 1959*). Most river cross-sections and floodplain areas have varying roughness. Often, different roughness values are selected for different parts of the river reach, or different parts of the cross-section. Chow (1959) offers procedures for estimating Manning's coefficients for channels and overbanks. Given that this coefficient is based on an empirical relation, it is used as a calibrating parameter. Often, it is "estimated" by the modeller, and then tuned during model calibration. Nowadays, GIS allows us to assign spatially distributed Manning's coefficients for each land use represented, given that global land use datasets are now available.

4.1.5 Data for Calibration

The last piece of information needed for a model is calibration and validation data. In general, flow and stage data, often taken during major flood events are used to calibrate and test hydraulic models. Remotely sensed data and satellite imagery can be used to calibrate and assess 2-D models that predict the extents of flooding (*Bates, 1997*). Furthermore, by acquiring inundation extents and depths over the course of a flood event, modellers can calibrate the model, either by varying Manning's n or varying the terrain itself, to ensure that hydraulic model results match with the real flood footprint (*Horritt and Bates, 2002*). The Manning coefficients for example can be adjusted to vary the friction of the riverbed and change the flow and therefore, the stage. A cautionary note on the use of Manning's n as a calibrating parameter is that it must be physically possible and realistic. Validation data to confirm the calibration must be undertaken with a different set of data to ensure that the model replicated observed values consistently.

4.2 DEM Generation: Data sources and methods

Several methods exist for creating a surface suitable for hydraulic modelling. The best method will depend on what kind of elevation data are being used. Many of the above mentioned data, acquired through remote sensing such as LiDAR and sonar, need to be processed before being used to create a terrain, since they include non-earth elevation points, such as trees, vegetation, bridges and decks. Furthermore, non-continuous raw data need to be interpolated to create a continuous surface. Table 2 summarizes the main sources of elevation data used to create a DEM and the relative advantages and disadvantages of using each.

Table 2: Summary of advantages and disadvantages of using DEM sources

Source	Advantages	Disadvantages
Topographic maps	-Economical and simple if maps are digitized and contours are already available -The resulting DEM will already be bare-earth	-Not very accurate. -Highly dependent on quality of the base map. -Microtopography and flat areas not well-represented in topo maps (so floodplains are not well represented). -Must be manually digitized, making it subject to human error
Ground Surveying	-Extremely accurate -Has other applications such as calibrating larger datasets	-Expensive and time consuming -Not cost effective for large areas. -Permission is required to enter property for data measurement
Digital Aerial Photogram-metry	-Within the field of remote sensing, is a relatively well understood approach -If matched well, can be very accurate -Provides other products; aerial imagery which is good for interpreting elevation and terrain -Relatively economical for surveys of large areas	-Takes long to process images, produce DEM. -Dependent on scale and quality of imagery -Manual measurements are tedious and require experienced observer -Limitations in the automatic matching algorithm
LiDAR	-Good for large scales as large areas can be covered -High resolution and accuracy -Has ancillary benefits and uses in other fields -Provides other products; for example surface maps that are used to measure height of vegetation	-Expensive and may need lots of flights for covering larger areas -Cannot operate in bad weather conditions -Often requires complementary data, to check the data, for example aerial photographs. -LiDAR often is used alongside digital aerial photography above.

4.2.1 Topographic Maps

A DEM can be produced by digitising contour lines and heights from a topographic map and then using an interpolation scheme to create a continuous surface. Unfortunately, the accuracy of the DEM depends on the quality and resolution of the map itself (*Lui, 2008*). While the method is economical if the maps are already available, the resolution of topographic maps is generally poor, especially in flatter areas such as floodplains.

4.2.2 Kinematic GPS and Ground Survey

Elevations can also be measured directly in the field using Global Position System (GPS). These elevation point values have to be interpolated, just like contour lines, to produce a continuous surface or grid. Real Time Kinematic (RTK) satellite navigation systems are used along with GPS for quality control purposes and increase the precision of these data. Thus, GPS-RTK is known to provide the most accurate elevation data possible (*Chang et al., 2004a*). The drawback is that they require lengthy surveys and fieldwork, so they are often used for providing validation data for other techniques or for filling gaps in data rather than for creating full scale DEMs (*Chang et al., 2004b*).

4.2.3 Digital aerial photogrammetry

DEMs can be constructed from overlapping high-resolution satellite images using stereo-photogrammetric techniques (*Chang et al., 2004a; Lui, 2008*). This involves identifying common points between two or more photographic images taken from different angles, and constructing a line of sight from the camera location to the point on the object. Where these rays intersect is recorded and used in estimating the three-dimensional coordinates of the point. When this has been done for many points, they are collected and interpolated onto a regular grid. The model however, is a surface model and still needs to be made bare earth (*Fabris, 2005; Lui, 2008*).

4.2.4 LiDAR

LiDAR stands for Light Detection and Ranging. It is an airborne technique that uses a laser scanner to send pulses towards the earth's surface, much like radar, and these are reflected off features. The round trip time allows the distance between the laser and the ground to be calculated. From that, the elevation is obtained. Many LiDAR systems collect multiple "returns" where the first return would come from vegetation and foliage while the last return would come from the ground. Ground returns are used to construct a bare-earth DEM while surface returns are used in estimating object heights. LiDAR also helps in identifying surfaces, since the intensity of the reflected pulse is also recorded and can provide useful information about the surface feature being imaged, for example whether it is water, vegetation etc. (*Marks and Bates, 2000; Lui, 2008*).
For LiDAR to be used in hydrodynamic model, ground returns must be filtered so that the final DEM produced is devoid of vegetation or structures that would not obstruct the flow of water. Once the ground points have been extracted, they are interpolated to produce a continuous surface. Several interpolation methods exist, with the common ones being Nearest Neighbour, Kriging, Inverse Distance Weighted and Spline (*Merwade et al., 2006*). Many interpolation techniques have been reviewed by Merwade (*2006*). In California, high resolution LiDAR data suitable for flood modelling are becoming increasingly available and a substantial amount of these data have been collected by the DWR as part of the Central Valley Floodplain Evaluation and Delineation (CVFED) effort.

4.3 Conclusions

The section above illustrates how GIS is being used in hydraulic modelling and its role in characterizing the topography. This role is likely to increase, given that further developments in data sources are anticipated and more software packages are being developed to deal with these new data. Further work remains in understanding how to best process remotely-sensed data. This includes determining better filtering algorithms for LiDAR, developing better interpolation methods for flood models, and minimizing uncertainties in the modelling process. There is likely to be a re-orientation for hydraulic engineers, as they need to learn more GIS and remote sensing to make better use of the more extensive and detailed data sets needed for 2-D and 3-D hydraulic models.

Finally, the aim of using GIS in hydraulic models is not to simply develop the most "complex" model, but rather a model that can help meet project objectives. Thus, in making a model more accurate, one should balance against the increased computational burden and investment in money and time needed in surveying, data collection and model set-up and testing (*Mason et al., 2009*). Therefore, a sensitivity analysis exercise was used to assess the effects of DEM resolution and accuracy, grid spacing and solution scheme on flooding extents and weigh the various levels of "complexity" with their computation time.

5 Chapter 5: Modelling Methods

This section summarizes the development of the smaller model for the Yolo Bypass, followed by a more thorough description of the larger Yolo-Sutter Bypass model covering the Lower Sacramento River area.

5.1 Creation of Bare-Earth DEM

5.1.1 LiDAR Filtering and interpolation

The main data source for the DEM was LiDAR collected as part of the Central Valley Floodplain Evaluation and Delineation (CVFED) program. The CVFED LiDAR data were available as a large point cloud dataset divided into smaller tiles for the study area and assembled as binary ASCII and LAS files with x, y, and z values. LAS files are currently the industry-standard binary format for storing airborne LiDAR data and can be easily accessed as a dataset within ArcGIS. The raw LiDAR data within the ASCII and LAS files included points for vegetation, structures, and other obstructions that needed to be removed before the dataset could be used for bare-earth DEM generation. Given that each LiDAR tile averaged more than 2 million points, the large LAS dataset size required thinning the points to be used in ArcMap. The thinning used was based on the "Window Size" method, since it was the only method that could filter such a large dataset. After LiDAR data were filtered and thinned, an LAS dataset was created for the study area using bare-earth returns and enforcing 'breaklines' - lines representing flow networks or boundaries. The dataset is then converted in to a raster of 1-meter resolution. While other workflows can convert LiDAR datasets to raster datasets, many other methods are not supported by ArcGIS. The newest version of ArcGIS, version 10.2, has a tool in the ArcToolbox to manage LAS Datasets and to convert them directly to rasters of a specified resolution. Although the processing time is quite long, this method was the most straightforward with the least error.

The resulting raster dataset created was not continuous and needed to be interpolated to a continuous surface. A number of interpolation methods were tested to see how they all compared in terms of accuracy. Kriging and Natural Neighbours gave generally good results, with low Root Mean Square Error (RMSE), but kriging required inputting GIS lines representing boundaries and those that define topographic features. Given that these lines were not available, "Natural Neighbours" was used as the interpolation method. Natural neighbour is based on the 'Sibson' interpolation (*Sibson, 1981*), where the user specifies how far to search for points by setting a neighbourhood threshold. After finding the closest set of points, weights are applied to them and finally they are interpolated through triangulation.

5.1.2 DEM generation

The DEM generated from CVFED LiDAR had fairly good coverage but had some missing data, for example in the Sutter Slough area. Older elevation datasets from DWR and USGS were used in areas lacking CVFED coverage. The highest resolution elevation data available is a 10 meter DEM, resampled from 2-meter data for the San Francisco Bay and Sacramento-San Joaquin Delta. This DEM was developed using LiDAR, single- and multi-beam sonar soundings and existing integrated maps collated from multiple sources (*Wang & Ateljevich, 2012; Carignan et al., 2010; Dudas, 2010; Fox Grover, Smith, & Jaffe, 2003*). A major strength of these data was its fairly good representation of bathymetry (*Wang & Ateljevich, 2012*). However, this version of the DEM does not extend north of I-80, so for areas above I-80, a publically available 10-meter San Francisco Bay NAVD 88 DEM, produced as part of joint efforts of NOAA, DWR and other public agencies, was used (*Carignan et al., 2010*). Finally, for any gaps or holes, the 10-meter USGS National Elevation Dataset (NED) DEM was used.

All of these DEMs were collected and projected to the same co-ordinate system, namely Universal Transverse Mercator (UTM), Zone 10 with a horizontal datum of North American Datum of 1983 (NAD83) with units of meters and a vertical datum of NAVD 88. They were all resampled to 1 m and mosaicked together with CVFED as the highest priority, followed by the Bay Delta DEM , the NOAA 10 m DEM and finally the 10 meter NED DEM of lowest priority.

5.1.3 Bathymetry Data and Hydrological Correction

Before the DEM can be used, it must characterize bathymetry. The CVFED LiDAR was completely devoid of bathymetry as shown by the figures below. The figures show cross sections of the Sacramento River using CVFED LiDAR (Fig. 6) and Delta DEM (Fig 7).

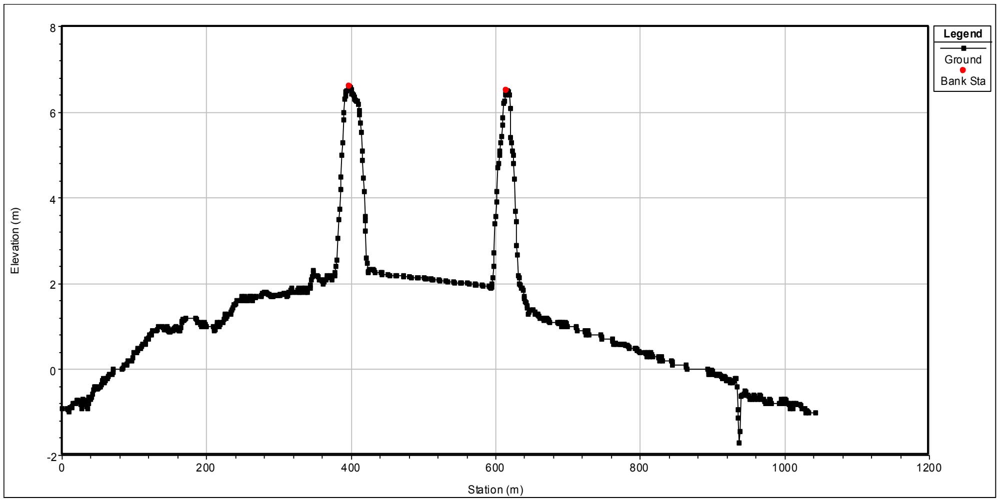

Figure 6: Cross Section obtained from CVFED LiDAR for the Sacramento River (River Mile = 20) at the point where Sacramento meets the Cache Slough Complex

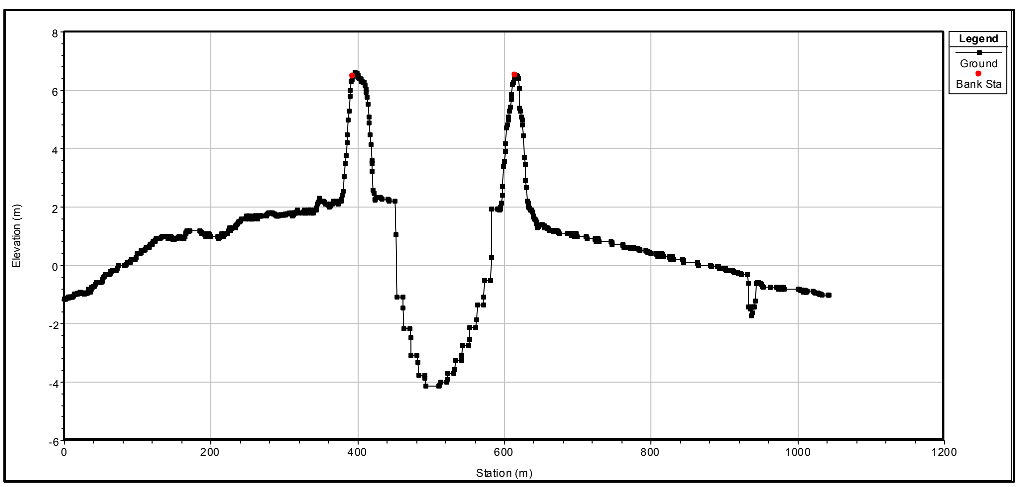

Figure 7: Cross Section obtained from Delta DEM LiDAR for the Sacramento River (River Mile = 20) at the point where Sacramento meets the Cache Slough Complex

It is evident that the CVFED LiDAR simply reflected from the surface of the water and is void of bathymetric data. As a result, multiple sources were used to incorporate the bathymetry into the DEM. Firstly, the bathymetry information in the San Francisco Bay and Sacramento-San Joaquin Delta DEM was extracted by clipping out the pixels within a polygon representing all river channels. These were clipped into the mosaicked DEM only if they were of a lower elevation. This was done using a CON statement. Other point-data bathymetry information was available from cbec eco-engineering, DWR and Environmental Data Solutions (EDS). Table 3 lists all the sources used for the construction of the composite DEM.

Table 3: Bathymetry and Elevation Sources

Data	Source	Notes
10 meter DEM	USGS National Elevation Dataset	Publically available, processed DEM
10 meter DEM	NOAA San Francisco Delta	Publically available, processed DEM with fairly good representation of bathymetry
10 meter DEM with bathymetry	Bay Delta Office	Publically available, processed DEM
CVFED LiDAR	DWR	Acquired as raw, unprocessed LiDAR, in ASCII and LAS
Liberty Island Bathymetry	EDS	Acquired as raw, unprocessed point data, in ASCII and shapefile
Cache Slough Bathymetry	EDS	Acquired as raw, unprocessed point data, in ASCII and shapefile
Barker Slough, Calhoun Cut, Lindsey Slough and Cache Creek Bathymetry	EDS, cbec eco-engineering	Acquired as raw, unprocessed data, point and TIN
Barker Slough Bathymetry	EDS, cbec eco-engineering	Acquired as raw, unprocessed data, point and TIN
West Delta (Part of Yolo Bypass)	EDS, cbec eco-engineering	Acquired as raw, point data.
Putah Creek Bathymetry	DWR	Acquired as raw, unprocessed point data,
North Sacramento River Bathymetry	Bay Delta Office	Publically available, processed DEM
Georgiana Slough Bathymetry	Bay Delta Office	Publically available, processed DEM
Miner Slough Bathymetry	Bay Delta Office	Publically available, processed DEM
Deep Water Ship Channel Bathymetry	EDS, cbec eco-engineering	Acquired as raw, unprocessed data, point and TIN
Toe Drain Bathymetry	EDS, cbec eco-engineering	Acquired as raw, unprocessed data, point and TIN
Knights Landing Ridge Cut Bathymetry	DWR	Acquired as raw, unprocessed point data, in ASCII and text file

5.2 Smaller Model Construction

5.2.1 Construction of Composite Digital Elevation Model

When the smaller bypass floodplain model was constructed, CVFED LiDAR was unavailable, so a composite DEM was created by mosaicking the 10 meter Bay Delta DEM, the 10-meter NOAA DEM and the 10-meter USGS DEM. The mosaicked DEM was made bare-earth by removing features such as vegetation and bridges and "drained" by digitizing polygons defining small channels and performing a raster algorithm to lower the elevation of the terrain that was covered by the polygon. Pre–processing within ArcGIS was needed to ensure that there were no gaps or holes in the DEM and a continuous surface was produced by using a "Natural Neighbors" interpolation scheme.

5.2.2 Construction of Bathymetry

Information on channel bathymetry was estimated through site visits and some bathymetry was made available by cbec eco-engineering. The modelling domain of the smaller model covers the complete Bypass from Fremont Weir to just north of Rio Vista. Figure 8 shows the schematic of the smaller model.

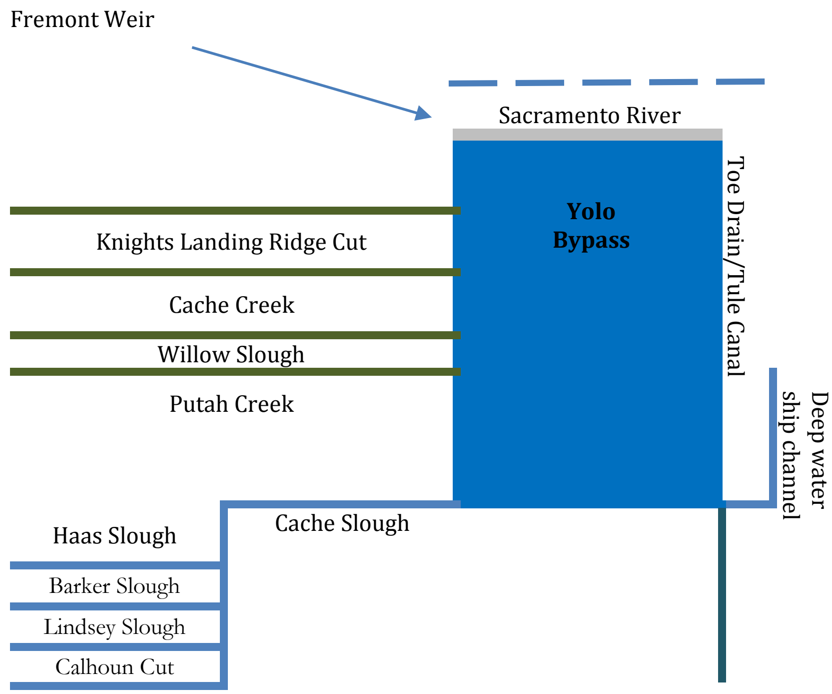

Figure 8: Schematic of Smaller Model

5.2.3 Boundary Conditions

Flow boundary conditions were set at Sacramento River, Barker Slough, Cache Creek, Knight's Landing Ridge Cut, Lindsey Slough, Toe Drain, Deep Water Ship Channel and West Liberty Island, with stages set at the confluence of Cache Slough and Sacramento River. Table 4 lists the boundary conditions and Table 5 lists the Initial Conditions set at these boundaries. The main purpose of this was to look at the flooding from the Fremont Weir, as opposed to the western tributaries given that there is interest in controlling how much flow comes through the Fremont Weir. For all flow scenarios, the Sacramento River was ignored.

Table 4: Boundary Conditions for smaller Yolo Bypass model

Reach	Boundary Condition Type	Boundary Value
West Liberty Island	Flow	10 cfs
Barker Slough	Flow	10 cfs
Hassel Slough	Flow	10 cfs
Cache Creek	Flow	10 cfs
Lindsey Slough	Flow	10 cfs
Toe Drain	Flow	Variable
Deep Water Ship Channel	Flow	10 cfs
Cache Slough	Stage	Tidal boundary

Table 5: Initial conditions for smaller Bypass model

Reach	Initial Flow
Sacramento River	3000 cfs
Barker Slough	10 cfs
Hassel Slough	10 cfs
Cache Slough (includes Miner Slough)	70 cfs
Lindsey Slough	10 cfs
Toe Drain	100 cfs
Deep Water Ship Channel	10 cfs
West Liberty Island	10 cfs

5.2.4 *Model Roughness*

The model Manning's roughness used for this project was 0.06 for the Bypass (Overland areas could only be assigned one roughness coefficient in the early version of RAS) and 0.03 for the river channel and 0.05 for the banks. These coefficients were based on the ground cover observed in field and site visits.

5.2.5 Contraction and Expansion Coefficients

The coefficients of contraction and expansion are used to capture the energy losses that occur from either flow contraction that occurs when approaching a constricted area like a bridge, or from increased flow expansion when leaving the bridge. These energy losses are not accounted for in the frictional loss co-efficient, so these are accounted for in the contraction and expansion coefficients. Typically, the coefficients for all cross-sections are kept as 0.3 for contraction and 0.5 for expansion (default), unless there are bridges or culverts in the vicinity. Since no bridges were modelled, the default coefficients are used. The culverts in the Toe Drain were also left unchanged after conducting a calibration of tidal flow.

5.2.6 Calibration

Calibration for low-flow cases was preliminary and based on tidal flow observations at Lisbon weir. Complete calibration as part of this study is described in Section 5.6, in the description of the larger model development. Validation for the models was not undertaken due to limitations discussed in Section 5.7.

5.2.7 Model Simulations

Model simulations are discussed in Chapter 7: Applications, where baseline simulation results and results of different scenarios are discussed.

5.3 Larger Model Development

This section describes the development of the hydrodynamic model for the Yolo-Sutter Bypass and the full Lower Sacramento River. A schematic of the model is shown in Figure 9, which shows all the reaches included in the model.

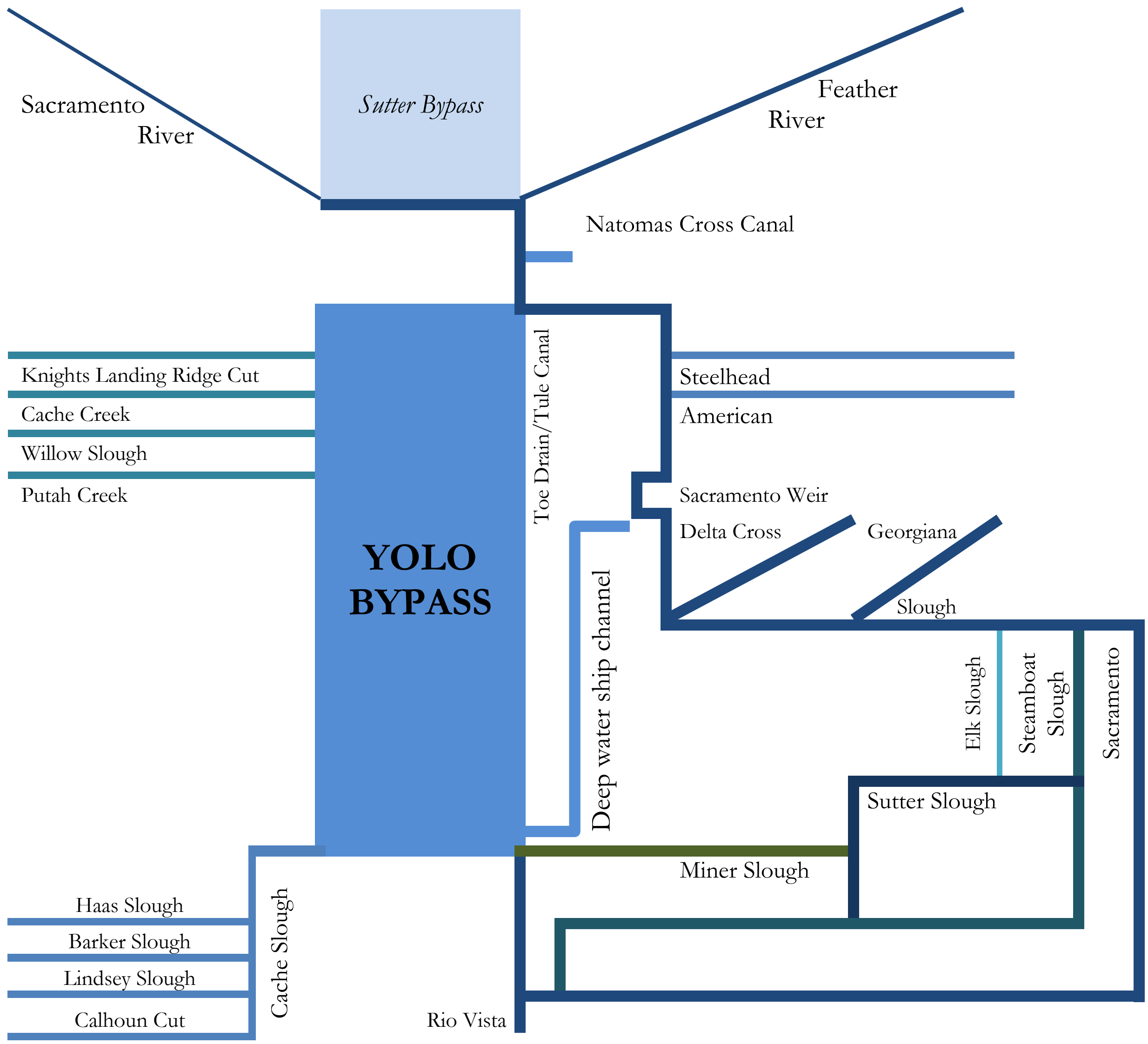

Figure 9: Simplified schematic of Larger Model (Source: CDEC)

5.4 HEC-RAS Pre-processing

5.4.1 Geometry Creation

Cross-sectional data for the Sacramento River upstream of the Feather River confluence were not represented in the DEM and therefore, obtained from DWR as part of the CVFED effort. Furthermore, information on bridges, culverts and weirs was obtained from DWR and was imported from the model (CVFED). For all other purposes, cross-sections were extracted from the composite DEM created according to the procedures outlined above. ArcGIS and HEC-GeoRAS Extension were used to create the Geometry for the HEC-RAS models. The corrected DEM, along with aerial imagery was used to guide where to digitize the river thalwegs and banks. Figure 10 illustrates a sample stream section with the stream, banks, flow paths and cross-sections.

Figure 10: Illustration of stream, banks, flow paths and cross-sections for a sample stream section. Sub-section is also indicated.

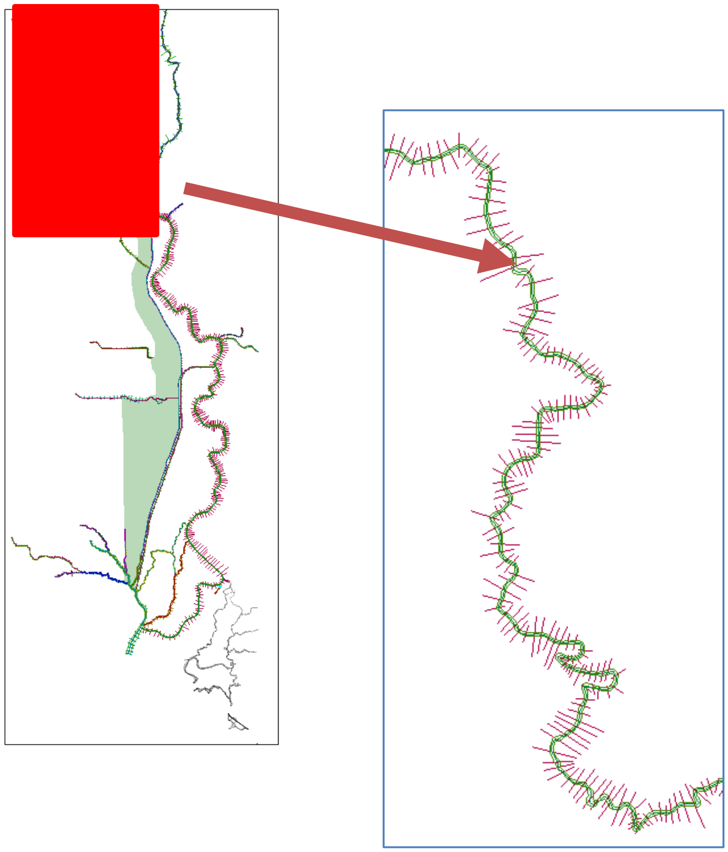

After digitizing the river centerline and banks, cross-sections were drawn at appropriate locations, checked if they were correct and finally exported, along with all other features. The final geometric data were exported into HEC-RAS. In total, the model region has 22 reaches and four 2-D flow areas. Figure 11 illustrates an example of the use of the geometry editor.

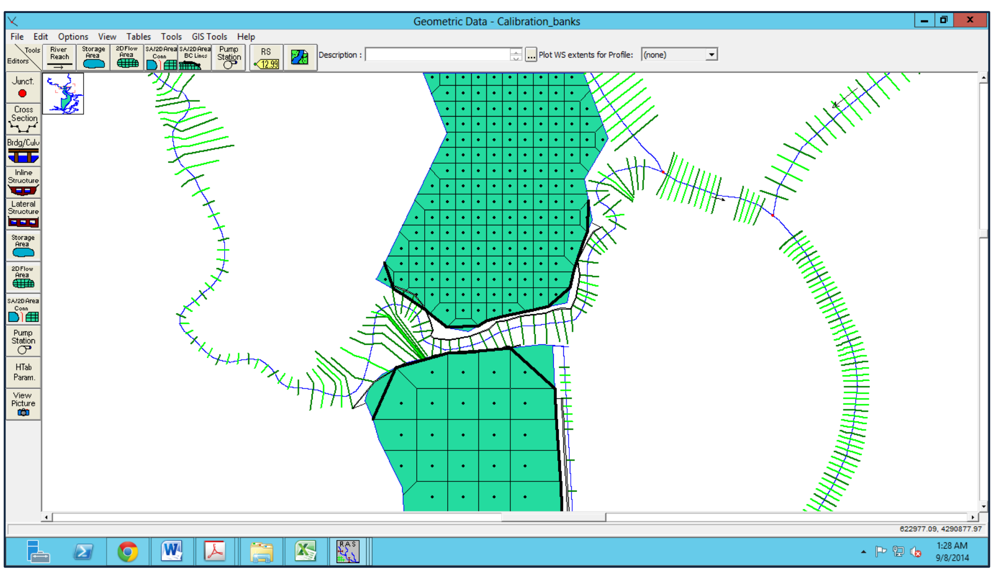

Figure 11: HEC-RAS Geometry Editor

5.4.2 Geometry Parameters

5.4.2.1 Roughness Coefficients

After conducting geometry checks, assigning bank and levee locations and ensuring their accuracy, roughness values were assigned to the cross-sections based on the HEC-RAS manual. Model roughness, or Manning's n, represents the impedance of flow, due to frictional forces, and is affected by vegetation in the channel or floodplain. An initial value of 0.035 was used for the channel sections in all the reaches and 0.05 was assigned to the bank stations. Since these were preliminary estimates, they were modified during the calibration exercise. The final coefficients varied for each river reach.

5.4.2.2 Expansion & Contraction Coefficients

The default expansion and contraction coefficients of 0.1 and 0.3 were used for all cross-sections. The only exception is that near bridges, which were imported from the CVFED model, given that their information was not otherwise available.

5.4.2.3 Grid Sizing and Grid Convergence Testing

In HEC-RAS, grid spacing needs to be specified to determine the size of the cells in the 2-D area. Each cell contains hydraulic properties based on the underlying DEM, and calculates elevation–volume, wetted perimeter, area, and roughness tables for each cell and cell face. In terms of computation, however, only one water surface elevation is calculated for each grid cell center at each time step (*HEC, 2014*).

The size of the grid has implications on model stability. If spacing is very small or the time step is too large, the model can become numerically unstable because the Courant number becomes too large. The value of the Courant number depends on the method used to solve the discretized equation, whether it is explicit or implicit. Depending on how much the velocity changes with time and distance, an appropriate cell size had to be selected to ensure that the model does not become unstable. Before deciding on the grid size, a grid convergence test using a 10 m DEM was carried out to demonstrate that the results did not depend on grid sizing. The test was carried out on the same smaller rectangular section of the Bypass to assess the differences in flooding for even finer grid sizes. Flooding extents were calculated within ArcGIS. Table 6 gives the results of flooding and range of depths achieved with various grid sizes.

Table 6: Grid Convergence Test Results

Grid Size	Timestep (mins)	Cell counts (from ArcGIS)	Flooding Extent (acres)	Range of depths (ft)
100 m by 100 m	15	171722	3,829.3	0 – 9.125
200 m by 200 m	15	171721	3,829.4	0 – 9.125
400 m by 400 m	15	171728	3,829.3	0 – 9.125
600 m by 600 m	15	171859	3,843.0	0 – 9.125
800 m by 800 m	30	171990.2	3,829.5	0 – 9.125
1000 m by 1000 m	30	172334	3,832.4	0 – 9.125

The results suggest that model results are not dependent on the grid resolution. Increasing grid resolutions using the same DEM gives almost the same inundation area as calculated in ArcGIS. The range of depth is also the same, although their distribution is only slightly different.

For this model for the entire Bypass however, the finest grid spacing computationally possible by the server was 100 m by 100 m. Any grid size below this number resulted in model instability. However, computational times were much larger, and therefore, a 200 m by 200 m grid was used.

5.5 Boundary Conditions

Observed stage and flow data from CDEC and Water Data Library were used for boundary conditions. For some ungauged river reaches, computed estimates of flow data, based off work of cbec eco-engineering was used. For all gauges, 15-minute or hourly data were used. All data computed by cbec eco-engineering however, were daily data. Table 7 provides a list of boundary conditions used and their respective sources. The respective boundary conditions taken from cbec eco-engineering also are plotted in Appendix A for a low flow period for the month of July.

Table 7: Boundary Conditions

Boundary Condition	Type	Source	Location
Sacramento Upstream	Flow	15 minute Gauge from CDEC.	Located at Wilkins, downstream of Tisdale Weir, near Grimes. Gauge: Station ID: WLK
Feather Upstream	Flow	Daily computed data from cbec eco-engineering	Computed based on data from the following gauges: USGS 11390500, USGS 1142500, A02930, A02945, Arcade Creek/EMC02.
American River	Flow	15 minute gauge from CDEC. Gauge Operated by USGS	American River at Fair Oaks. It is located below Nimbus Dam (Gauge: USGS 11446500 and CDEC ID: AFO)
Natomas Cross Canal	Flow	Daily computed data from cbec eco-engineering	Estimated based on Arcade Creek gauge
Steelhead Creek	Flow	Daily computed data from cbec eco-engineering	Estimated based on Arcade Creek gauge
Cache Creek	Flow	Daily computed data from cbec eco-engineering	Gauge at Cache Creek Settling Basin
Putah Creek	Flow	Daily computed data from cbec eco-engineering	South Fork, on Old Davis Road
Cache Slough	Flow	Daily computed data from cbec eco-engineering	Estimated flow based on CDEC Gauge data (Station ID: UCS)
Calhoun Cut	Flow	Daily computed data from cbec eco-engineering	Estimated flow based on CDEC Gauge data Station ID: UCS)
Barker Slough	Flow	Daily computed data from cbec eco-engineering	Estimated flow based on CDEC Gauge data from North Bay Aqueducts.
Haas Slough	Flow	Daily computed data from cbec eco-engineering	Estimated flow based on CDEC Gauge data
Lindsey Slough	Flow	Daily computed data from cbec eco-engineering	Estimated flow based on CDEC Gauge data Station ID: LSHB)
Knights Landing Ridge Cut	Flow	Daily computed data from cbec eco-engineering)	Estimated flow based on DWR gauges, A02930, A02976 and A02945/
Knights Landing Outfall Gates	Flow	15-minute gauge from Water Data Library	Hourly gauge/ DWR A02945
Delta Cross Canal	Flow	Daily computed data from cbec eco-engineering	Estimations from DWR Dayflow program
Georgiana Slough	Flow	Daily computed data from cbec eco-engineering)	Estimations from DWR Dayflow program
Deep Water Ship Channel	Flow	10 m^3/s	Assumed constant based on data from Water Data Library
Elk Slough	Flow	No hydraulic connection	Assumed no flow. - Just an empty channel
Downstream Sacramento	Stage	Hourly data available from CDEC. Station ID: RVB	Rio Vista Stage, NAVD 88, Available as hourly timestep

5.6 Model Calibration

Calibration is a necessary step that ensures that the model matches a real system, and requires adjusting model parameters in an iterative process to obtain computed results that are close to the measured result. The calibration exercise was complicated by the challenges of obtaining floodplain wetting and drying data, geometrical changes occurring due to levee breaches, datum inconsistencies and incomplete or unreliable stage and flow data for a particular time period. Given these complications, the calibration efforts (seen as preliminary) were conducted simply for low flows with no overland flooding, since drainage times for the Bypass were not available. The calibration effort was also limited to the Toe Drain and the Sacramento River, given that these river reaches were seen to be the most important ones.

Computed stages were compared to observed stages for the period from 1st July, 2006 to 10th July 2006, using CDEC data to ensure consistency. Most of the CDEC stage data was reported using United States Engineering Datum (USED), and had to be converted initially to National Geodetic Vertical Datum 1929 (NGVD29) and later to North American Vertical Datum 1988 (NAVD88). This was done at all locations except for the Lisbon and Liberty Island gauge data, where data was already available in NAVD88 standard. Table 8 lists the river stations where observed and computed stages were compared. Appendix B includes the location co-ordinates and other pertinent information of these gauges.

Table 8: Gauging Stations used for Calibration and Validation

River Reach	Gauging Station	Gauge ID	Datum
Sacramento River	Sacramento River at Wilkins	Station ID: WLK	USED
	Sacramento River at Fremont	Station ID: FRE	USED
	Sacramento River at Knights Landing	Station ID: KNL	USED
	Sacramento River at Verona	Station ID: VON	USED
	Sacramento River below Georgiana Slough	Station ID: GES	NGVD29
	Sacramento River at Freeport	Station ID: FPT	USED
Toe Drain	Yolo Bypass at Lisbon Weir	Station ID: LIS	NAVD88
	Yolo Bypass at Liberty Island	Station ID: LIY	NAVD88

The first calibration exercise was done for the Toe Drain where tidal behavior was checked below Lisbon weir. An oscillatory river stage below the Lisbon weir characteristic of tidal behavior should be observed. The Lisbon Weir creates an elevated tidal backwater pool in the Toe Drain so tidal influence is felt downstream of the weir. Upstream of the weir, the hydrograph should be flattened out. Figure 12 shows observed and computed stage measurements below the Lisbon Weir stage as well as the stage computed upstream of the weir.

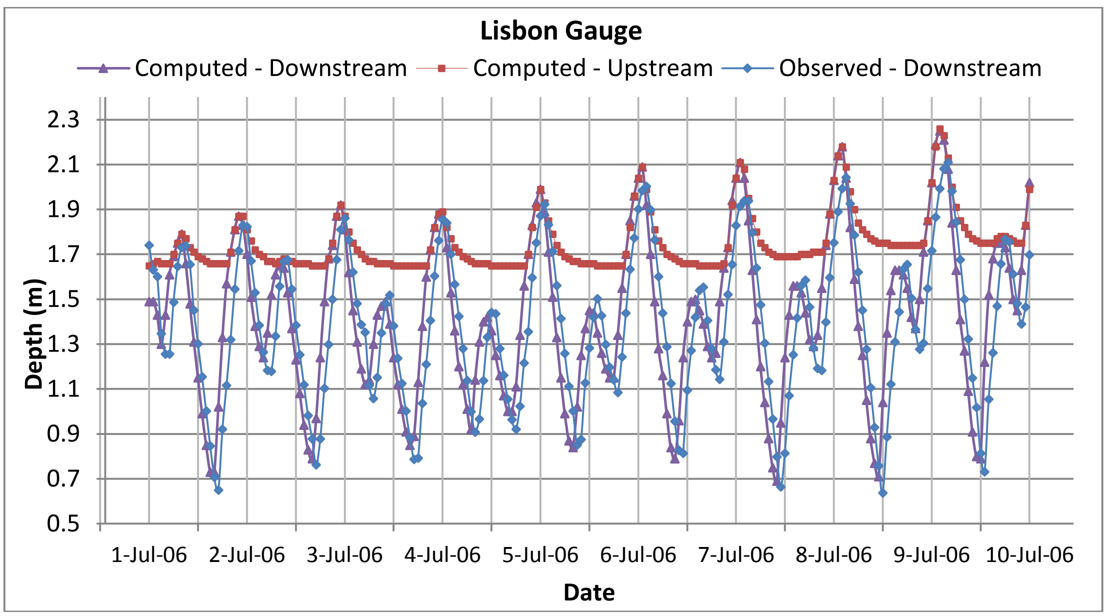

Figure 12: Lisbon Gauge Tidal Boundary

As the figure shows, computed stages below the Lisbon weir match the observed values quite well. The oscillatory behavior, typical of tidally influenced areas can be seen below the weir. Above the weir, the hydrograph is flattened as expected, because the weir increases water elevations and allows surcharging of the northern part of the Toe Drain. The final Manning's coefficient was reduced from 0.03 to 0.025 for the channel and 0.035 for the banks to match observed data.

The computed stage is 15 minutes behind the observed stage, and over-predicts the peaks beyond day 6. A possible reason for this could be that different sources were used as boundary conditions. While CDEC data was used for upstream boundary conditions at Sacramento and downstream boundary condition at Rio Vista, computed values (by cbec) based on USGS and Water Data Library gauges were used for the upstream boundary conditions at Feather River. This could result in the hydrograph getting out of sync. Another reason for the difference could be the behavior of pumps in the Lisbon weir, which were not taken into account in this model. These pumps recycle water at Lisbon weir, moving it upstream along the Toe Drain to the northern part, so including them in our model would have otherwise increased the stage upstream of the weir, and lowered it downstream.

As part of the calibration, the stage at Liberty Island was also checked and compared to CDEC data. Figure 13 shows the observed and computed Liberty Island stage measurements over time. The results show that the tidally influenced Liberty Island computed stage is within 0.1 meters of the observed stage with a slight time delay in the hydrograph.

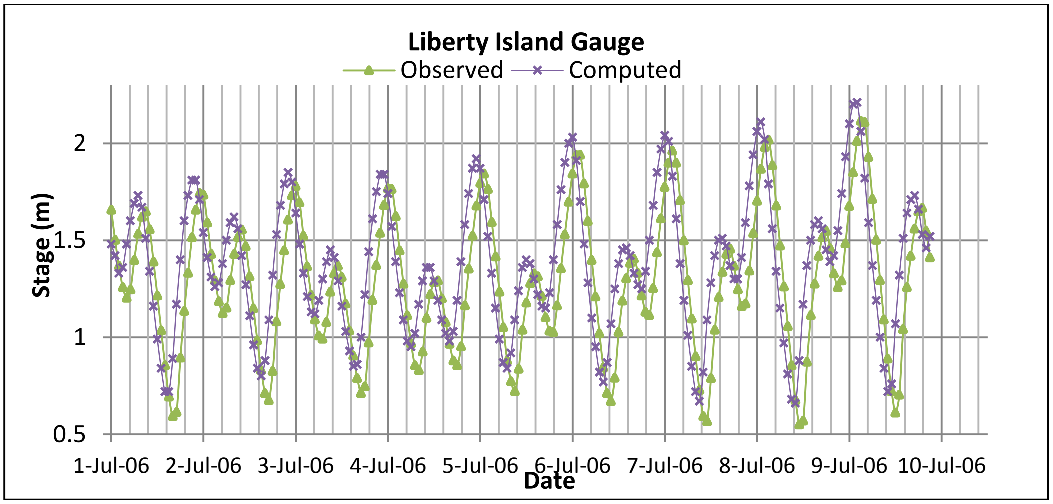

Figure 13: Liberty Island Upstream and Downstream Tidal Boundary

Within the Sacramento River, stages were checked at six locations, namely at Wilkins, Knight's Landing, Fremont, Verona, below Georgiana Slough and at Freeport. The computed stages were found to be much higher than observed stages at almost all of the locations so the Manning's coefficient for the channel was reduced for all reaches within the Sacramento River, varying from 0.025 to 0.027. Figure 14 and 15 show the observed and computed stages at Wilkins and Knight's landing. The computed values at both these locations is slightly higher than observed values by less than 0.2 meters. The shape of the hydrograph is relatively comparable at these locations except that observed hydrograph is slightly flatter at Knight Landing. A thing to bear in mind is that the computed stages of the Sacramento River at Wilkins are at an hourly time-step while the observed data was obtained from a 15-minute time-series. However, there does not seem to be any significant phase shift.

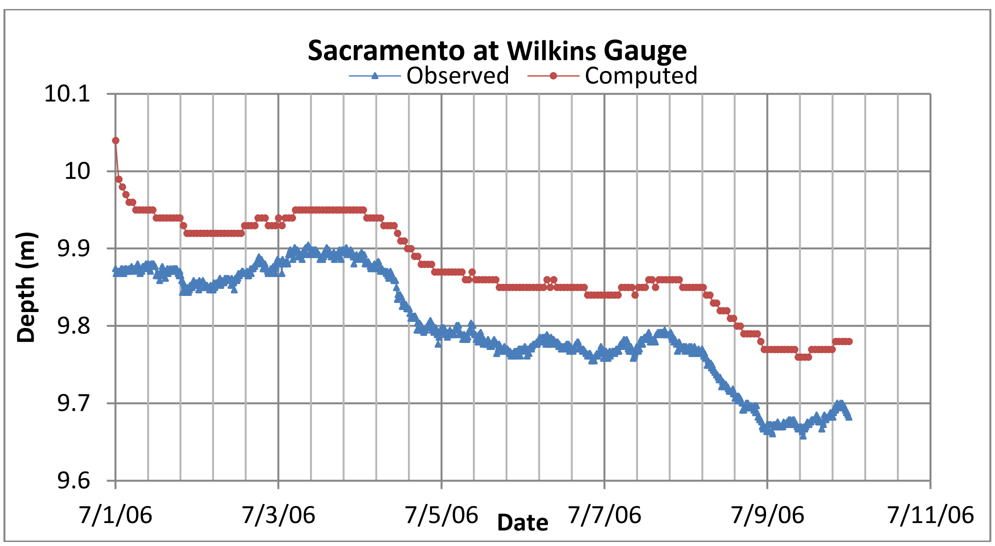

Figure 14: Observed and computed stage of Sacramento at Wilkins

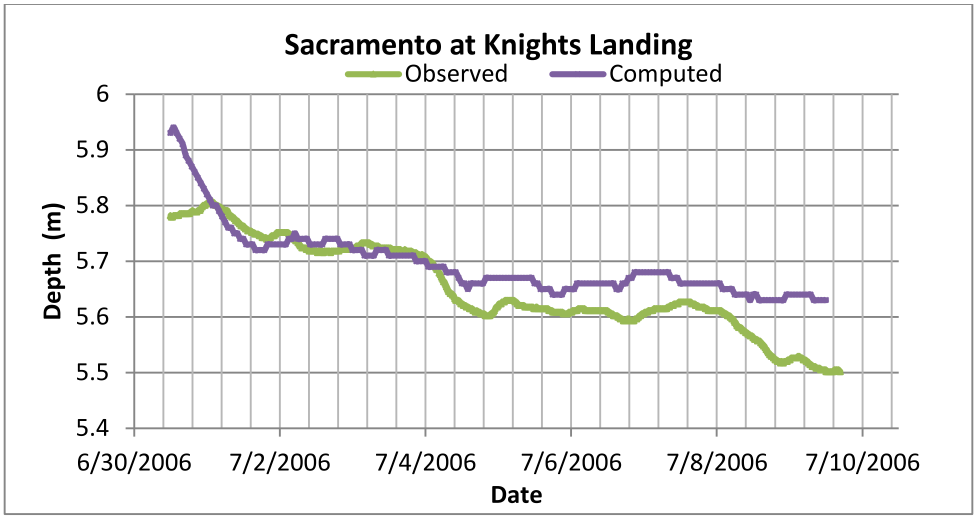

Figure 15: Observed and computed stage of Sacramento at Knight's Landing

Observed and computed stages at the west end of Fremont and Verona were also compared and after extensive calibration, the best possible match was found to still be off by 0.3 meters. Figure 16 and 17 show the final observed and computed stages at these two locations.

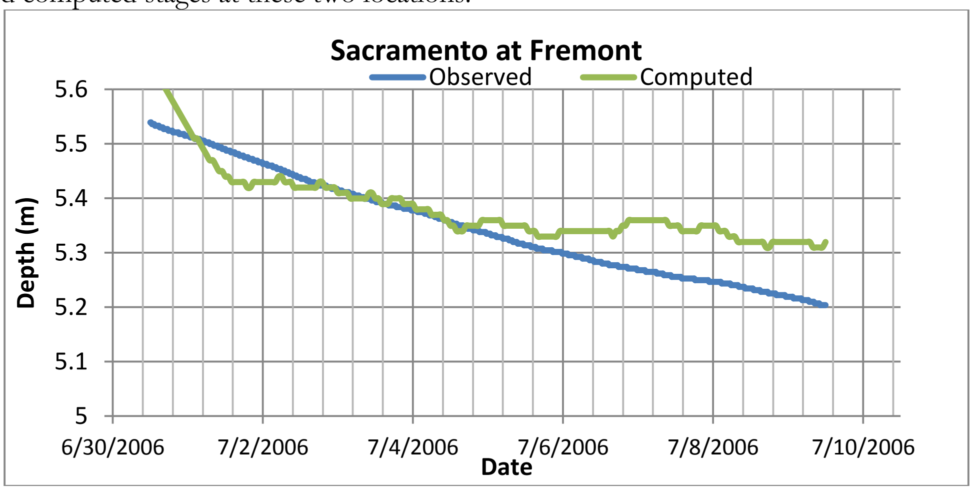

Figure 16: Observed and Computed Stage at Fremont (Western end)

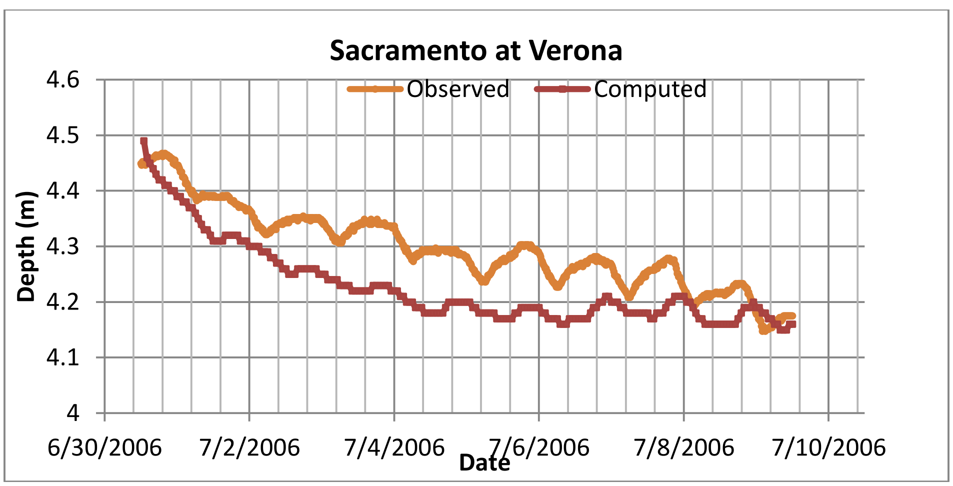

Figure 17: Observed and Computed Stage of Sacramento River at Verona

Minor loss coefficients ranging from 0.1 to 0.3 were added between the section from Fremont and Verona since the river bends extensively here. These loss coefficients raised the stage at Verona and lowered it at Fremont. However, despite multiple attempts, the computed hydrograph fails to follow the smooth oscillatory shape of the observed hydrograph, particularly at Verona and Fremont. Part of the reason for this could be that no surveyed cross-sections were available to confirm the geometry within this section. Furthermore, the combination of data of different time series, from 15-minute, hourly and daily makes it difficult to compare the timing of the hydrograph and compare phase shifts when input flow data for the location is 15-minute discharge data but calibration data is hourly stage data (in Verona).

Computed stages at Georgiana and Freeport were found to follow the observed stage quite well, given that both these locations are closer to the downstream boundary. The hydrograph shape and timing is consistent with observed data. Figure B-1, B-2, B-3, B-4, B-5, B-6, B-7 and B-8 in the Appendix show the observed and computed stages of the Sacramento River and the Toe Drain at all the aforementioned locations.

For the rest of the reaches where there was no calibration data, the Manning's coefficient was left as 0.03 for the banks and 0.04 for the overbank areas. The exceptions are the slough reaches, where the Manning's coefficient was raised to 0.035 for the channel and 0.05 for the overbank areas.

Given limitations in reliable, consistent and accurate data availability, the current calibration exercise was found to be satisfactory, sine the final computed surface profiles match observed stages from CDEC reasonably well and were within 0.2 meters of one another.

5.7 Calibration and Validation Limitations and Next Steps

The calibration exercise revealed major discrepancies while collecting stage data from different sources, either due to datum errors among different gauges or simply mislabeled datums. Much of the CDEC data varied with respect to the datum used and in some places, the data were inconsistent with USGS and Water Data Library stage data, even after converting it to NAVD 88 meters. This was found to be the case at Rio Vista, Lisbon Weir, Sacramento River at Wilkins and Sacramento at Verona.

Another limitation with the existing model is that much of the boundary inflow conditions have been computed values obtained from cbec eco engineering as well as from the Department of Water Resources. These computed values have their own associated assumptions and also use diffirent time seroes (hourly, 15 minute etc) - To the extent possible, all computed values were cross-checked with literature and observations. For example, computed values for the Feather River were checked with observed stages at Fair Oaks, CA and the Feather River at Verona. Furthermore, 15-minute data, where available was used for the calibration to ensure that any differences in the phasing and timing are captured (as in Fig 13) and do not get averaged out. In Verona (Fig 17), the phasing is difficult to compare as the computed stage is hourly data but observed data is 15-minute.

Given time constraints, obtaining an entire set of flow and stage data for validation purposes was not possible. As a possible continuation of this study, validation should be carried out using a flow data in a low-flow period from another year. Furthermore, CDEC data should be used for boundary conditions on the Sacramento River for fair comparison purposes and all stage data should be converted to NAVD 88 datum.

6 Chapter 6: Model Sensitivity

6.1 DEM Resolution and Accuracy

Terrain resolution and accuracy can affect the results of 2-D hydraulic models in various ways; it can affect the flood depth, extent and velocity by averaging out features. This in turn would affect the hydraulic properties within the cells. Another way the DEMs can affect results is through the geometry of channels, since DEMs are used to extract channel geometry needed for HEC-RAS. Thus, they are in fact inputs for generating other inputs.

A sensitivity analysis was done to assess the effects of DEM resolution and DEM accuracy on our 2-D hydraulic model. Four digital elevation models (DEMs) were used for the sensitivity analysis conducted in this exercise. Their main features are in Table 9 below:

Table 9: Main properties of DEMs used for testing and sensitivity

DEM	Resolution (horizontal)	Accuracy	Bathymetry represented	Processed for errors or holes	Notes
Composite DEM (New)	1 meter	High	Yes	Yes	Produced from CVFED LiDAR, Bay Delta DEM and NOAA DEM
Bay Delta DEM	10 meter	High	Yes	No	2-meter DEM resampled to 10 meter.
Composite DEM (Small)	2 meter	High	Yes	Yes	Produced from Delta DEM, and NOAA 10 meter DEM
NOAA DEM	10 meter	Medium	Some	No	Produced by NOAA but uses some USGS NED data

Three of the four DEMs, the 1-meter composite DEM, 1-meter CVFED Base DEM and the 10-meter NOAA DEM were used to extract cross-sections to compare their respective geometries. All DEMs are of slightly different quality. Figure 18 shows the cross section of the Sacramento River just above Rio Vista, before it joins with Steamboat Slough and Cache Slough.

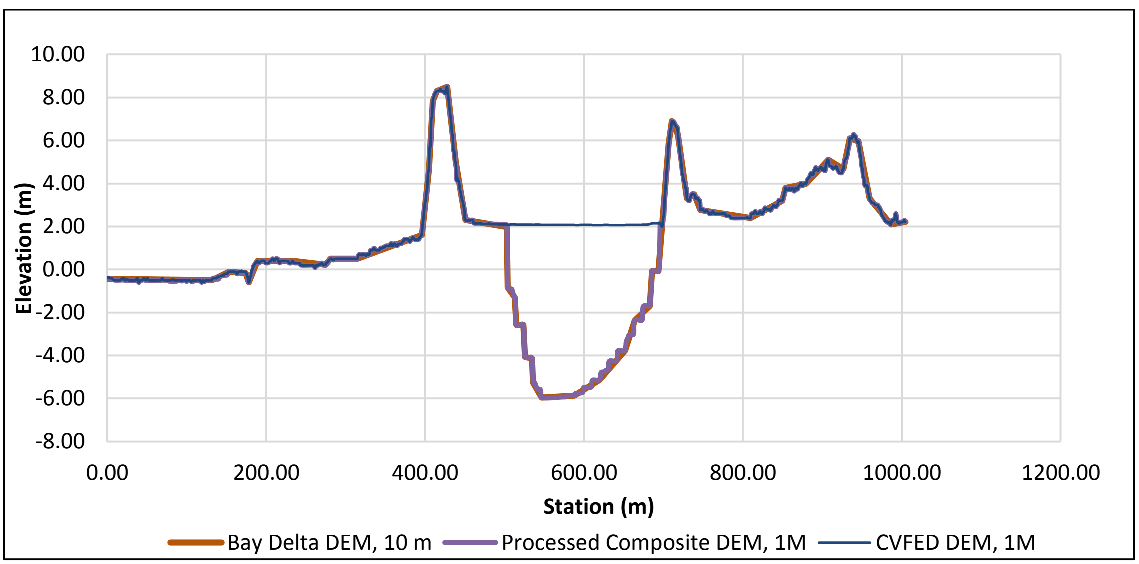

Figure 18: DEM effects on geometry

The cross sections extracted from the 1-meter composite DEM and 10-meter Delta DEM have a similar shape since their source of bathymetry is the same, but the 1-meter DEM provides more points and slightly more detail. However, the 1-meter CVFED DEM fails to provide the shape for the channel. The above results show that the bathymetry generated from the DEM is more sensitive to the quality and accuracy than its resolution. In fact, for generating cross sections, as long as the shape and depth of the channel can be captured, small changes in DEM resolution are of no great consequence.

With respect to the results of hydraulic models, including the extents, depths and velocities of flood derived from the model, the input DEM has significant implications. A test on a smaller rectangular section of the Bypass of 6,000 acres was conducted with one upstream flow value and one downstream stage, modelled as a 2-D flow area. Only one reach (small portion of the Toe drain) was modelled. Table 10 shows the results of using different DEM's to get the flood inundation extents for this area.

Table 10: Effects of DEM resolution of inundation extents and depths

DEM USED	Extent of flooding (acres)	Range of flooding depths (m)
1-meter DEM (New Composite DEM)	4187.2	0 -9.125
2-meter DEM (Older Composite DEM)	4130.1	0 – 11.74
10-meter DEM (Bay Delta)	4180.4*	0 -6.14
10-meter DEM (NOAA, resampled)	4241.5	0 – 9.125

** The Bay Delta DEM was spotty and had to be interpolated to get a continuous raster. This allows the extents to be comparable but the range will differ due to missing data that had to be interpolated.*

In general, the lower resolution DEMs give higher estimates of flooding. As resolution increases from 10 meter to 1 meter and 2 meter respectively, the inundation areas of both the composite DEMs decrease by up to 0.50%. One reason is that in a lower resolution DEM, sinks are filled and averaged out, increasing the conveyance of water. Coarser DEMs might also average out high structures such as levees, embankments and other obstructions to the flow of water. Due to the averaging of local elevations, flow will face less resistance and increase the extent of flooding. A second reason for more flooding in coarser DEMs has to do with how the extents are calculated. When calculating the area flooded, "cells" that flooded even slightly will be counted, while the rest will not. In a 2-meter DEM, fewer cells within a given area will be counted since the cells are smaller. But in a 10 meter DEM, cells are larger and the entire cell will be counted even if it is slightly flooded. It is hard to make this a rule however, since the inundation area from the 2-meter composite DEM is slightly lower than the 1-meter DEM. This could be due to their different sources. The 2-meter composite DEM is a composite of the Bay Delta and NOAA DEM, resampled to 2 meters. Resolution might not be as important as the source of data.

Given that at the time this thesis was published, counting extents through this method was the only available option, but there is the hope that improvements in user interface will allow flooding extents to be calculated in a better, simpler method.

6.2 Effects of solution scheme on model results

The final test compared model results using a full momentum equation and a diffusion equation. For three different flows through the Toe Drain, the entire 69,000 acre Yolo Bypass model was run using diffusive wave and dynamic wave formulations and solutions. Table 11 presents the inundation extents with the two different solution schemes.

Table 11: Flooding from different Solution Schemes

Flow Scenario	Inundation (acres) - Diffusive	Inundation (acres) - Dynamic
2000 cfs	8,113.53	7,601.342 (-6.3%)
4000 cfs	17,253.44	15,652.13 (-9.3%)
6000 cfs	21,291.92	22,999.88 (8%)

The results show that using the full momentum model to solve the equation gives us lower inundation with 2,000 and 4,000 cfs but slightly higher inundation results with 6,000 cfs compared to using only diffusive wave. The difference is due to any inertial effects that are ignored in the diffusive wave model but are solved for in a full dynamic wave model. Appendix B presents the Water Surface Elevations and Channel Velocity of the Toe Drain for both solution schemes.

Given the scale of the Bypass, this difference is not extremely significant. A difference of even 1000 acres within the large Bypass is just 1.5%.

Our sensitivity analysis indicates that model results in HEC-RAS 5.0 are most sensitive to the kind of DEM being used. This DEM sensitivity extends not only to the DEM resolution, but its quality and accuracy as well. The results are also sensitive to solution scheme but to a much smaller extent.

7 Chapter 7: Model Applications

To achieve habitat and fisheries improvement goals, several modifications to the Bypass system have been proposed. However, these modifications need to be tested to see if they will achieve the intended goals. A calibrated public domain 2-D model like the one created as part of this thesis can help simulate various alternatives. Some example applications are:

1. Assessing the impacts of physical modifications to the Fremont Weir that have been suggested as part of the BDCP and the Yolo Bypass Management Study. This includes introducing a notch, lowering the weir elevation or developing a fish ladder to improve fish passage. A hydraulic model is useful to investigate various designs and operations of the weir (*BDCP, 2001; Jones and Stokes, 2001*).
2. Assessing physical and operational modifications to the Sacramento and Lisbon weirs to enhance fish habitat quality through alteration of the flooding extent, duration and timing in the Bypass.
3. Assessing the effects of diversion channels from west side tributaries into the Bypass. Examples are the re-alignment of the South fork of Putah Creek. It has been suggested that constructing a 5-mile long channel from Putah Creek to Toe Drain would allow adult salmon to enter the stream. Other modifications at Knights Landing Ridge Cut have also been suggested to reduce adult fish straying (*BDCP, 2012*).
4. Assessing effects of improving conveyance in the Toe Drain. Several agricultural crossings and obstructions exist in the Tule Canal and Toe Drain. Removing them might improve fish passage (*cbec, 2012*).
5. Controlling the timing and duration of flooding and obtaining an optimal flood footprint (*Suddeth 2014*).

Given the many applications of a hydraulic model, a smaller model for the Yolo Bypass was developed to explore multiple cases and compare them with a base case. The following section details development of the smaller model and presents two case study applications for restoration purposes.

7.1 Case Study 1: Controlled Flows and Flood footprint

7.1.1 Modelling objectives

As part of efforts to restore ecosystem function within the Yolo Bypass and the Delta, the draft BDCP had proposed in 2012 lowering part of the Fremont weir to increase the frequency of flooding in the Bypass. It also proposed an operable gate at the weir to control the duration of flooding, since ecosystem habitat function depends on not just on the magnitude of flooding, but its duration and timing (*BDCP, 2012*). Although the exact amount of flooding has not been established, annual flooding between 3,000 cfs and 6,000 cfs has been proposed with end dates from February 15th to May 15th (*BDCP, 2012*).

Public agencies and stakeholders involved with the Yolo Bypass, and the Delta are interested in knowing the effects of restoration projects on overall flood conveyance and capacity in the Bypass, and more specifically on various private lands. The results of a hydraulic model are particularly valuable as inputs to other models used in the effects analysis for such proposals, including environmental impact and agricultural impact assessments.

The agricultural production model developed by Howitt et al. (2013), for example, used flood inundation acreages from the 1-D HEC-RAS model to estimate economic impacts of incremental flooding due to notched flows through the Fremont Weir. Howitt et al. (2013) estimated losses to Yolo County's economy of $3.8 million and $8.9 million for 3,000 cfs and 6,000 cfs, respectively, based on assuming that 3,000 and 6,000 cfs would inundate 12,200 to 25,000 acres of the Bypass (including Liberty Island). This study therefore has a limitation in that it uses 1-D model results that cannot give a detailed flood footprint.

Given the need to assess how much incremental flooding will occur and what specific land uses might be affected by increasing flows through the Fremont Weir, the smaller Yolo Bypass floodplain model (described earlier) was run area for 2000 cfs, 4000 cfs and 6000 cfs coming through the Fremont Weir and low flow conditions in the west side boundaries. Since the Sacramento River was not modeled, a constant flow input was assigned to the upstream portion of the Toe Drain. These three flow cases were run for the duration of 15 days from 1st of February to the 15th of February, with a time step of 30 seconds.

7.1.2 Model Results and Discussion

For all three runs, the upper Bypass system reaches steady state by day 5 while the lower part of the Bypass takes 9 days to achieve complete steady state. By shutting off flows, drainage time of the entire system was 4 to 5 days for the upper Bypass. The Toe Drain begins to overflow as soon as the water surface elevation reaches around 15 to 20 feet in the upper Tule Canal section north of KLRC.

Table 12 shows the average velocities, flooding acreage, travel times and drainage times achieved for the three flow conditions. Detailed velocity and water surface elevations for each cross-section and flood inundation maps can be found in Appendix C.

Table 12: Summary of output

Q(cfs)	Mean Velocity (m/s)	Maximum inundation (Calculated from ArcGIS) (acres)	Average Travel Time (hrs)	Approximate drainage times (hrs)
2,000	0.332	8,114	110	78
4,000	0.463	17,253	44	81
6,000	0.5323	21,292	32	100

The profile of the Tule/Canal Toe Drain, as a representation of the Yolo Bypass with the water surface elevation for 2,000, 4,000 and 6,000 cfs is shown in Figure 19. These elevations are in meters and from downstream to upstream.

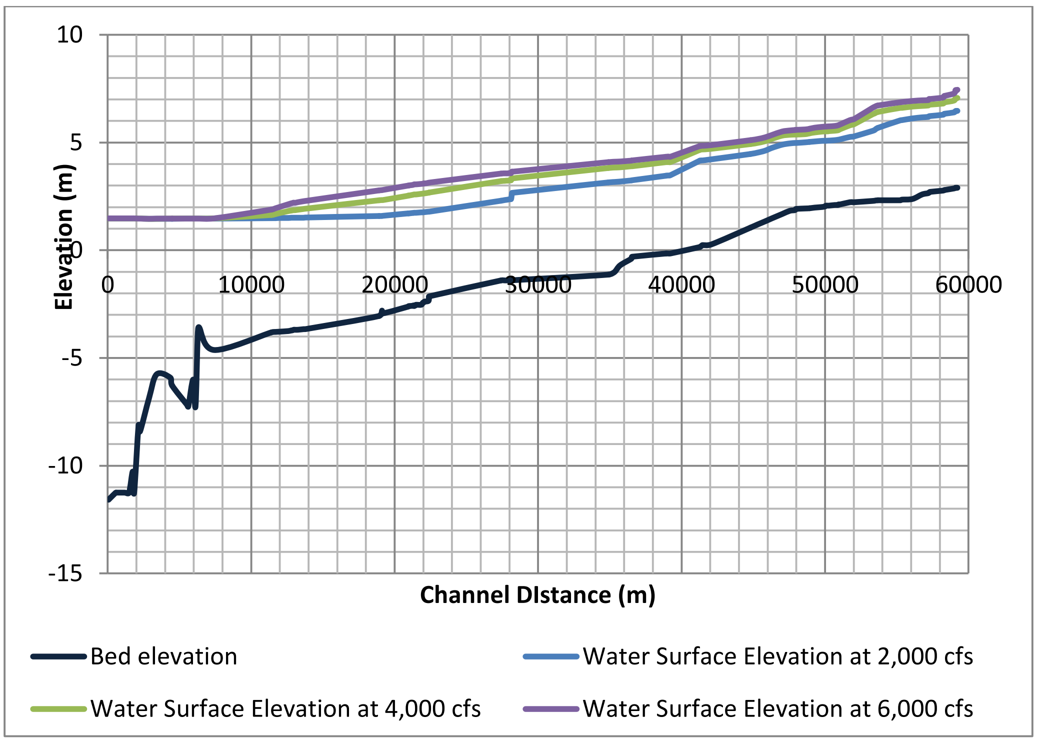

Figure 19: Profile Plot of the Toe Drain (Downstream to Upstream)

The water surface levels in the Toe Drain do not significantly differ for the three different flows in the southern part of the Bypass, but there are differences in the northern Bypass. However, depths for 2,000 cfs are relatively high because they do not spill over and are contained within the channel. Howitt et al. (2013) estimated losses to Yolo County's economy of \$3.8 million and \$8.9 million for 3,000 cfs and 6,000 cfs, respectively, but these were based on the assumption that 3,000 and 6,000 cfs would inundate between 12,200 and 25,000 acres of the Bypass (that include Liberty Island). Our 2-D model however, estimates that 2,000 cfs, 4,000 cfs and 6,000 cfs would inundate 8114, 17,253 and 21,292 acres respectively. These flooded acreages so not include Liberty Island. Using these results would therefore effect the results of the agricultural model, which is driven by inundation acreages (*Howitt et al., 2013*).

Zone-specific inundation extents and depths were calculated for the Bypass, based on the seven agro-ecological zones defined by Howitt et al. (2013). These seven different zones reflect location-specific agro-economic realities (Figure 20).

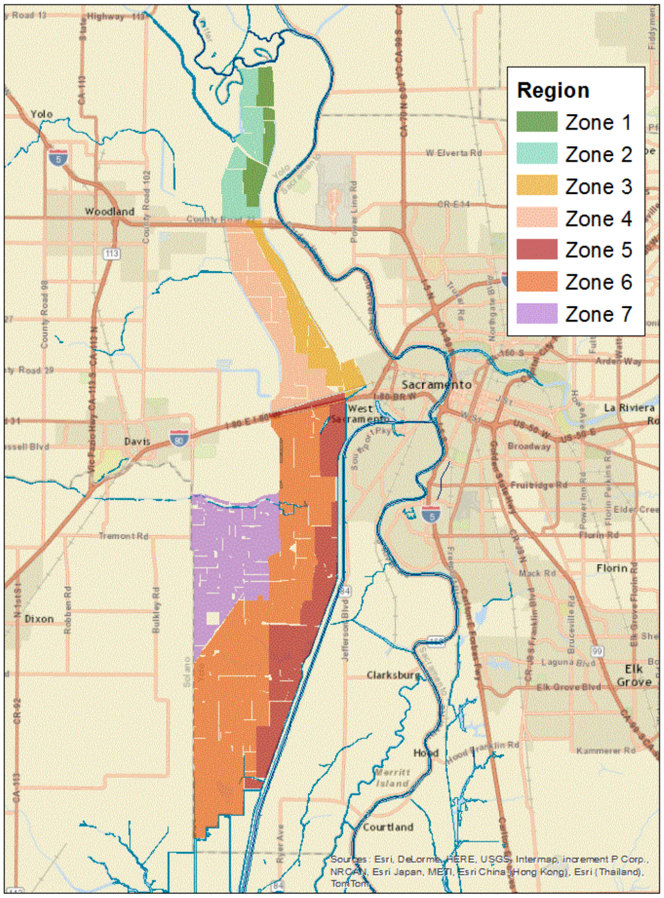

Figure 20: Modelling Extents and agricultural zones

Table 13 shows the extent of maximum inundation in the Bypass at day 15 within each of the zones. Note that these numbers do not include the inundation in Liberty Island, which remains submerged most of the year.

Table 13: Zone-specific inundation for 2,000 cfs, 4,000 cfs and 6,000 cfs

	Area inundation (acres) with 2000 cfs	Area inundation (acres) with 4000 cfs	Area inundation (acres) with 6000 cfs
Zone 1	1038	1600	1674
Zone 2	351	945	1490
Zone 3	2144	2501	2553
Zone 4	973	1709	2226
Zone 5	1848	6035	7066
Zone 6	1733	4436	6255
Zone 7	27	27	27
All zones	8114	17253	21292

The results show that the northern part of the Bypass is not as sensitive to increased flows as much as the southern part. Going from 2,000 cfs to 4,000 cfs, the inundation extents in Zone 1 and Zone 2 do not dramatically change. However for Zone 5 and 6, they change by a relatively larger amount.

Unlike a 1D model the results of a 2D model also give the extents of flooding for each depth class, allowing us to conduct more accurate economic assessments, as losses will also depend on the depth of flooding, not merely the extant. Depths for each zone are presented in Appendix C.

7.2 Case Study 2: Multi-objective Optimization Cases

Suddeth (2014) has developed a **m**ulti-objective **o**ptimization **m**odel for the **Y**olo **B**ypass (YBMOM) to assess impacts of varying inundation schemes on regional agriculture, wildlife, and recreation. Her study presents a multi-objective analysis for balancing ecosystem functions with human uses in the Yolo Bypass, an approach identified as "reconciliation ecology" (*Rosenzweig, 2003)*. The results of her model prescribe an optimal flood footprint, and a hydraulic model would help see if and how this footprint can be achieved.

7.2.1 Model Background

Suddeth's model looks at three main objectives: net profitability from agriculture, fish habitat quality, and bird habitat quality. These objectives are constrained by the condition that the Bypass maintains its flood control function, and by other external factors such as soil, climate, and other conservation requirements. How the objectives perform depends on the extents and depths of inundation within different land uses as well as the timing and duration of inundation. A more thorough description of the YBMOM is available in Suddeth, (2014).

The economic objective in Suddeth's model is determined primarily by agricultural costs and revenues using weights or parameters developed by an earlier study of an agronomic model for the Yolo Bypass (*Howitt et al., 2013*). The habitat quality objectives are divided into fish habitat and bird habitat. Fish habitat quality is described by habitat preferences for Chinook salmon and split-tail while bird habitat quality for dabbling ducks and shorebirds. The weights used to describe habitat preferences were obtained from surveys of experts (*Suddeth, 2014*). For the base case in this thesis, it is assumed that improvements in either fish or bird habitat quality contribute equally to overall habitat quality. Suddeth (2014) provides trade-off curves which show how one objective performs compared to others and looks at different management cases, for example how additional flooding or changing land uses could benefit the objectives (*Suddeth, 2014*). YBMOM prescribes with respect to the flood footprint for particular land uses, in zones defined by Howitt et al., (2013) and shown in Figure 20.

7.2.2 Objectives: Matching the optimization footprint

Here, we use Suddeth's model to prescribe an optimal flooding footprint after running the base runs for 2,000, 4,000 and 6,000 cfs of water coming down the toe-drain. An initial HEC-RAS model was run to obtain the maximum acres of flooded land. This was used as a constraint to run the optimization model, for a duration of 1- and 8-weeks. The overall objective was to maximize achievable profits in which all objectives were maximized within the constraints. The optimization footprints for 2000, 4000 and 6000 cfs for two different flooding cases are compared to the simulated hydraulic footprint, the results of which are displayed in Table 14-15 and are discussed below. Actual inundations in acres prescribed by the optimization model are shown in the Appendix D.

Table 14: Flooded Acreage as a Percent of Total Acreage for that Agricultural Zone (or Region) – Week 1

ZONE	6000 cfs (Model constrains flooding to 21263 acres)			4000 cfs, 17226 acres			2000 cfs, 8087 acres		
	HEC-RAS Footprint	**Optimization Scenario 1***	**Optimization Scenario 2****	**HEC-RAS footprint**	**Optimization Scenario 1***	**Optimization Scenario 2****	**HEC-RAS footprint**	**Optimization Scenario 1***	**Optimization Scenario 2****
Zone 1	84%	35%	34%	81%	32%	28%	52%	0%	0%
Zone 2	46%	0%	0%	29%	0%	0%	11%	0%	0%
Zone 3	68%	78%	33%	67%	52%	34%	57%	22%	22%
Zone 4	37%	11%	11%	29%	11%	11%	16%	11%	0%
Zone 5	83%	100%	71%	71%	82%	57%	22%	39%	31%
Zone 6	28%	38%	56%	20%	31%	44%	8%	15%	20%

Table 15: Flooded Acreage as a Percent of Total Acreage for that Agricultural Zone (or Region) – Week 8

ZONE	6000 cfs, 21263 acres			4000 cfs, 17226 acres			2000 cfs, 8087 acres		
	HEC-RAS Footprint	**Optimization Scenario 1***	**Optimization Scenario 2****	**HEC-RAS footprint**	**Optimization Scenario 1***	**Optimization Scenario 2****	**HEC-RAS Footprint**	**Optimization Scenario 1***	**Optimization Scenario 2****
Zone 1	84%	32%	32%	81%	32%	28%	52%	0%	0%
Zone 2	46%	0%	0%	29%	0%	0%	11%	0%	0%
Zone 3	68%	29%	29%	57%	52%	34%	57%	22%	22%
Zone 4	37%	11%	11%	29%	11%	11%	16%	11%	0%
Zone 5	83%	84%	71%	71%	82%	57%	22%	39%	31%
Zone 6	28%	36%	49%	20%	31%	44%	8%	15%	20%

Scenario 1: *There is no flooding in zone 2, very limited flooding in zone 4, and zone 6 flooding is less than or equal to acres flooded in zone 5.*
****Scenario 2:*** *No flooding in zone 2 and very limited flooding in zone 4, but zone 6 can be flooded without restriction*

The results of YBMOM indicate that flooding should be concentrated in the southern Bypass (Zones 5 and 6), with less flooding in the northern Bypass. Given that optimization calls for a much higher proportion of flooding in the south than in the north, constructing a berm along the Tule Canal/Toe Drain to reduce flooding in the north, and installing an inflatable dam in the lower Bypass would allow us to get results that match YBMOM.

7.2.2.1 *Matching the footprint*

To obtain a hydraulic footprint that would match the results from the optimization model, several alternatives were developed using inflatable dams and different widths and length berms on the northern Bypass. Since most flooding is low-flow flooding, several options were simulated to see if they can match the footprint. All options are simulated for 2,000 cfs, without constraints on where flooding should take place, and then compared to the optimization model. These options are described in Table 16 and there scope shown in Figure 21:

Table 16: Summary of options tested

Options	Description
Option 1	Berm 5 feet high, 10 mile long berm, along the northern part of the Yolo Bypass.
Option 2	Berm 5 feet high, 25 mile long, all along Zone 1, 3 and part of zone 6 of the Yolo Bypass.
Option 3	Same as option 2 but with a dam at the bottom. See Figure 21 for the location of the dam
Option 4	Same as option 3 but with a dam more upstream. See Figure 21.

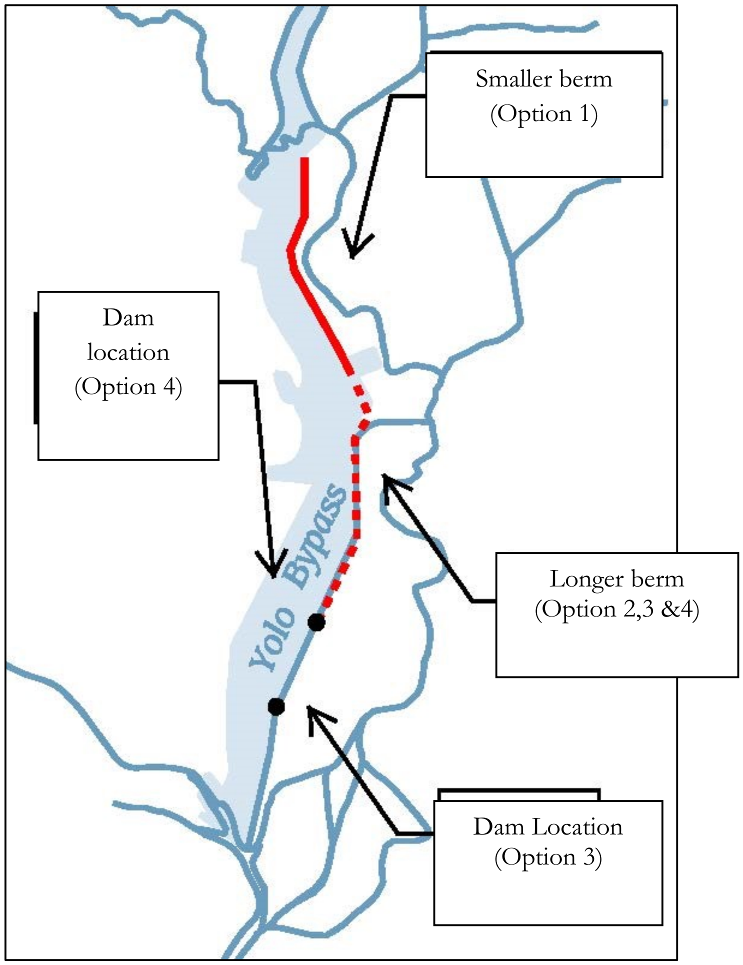

Figure 21: Dam and Berm locations

7.2.2.2 Results and discussion

The results of flooding from these simulations are summarized in the Table 17 (Figures of the results can be found in Appendix D). Given that Zone 1 and Zone 3 are significantly smaller than Zone 5, actual number of acres is reported in each subsection.

Table 17: Compiled Results of Options, compared to Optimization and Base Case

	Zone 1	Zone 2	Zone 3	Zone 4	Zone 5	Zone 6	Zone 7
Optimization	0%	0%	22%	6%	35%	17%	0%
HEC-RAS Base	52%	11%	57%	16%	22%	8%	0.08%
Option 1	37.69%	6.59%	50.59%	14.52%	15.85%	5.98%	0.27%
Option 2	35.75%	5.75%	18.14%	2.69%	10.38%	2.20%	0.27%
Option 3	16.58%	6.63%	4.34%	8.22%	34.32%	18.00%	0.27%
Option 4	2%	7.69%	4.88%	13.43%	38.00%	31.82%	0.27%

Option 1:

This option makes one modification to the base geometry, by adding a berm 10 miles long and 5 feet high along the right bank of the Toe Drain. The model is run for the same amount of time, i.e. 15 days. From day 1 – 8, the berm keeps the water inside the Toe Drain, but on day 9, the flood water reaches the lower end of the berm, flowing around it and backing north into the 2-D area. In reality, water may not behave this way, but simulation using the HEC-RAS 5.0 model ends up moving water upwards in the Bypass. Exact inundation is reported in Table 18.

Table 18: Flooding from Option 1: Shorter Berm

	Option case (acres)	Base case (acres)	Option case (%)	Base case %	Optimization case – Average (%)
Zone 1	**747**	1,037	37.69%	52%	0%
Zone 2	**213**	351	6.59%	11%	0%
Zone 3	**1902**	2,144	50.59%	57%	22%
Zone 4	**869**	973	14.52%	16%	6%
Zone 5	**1345**	1,848	15.85%	22%	35%
Zone 6	**1349**	1,733	5.98%	8%	17%
Zone 7	**24**	27	0.27%	0.08%	N/A

The construction of a berm helps to reduce flooding in Zone 1, but doesn't help in reducing flooding in Zone 3 and Zone 4. Since optimization calls for reduced flooding in Zone 3 & 4 (22% and 6%), a longer berm was needed.

Option 2:

Option 2 is a longer berm (25 miles) and performs better in reducing flooding in Zone 3 and 4, relative to Option 1. There is little flooding outside of the berm until day 11 when water overtops the 5 foot berm. However, the southern part of the Bypass still is not achieving the flooding extents recommended by YBMOM, so installing bladder dams or gates in the lower Bypass was considered. Results are shown in Table 19.

Table 19: Flooding from Option 2: Longer Berm

	Option case (acres)	Base case (acres)	Option case (%)	Base case %	Optimization case – Average (%)
Zone 1	709	1,037	35.75%	52%	0%
Zone 2	186	351	5.75%	11%	0%
Zone 3	682	2,144	18.14%	57%	22%
Zone 4	161	973	2.69%	16%	6%
Zone 5	881	1,848	10.38%	22%	35%
Zone 6	496	1,733	2.20%	8%	17%
Zone 7	24	27	0.27%	0.08%	N/A

Two dam locations were considered and tested (See Option 3 and Option 4) to see what the effect would be of each dam on the flood footprint. The operation of each dam is the same - both close when water surface elevation upstream reaches 8 feet.

Option 3

Option 3 is the same as Option 2, except that there is a dam located on the Toe Drain, close to Prospect Slough (See Figure 21). Option 3 (Table 20) gives us generally good results for Zone 2 and 3, much like Option 2, but still does not cause the flooding we need in Zone 5, 6 and 7 as we had hoped. These zones are also much larger, in terms of acreage, so to increase the percentage of flooding within that area, more acres need to be flooded. As a result, another simulation was carried out to locate the dam further north along the Toe Drain, midway between Lisbon Weir and where the dam in this option (Option 3) was located.

Table 20: Flooding from Option 3: Berm and gate

	Option case (acres)	Base case (acres)	Option case (%)	Base case %	Optimization case – Average (%)
Zone 1	329	1,037	16.58%	52%	0%
Zone 2	215	351	6.63%	11%	0%
Zone 3	163	2,144	4.34%	57%	22%
Zone 4	492	973	8.22%	16%	6%
Zone 5	2912	1,848	34.32%	22%	35%
Zone 6	4064	1,733	18.00%	8%	17%
Zone 7	24	27	0.27%	0.08%	N/A

Option 4

Option 4 operates the same as Option 3, except that the location of the dam is further upstream on the Toe Drain (See Figure 21). The final results of Option 4 are quite close to Optimization results, and allow significant flooding in Zones 5 and 6. To get more water in the western part of the Bypass from the Eastern pass would require diversion channels from the Toe Drain to the Western Bypass, once enough water is available in the Toe Drain at the particular point.

Table 21: Flooding from Option 4: Berm and gate more north

	Option case (acres)	Base case (acres)	Option case (%)	Base case %	Optimization case – Average (%)
Zone 1	35	1,037	1.77%	52%	0%
Zone 2	249	351	7.69%	11%	0%
Zone 3	184	2,144	4.88%	57%	22%
Zone 4	804	973	13.43%	16%	6%
Zone 5	3225	1,848	38.00%	22%	35%
Zone 6	7184	1,733	31.82%	8%	17%
Zone 7	24	27	0.27%	0.08%	N/A

While Options 1 and 2 do not seem to show any significant effects in the extents of flooding, they affect the depths considerably. This is important in restoration projects where fish habitat preferences depend not only on the magnitude of flooding and the extents, but the depths and velocities as well. The depths and extents achieved with each option compared to the base case can be found in Appendix D.

The results above show that including hydraulic structures within the Bypass can give us insights as to how to best convey water. It also allows us to determine the best location for bladder dams, if we want flooding in a particular region.

8 Chapter 8: Conclusions

Structural or operational modifications to the Bypass for enhancing habitat quality can affect the flooding extents and depths, thereby affecting existing land uses in the Bypass. In order to examine what these effects are and reconcile ecological objectives with economic ones, a hydraulic model is needed to serve as an effective decision support tool. This thesis documents the development of such a 2D hydraulic model for the Yolo and Sutter Bypass system for the purpose of assessing flooding extents and depths for environmental restoration projects.

The software used for this assessment is a public domain software, HEC-RAS 5.0, produced by the US Army Corps of Engineers. The resulting model has been calibrated with stage and flow data available on key sites and tested for case studies. It is used to test the effects of bladder dams and gates on the floodplain and finds them to be effective in increasing flooding in the lower Bypass and allowing much of the depths and extents needed for habitat quality to be achieved.

A sensitivity analysis is conducted to determine whether additional complexity makes the model any more accurate and where additional improvements can be made. The results of the sensitivity analysis suggest that flooding extents were sensitive to the DEM used, and therefore improvements in DEM processing and verification can make results more accurate and give detailed flooding footprints with less errors.

The application of HEC-RAS 5.0 to the Yolo Bypass is an illustration of the ways by which we can use computational tools and GIS to not only assess environmental restoration projects but also design or develop the most optimum operations for a restoration project. .

References

Andreadis, K. M., Clark, E. A., Lettenmaier, D. P. and Alsdorf, D. E. (2007). Prospects for river discharge and depth estimation through assimilation of swath-altimetry into a raster-based hydrodynamics model. *Geophysical Research Letters* 34. doi:10.1029/2007GL029721.

Allan James, L., & Singer, M. B. (2008). Development of the lower Sacramento Valley flood-control system: Historical perspective. *Natural Hazards Review*, *9*(3), 125-135.

ASCE, Ettema, R. (Ed.). (2000). *Hydraulic modelling: Concepts and practice* (No. 97). ASCE Publications.

Bates PD, Anderson MG. (1993). A two dimensional finite element model for river flood inundation. *Proceedings of the Royal Society of London*; 440(A):481–491.

Bates, P. D., Anderson, M. G., and Hervouet, J.-M. (1995).An initial comparison of two 2-dimensional finite element codes for river flood simulation. *Proceedings of the ICE-Water Maritime and Ene*rgy, 112(3), 238-248.

Bates, P. D., Horritt, M. S., Smith, C. N. and Mason, D. C. (1997). Integrating remote sensing observations of flood hydrology and hydraulic modelling. *Hydrological Processes* 11, 1777–1795.

Bates, P.D. (2000), Development and testing of a subgrid-scale model for moving-boundary hydrodynamic problems in shallow water. *Hydrological Processes*, 14 (11-12), 2073-2088.

Bates, P.D., Marks, K.J. and Horritt, M.S. (2003). Optimal use of high-resolution topographic data in flood inundation models. *Hydrological Processes*, 17, pp. 537-557.

Bates, P.D., Wilson, M.D., Horritt, M.S., Mason, D., Holden, N., and Currie, A. (2006). Reach scale floodplain inundation dynamics observed using airborne Synthetic Aperture Radar imagery: data analysis and modelling. *Journal of Hydrology*, 328, 306-318.

Bay-Delta Conservation Plan (BDCP). (2012). February 2012 Draft Report. Available at : http://www.baydeltaconservationplan.com. Last Accessed August 5, 2014.

Bay-Delta Conservation Plan (BDCP). (2010). "Bay Delta Conservation Plan." Progress Report.

Bay-Delta Conservation Plan (2008). Evaluation of North Delta Migration Corridors: Yolo Bypass.

California Division of Water Resources. (1951). *Report to the State Reclamation Board on Authorization, Construction, Maintenance and Operation of Sacramento River Flood Control Project*. Sacramento, CA.

California Department of Water Resources, (2011). *Central Valley Flood Protection Plan Progress Report*.. Sacramento, CA.

California Department of Water Resources. (2003). *Bulletin 69-95: High Water in California*. Sacramento, CA.

California Department of Water Resources, (2007). *2007 California Flood Legislation – Summary*. Sacramento, CA.

California Department of Water Resources, (2009). *Yolo Bypass - Aquatic Ecology Section Research*. Sacramento, CA.

California Department of Water Resources, (2011). *Central Valley Flood Protection Plan Progress Report*. Sacramento, CA. Central Valley Flood Protection Plan [http://www.cvfpb.ca.gov/CVFPP/ (accessed 6.5.12).

Casas, A., Lane, S. N., Yu, D., & Benito, G. (2010). A method for parameterising roughness and topographic sub-grid scale effects in hydraulic modelling from LiDAR data. *Hydrology and Earth System Sciences*, 14 (8), pp.1567-1579.

Casulli, V. (1990). Numerical simulation of shallow water flow. *Computational methods in surface hydrology* 3 : 13-22.

Chang, Hsing-Chung, et al. (2004a).Validation of DEMs derived from radar interferometry, airborne laser scanning and photogrammetry by using GPS-RTK. *Geoscience and Remote Sensing Symposium, 2004. IGARSS'04. Proceedings. 2004 IEEE International*. Vol. 5. IEEE.

Chang, Hsing-Chung, L. L. Ge, and Chris Rizos. (2004b). Assessment of digital elevation models using RTK GPS. *Journal of Geospatial Engineering* 6.1: 13.

cbec . eco engineering. (2010). *BDCP Effects Analysis: 2D Hydrodynamic Modelling of the Fremont Weir Diversion Structure*. Report prepared for SAIC and the California Department of Water Resources (DWR). Project

cbec . eco engineering.(2012). *Yolo Bypass Drainage And Water Infrastructure Improvement Study*

Chow, V. T. (1959), *Open channel hydraulics*, McGraw-Hill, New York.

Domeneghetti, A., Tarpanelli, A., Brocca, L., Barbetta, S., Moramarco, T., Castellarin, A., & Brath, A. (2014). The use of remote sensing-derived water surface data for hydraulic model calibration. *Remote Sensing of Environment*, 149, 130-141.

Fabris, Massimo, and Arianna Pesci. (2005). Automated DEM extraction in digital aerial photogrammetry: precisions and validation for mass movement monitoring. *Annals of Geophysics*.

Feyrer, F., Sommer, T., & Harrell, W. (2006). Managing floodplain inundation for native fish: production dynamics of age-0 splittail (Pogonichthys macrolepidotus) in California's Yolo Bypass. *Hydrobiologia*, *573*(1), 213-226.

Hydrologic Engineering Center. (2014). *HEC-RAS River Analysis System 5.0: Combined 1D and 2D Modelling with HEC-RAS*. US Army Corps of Engineers, Davis, CA.

Hydrologic Engineering Center. (2001). *HEC-RAS River Analysis System: User's Manual.* (2001). US Army Corps of Engineers, Davis, CA.

Hydrologic Engineering Center. (1995). *HEC-RAS River Analysis System, Version 1.0: User's Manual.*. US Army Corps of Engineers, Davis, CA.

Horritt, M.S., Bates, P.D. (2001). Predicting floodplain inundation: raster-based modelling versus the finite element approach. *Hydrological Processes* 15, 825–842.

Horritt, M. S., and P. D. Bates. (2002) Evaluation of 1D and 2D numerical models for predicting river flood inundation. *Journal of Hydrology* 268.1: 87-99.

Horritt, M. S., P. D. Bates, and M. J. Mattinson. (2006) Effects of mesh resolution and topographic representation in 2D finite volume models of shallow water fluvial flow. *Journal of Hydrology* 329.1: 306-314.

Howitt, R, MacEwan D, Garnache C, Medellín-Azuara J, Marchand P, Brown D, Six Johan, and Lee Juhwan, (2013). *Agricultural and Economic Impacts of Yolo Bypass Fish Habitat Proposals*, UC Davis, CA.

Horritt, M.S. (2006). A methodology for the validation of uncertain flood inundation models. *Journal of Hydrology* 326, 153–165.

Horritt, M.S. and Bates, P.D. (2001a), Effects of spatial resolution on a raster based model of flood flow. *Journal of Hydrology*, 268, 87-99.

Horritt, M. S., Mason, D. C. and Luckman, A. J. (2001b). Flood boundary delineation from synthetic aperture radar imagery using a statistical active contour model. *International Journal of Remote Sensing* 22 (13), 2489–2507.

Horritt, M.S., Bates, P.D. and Mattinson, M.J., (2006a). Effects of mesh resolution and topographic representation in 2-D finite volume models of shallow water fluvial flow. *Journal of Hydrology*, 329, 306-314

Horritt, M. S. (2006b). A methodology for the validation of uncertain flood inundation models. *Journal of Hydrology*, 326(1), 153-165.

Hunter N.M., Bates P.D., Neelz S., Pender G., Villanueva I., Wright N.G., Liang D., Falconer R.A., Lin B., Waller S., Crossley A.J. and Mason D.C. (2008), Benchmarking 2D hydraulic models for urban flood simulations. *Water Management,* 161 (1), 13-30.

Jenson, Susan K. (1991). Applications of hydrologic information automatically extracted from digital elevation models. *Hydrological Processes* 5.1: 31-44.

Kelley, R. (1998). *Battling the inland sea: floods, public policy, and the Sacramento Valley*. Univ of California Press.

Lane, S.N., Bradbrook, K.F., Richards, K.S., Biron, P.M. and Roy, A.G. (1999). The application of computational fluid dynamics to natural river channels: three-dimensional versus two-dimensional approaches. *Geomorphology*, 29, 1-20.

Liggett, James A., and Jean A. Cunge. (1975). Numerical methods of solution of the unsteady flow equations. *Unsteady flow in open channels* 1: 159-179.

Lighthill, M. and G. Whitham. (1955) On kinematic waves. II: A theory of traffic flow on long crowded roads *Proceedings of the Royal Society of London. Series A: Mathematical and Physical Sciences* (1934–1990), 229 (1178) (1955), pp. 317–345

Marks, K.J. and Bates, P.D. (2000), Integration of high resolution topographic data with floodplain flow models. *Hydrological Processes*, vol. 14, pp. 2109-2122.

Mason, D. C., Bates, P. D., & Dall'Amico, J. T. (2009). Calibration of uncertain flood inundation models using remotely sensed water levels. *Journal of Hydrology*, *368*(1), 224-236.

Mason D.C., Cobby D.M., Horritt M.S. and Bates P.D. (2003), Floodplain friction parameterization in two-dimensional river flood models using vegetation heights derived from airborne scanning laser altimetry. *Hydrological Processes* **17**, 1711-1732.

Mason D.C., Horritt M.S., Hunter N.M. and Bates P.D. (2007a), Use of fused airborne scanning laser altimetry and digital map data for urban flood modelling. *Hydrological Processes*, **21**, 1436-1447.

Mason, D. C., Horritt, M. S., Dall'Amico, J. T., Scott, T. R. and Bates, P. D. (2007b). Improving river flood extent delineation from Synthetic Aperture Radar using airborne laser altimetry. *IEEE Transactions on Geoscience and Remote Sensing* 45, 3932–3943.

Mason, D. C., Speck, R., Devereux B., Schumann, G., Neal, J. and Bates, P.D. (2010). Flood detection in urban areas using TerraSAR-X. *IEEE Transactions on Geoscience and Remote Sensing* 48(2).

Merwade V. M., Maidment D. R., and Hodges B. R., (2005) Geospatial Representation of River Channels. ASCE *Journal of Hydrologic Engineering*, Vol. 10 (3), pp. 243-251.

Merwade V. M., Maidment D. R., and Goff J. A., (2006) Anisotropic considerations while interpolating river channel bathymetry. *Journal of Hydrology*, Vol.331(3-4), pp. 731-741.

Merwade V. M., (2007). An automated GIS approach for delineating river and lake boundaries, *Transactions in GIS*, 11(2), pp. 213–231.

Merwade, V., (2009). Effect of spatial trends on interpolation of river bathymetry. *Journal of Hydrology*, Vol. 371 (1-4), pp. 169–181.

Merwade V., Cook A., and Coonrod J., (2008a) GIS techniques for creating river terrain models for hydrodynamic modelling and flood inundation mapping. *Environmental Modelling & Software*, Vol. 23/10-11, pp. 1300-1311 (2008a).

Merwade V. M., Olivera F., Arabi M., and Edleman S., (2008b). Uncertainty in Flood Inundation Mapping - Current Issues and Future Directions. *ASCE Journal of Hydrologic Engineering*, Vol. 13(7), pp. 608-620.

National Hydraulic Consultants. (2012) *MIKE 21 2D Yolo Bypass Model Strengths and Limitations*.

Natural Heritage Institute et.al. (2002). *Habitat Improvement for Native Fish in the Yolo Bypass*. Accessed December 2011. <http://www.n-h-i.org/uploads/tx_rtgfiles/5605_FinalYoloReport.pdf>.

Miller, Andrew J., and Brian L. Cluer. (1998). Modelling considerations for simulation of flow in bedrock channels. Rivers over rock: fluvial processes in bedrock channels: 61-104.

Niedermeier, A., Romaneessen, E., Lehner, S., (2000). Detection of coastlines in SAR images using wavelet methods. *IEEE Transactions on Geoscience and Remote Sensing* 38 (5), 2270–2281.

Pappenberger, F., Beven, K., Horritt, M.S., Blazkova, S. (2005). Uncertainty in the calibration of effective roughness parameters in HEC-RAS using inundation and downstream level observations. *Journal of Hydrology* 302, 46–69.

Pappenberger, F., Matgen, P., Beven, K., Henry, J., Pfister, L., Fraipont de, P. (2006). Influence of uncertain boundary conditions and model structure on flood inundation predictions. *Advances in Water Resources* 29 (10), 1430–1449.

Pappenberger, F., Beven, K., Frodsham, K., Romanowicz, R., Matgen, P. (2007). Grasping the unavoidable subjectivity in calibration of flood inundation models: a vulnerability weighted approach. *Journal of Hydrology* 333 (2–4),275–287.

Pappenberger, F., Matgen, P., Beven, K., Henry, J. B., Pfister, L. and De Fraipont, P. (2006). Influence of uncertain boundary conditions and model structure on flood inundation predictions. *Advances in Water Resources* 29, 1430–1449.

Pappenberger, F., Frodsham, K., Beven, K., Romanowicz, R. and Matgen, P. (2007). Fuzzy set approach to calibrating distributed flood inundation models using remote sensing observations. *Hydrology and Earth System Sciences* 11, 739–752.

Pelletier, Patrice M. (1988). Uncertainties in the single determination of river discharge: a literature review. *Canadian Journal of Civil Engineering* 15.5 : 834-850.

Ramamoorthi, A. S. (1990). Flood damage forecasting by satellite remote sensing', Proceedings, International Symposium on Remote Sensing in Water Resources. *International Association of Hydrogeologists Publicatio*n, The Netherlands. pp. 433±442.

Rosenzweig, M. L. (2003). *Win-win ecology: how the earth's species can survive in the midst of human enterprise*. Oxford University Press.

Russo, M., (2010). *Sacramento River Flood Control Project Weirs and Flood Relief Structures - Fact Sheet.* CA Department of Water Resources - Northern District, Sacramento, CA.

Singer, M. B., Aalto, R., & James, L. A. (2008). Status of the lower Sacramento Valley flood-control system within the context of its natural geomorphic setting. *Natural Hazards Review*, *9*(3), 104-115.

Schumann, G., Matgen, P., Pappenberger, F., Hostache, R., Puech, C., Hoffmann, L. and Pfister, L. (2007a). High-resolution 3D flood information from radar for effective flood hazard management. *IEEE Transactions on Geoscience and Remote Sensing* 45, 1715–1725.

Schumann, G., Matgen, P., Pappenberger, F., Hostache, R. and Pfister, L. (2007b). Deriving distributed roughness values from satellite radar data for flood inundation modelling. *Journal of Hydrology* 344, 96–111.

Schumann, G., Matgen, P. and Pappenberger, F. (2008a). Conditioning water stages from satellite imagery on uncertain data points. *IEEE Geoscience and Remote Sensing Letters* 5, 810 – 813.

Schumann, G., Matgen, P., Pappenberger, F., Black, A., Cutler, M., Hoffmann, L. and Pfister, L. (2008b). Evaluating uncertain flood inundation predictions with uncertain remotely sensed water stages. *International Journal of River Basin Management* 6 (3), 187-199.

Singh, V. P. (2001). Kinematic wave modelling in water resources: a historical perspective. *Hydrological processes*, 15(4), 671-706.

Smith, B. and Sandwell, D. (2003), Accuracy and Resolution of Shuttle Radar Topography Mission Data, *Geophysical Research Letters*, vol. 30, no. 9.

Smith, L. C. (1997). Satellite remote sensing of river inundation area, stage, and discharge: a review. *Hydrological Processes* 11, 1427–1439.

Smith, M.J., Edwards, E.P., Priestnall, G. and Bates, P.D. (2006), Exploitation of new data types to create Digital Surface Models for flood inundation modelling. *FRMRC Research* report UR3, June 2006. 78pp.

Sommer, T., Harrell, B., Nobriga, M., Brown, R., Moyle, P., Kimmerer, W., & Schemel, L. (2001). California's Yolo Bypass: Evidence that flood control can be compatible with fisheries, wetlands, wildlife, and agriculture. *Fisheries*, *26*(8), 6-16.

Salcido, R. E. (2012). Success and Continued Challenges of the Yolo Bypass Wildlife Area: A Grassroots Restoration, The. *Ecology LQ*, *39*, 1085.

Schemel, L. E., Sommer, T. R., Müller-Solger, A. B., & Harrell, W. C. (2004). Hydrologic variability, water chemistry, and phytoplankton biomass in a large floodplain of the Sacramento River, USA. *Hydrobiologia*, *513*(1-3), 129-139.

Sibson, R. (1981) A Brief Description of Natural Neighbor Interpolation, Chapter 2 in Interpolating Multivariate Data. New York: John Wiley & Sons. 21–36.

Stoker, J. J. (1957) "Water Waves: The Mathematical Theory with Applications."

Tate, E. C., Maidment, D. R., Olivera, F., & Anderson, D. J. (2002). Creating a terrain model for floodplain mapping. *Journal of Hydrologic Engineering*, *7*(2), 100-108.

Tockner, K. and J.A. Stanford, 2002. Riverine Floodplains: Present State and Future Trends. *Environmental Conservation* **29**:308-330.

US Army Corps of Engineers Sacramento District 2007. (2007). *Yolo Bypass 2-D Hydraulic Model Development and Calibration.*

Yolo Basin Foundation, and Jones & Stokes (2001)." *A Framework for the Future: Yolo Bypass Management Strategy Final Report*.

Appendices

A. Appendix A

Boundary conditions using data from cbec eco-engineering is shown in the following charts and figures.

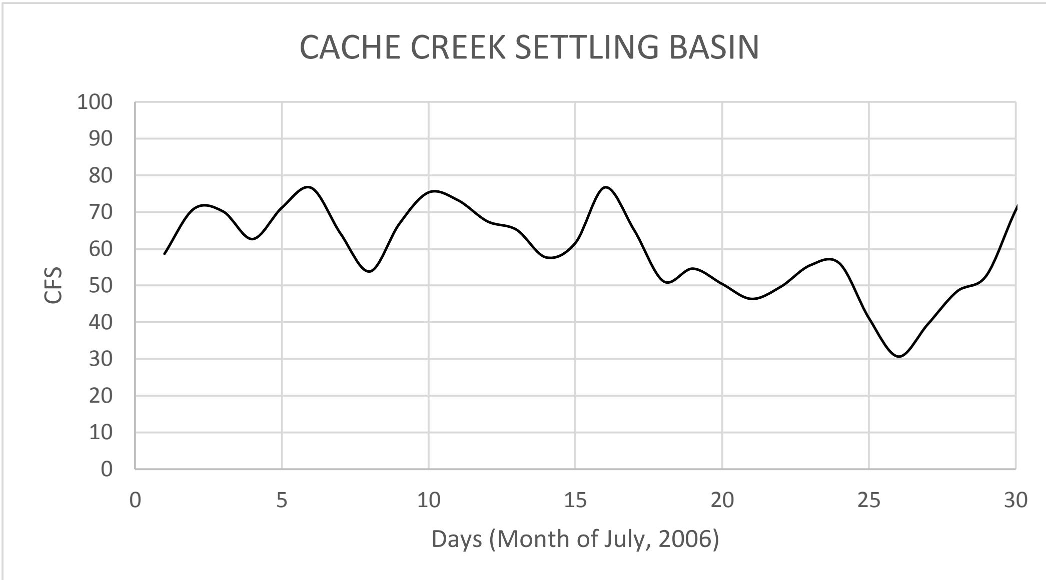

Figure A-1: Cache Creek Settling Basin

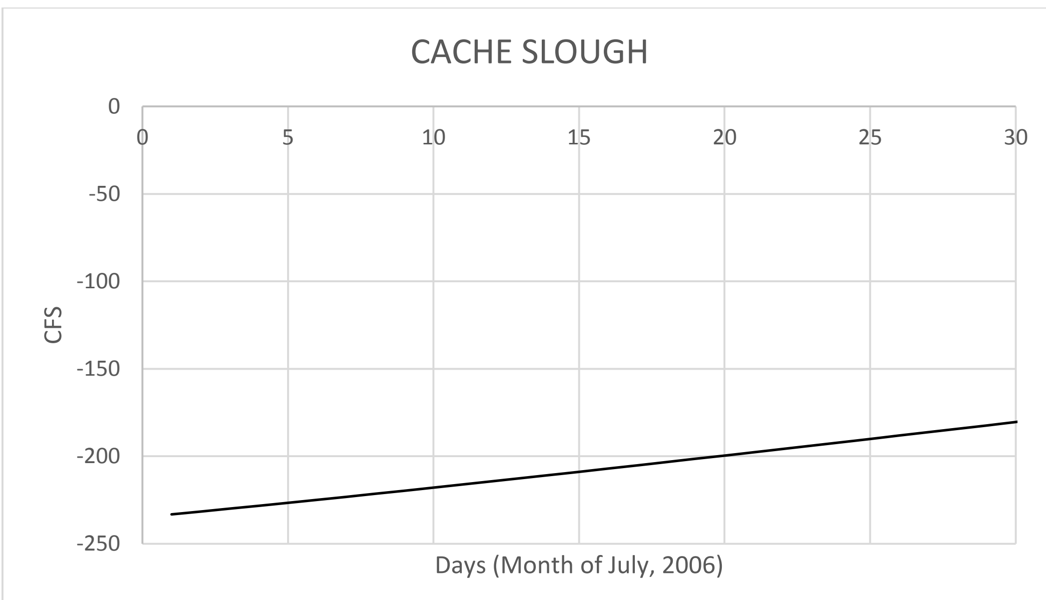

Figure A-2: Cache Slough

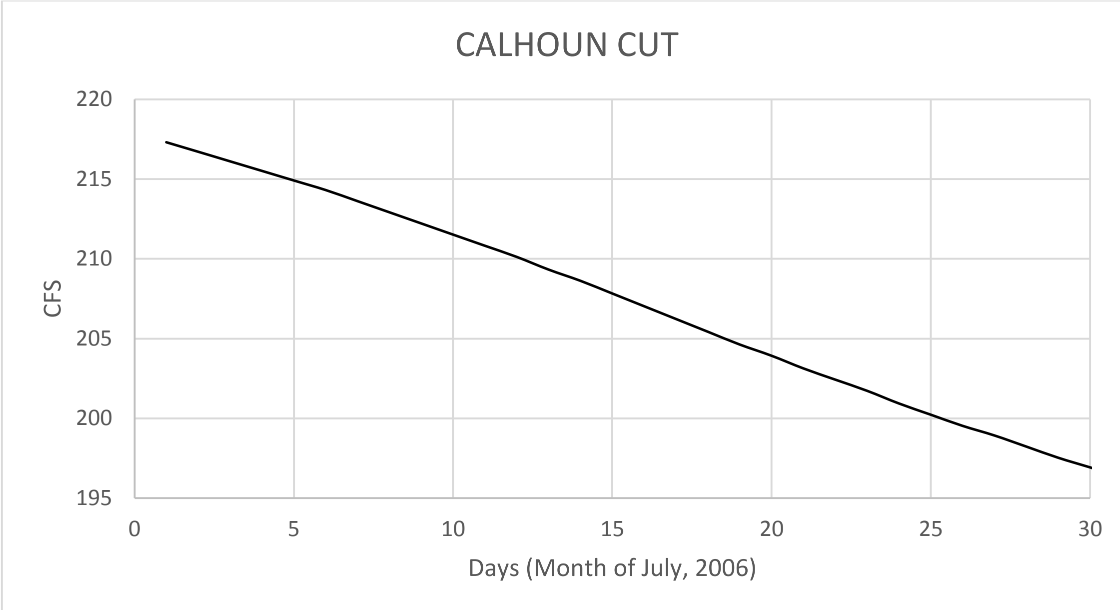

Figure A-3: Calhoun Cut

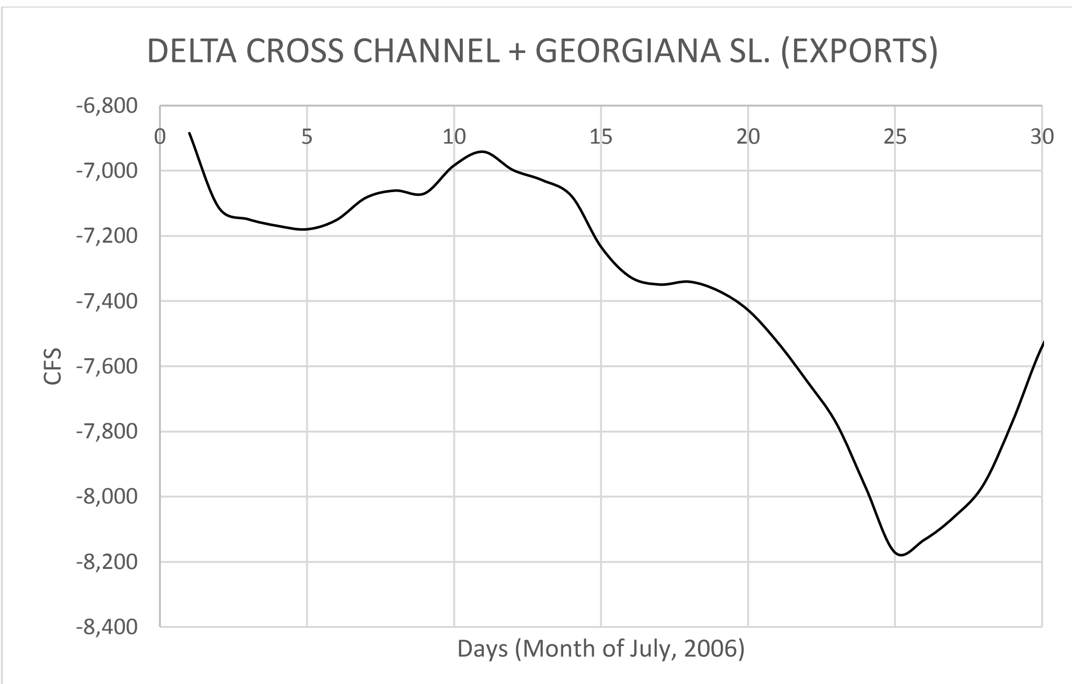

Figure A-4: Delta Cross and Georgiana Slough

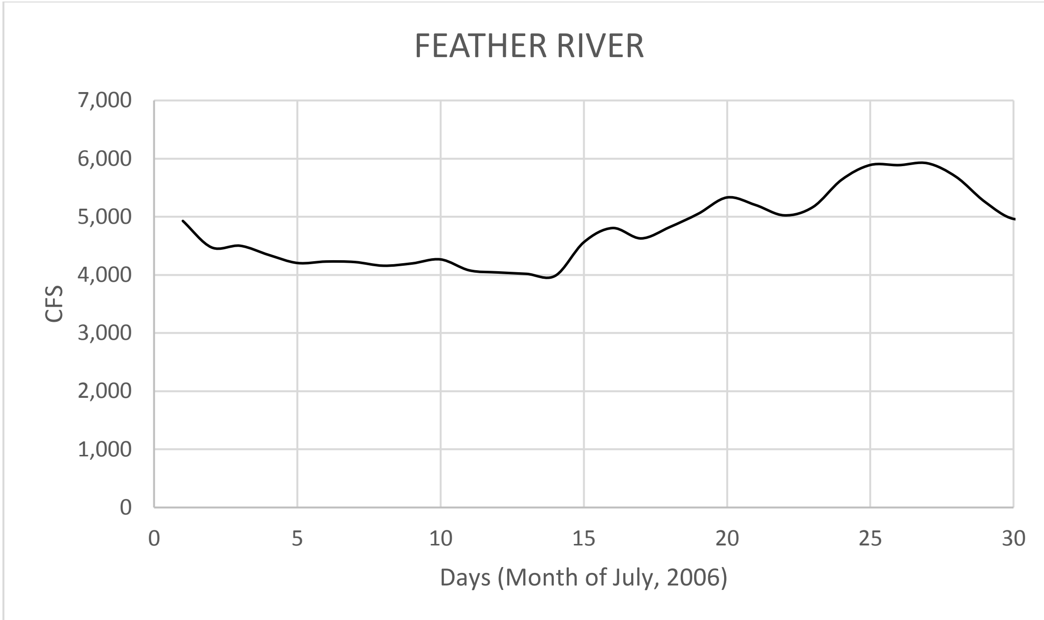

Figure A-5: Feather River

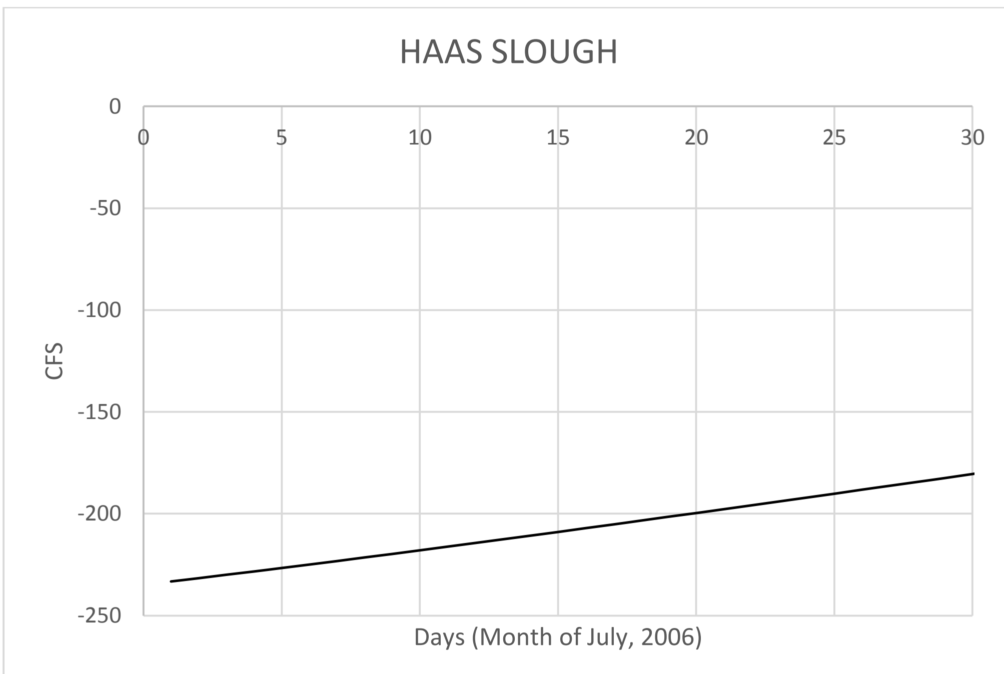

Figure A-6: Haas Slough

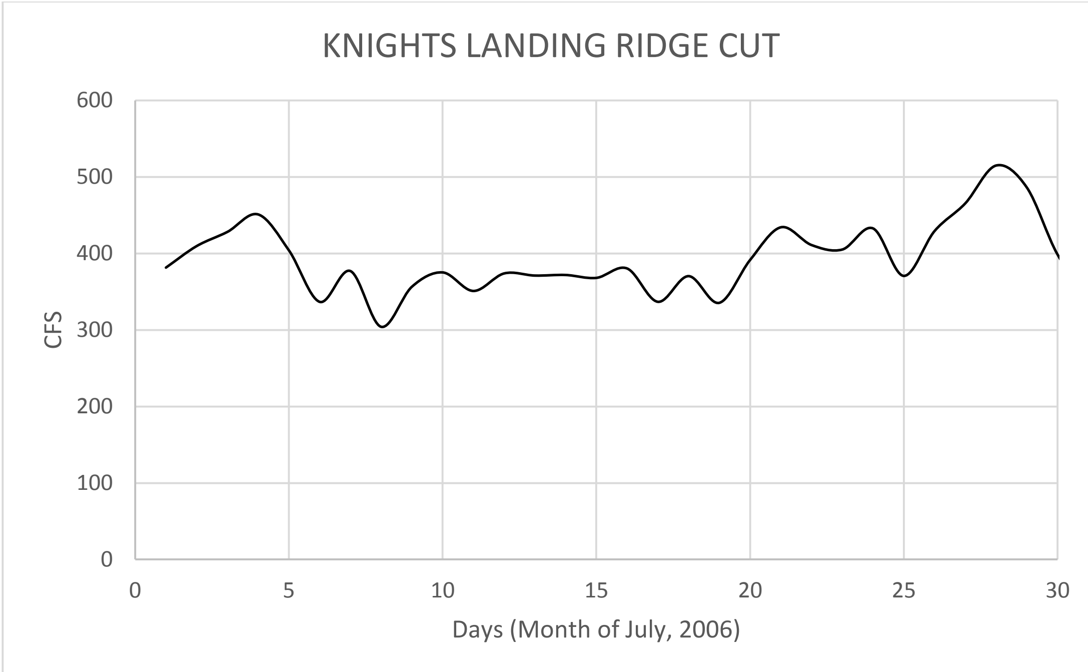

Figure A-7: Knight's Landing Ridge Cut

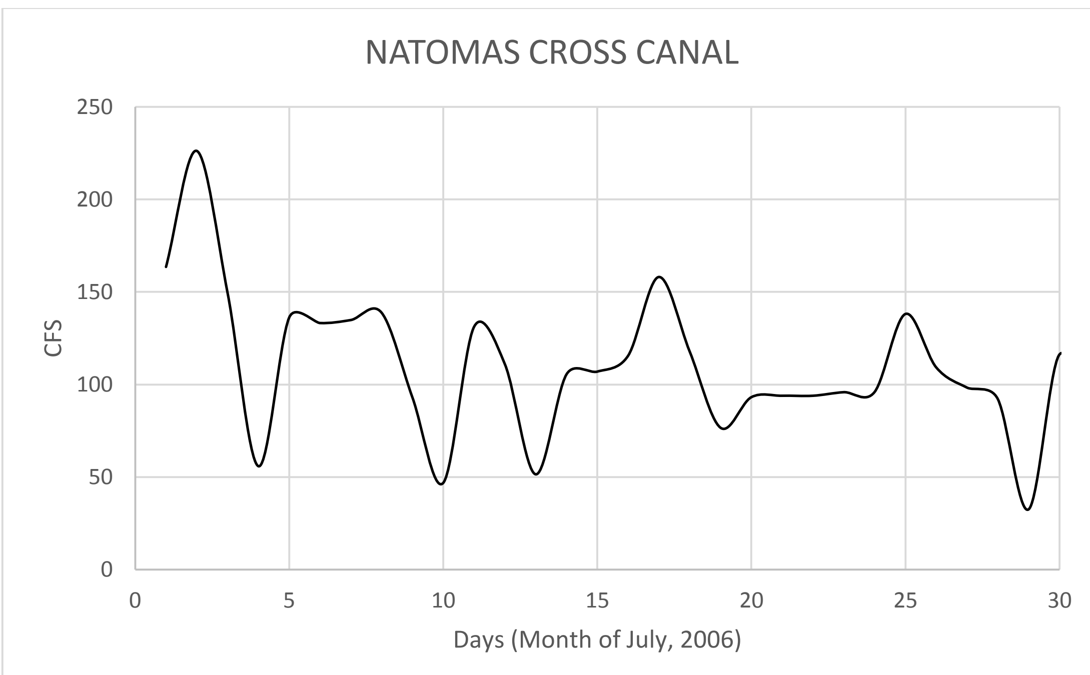

Figure A-8: Natomas Cross Canal

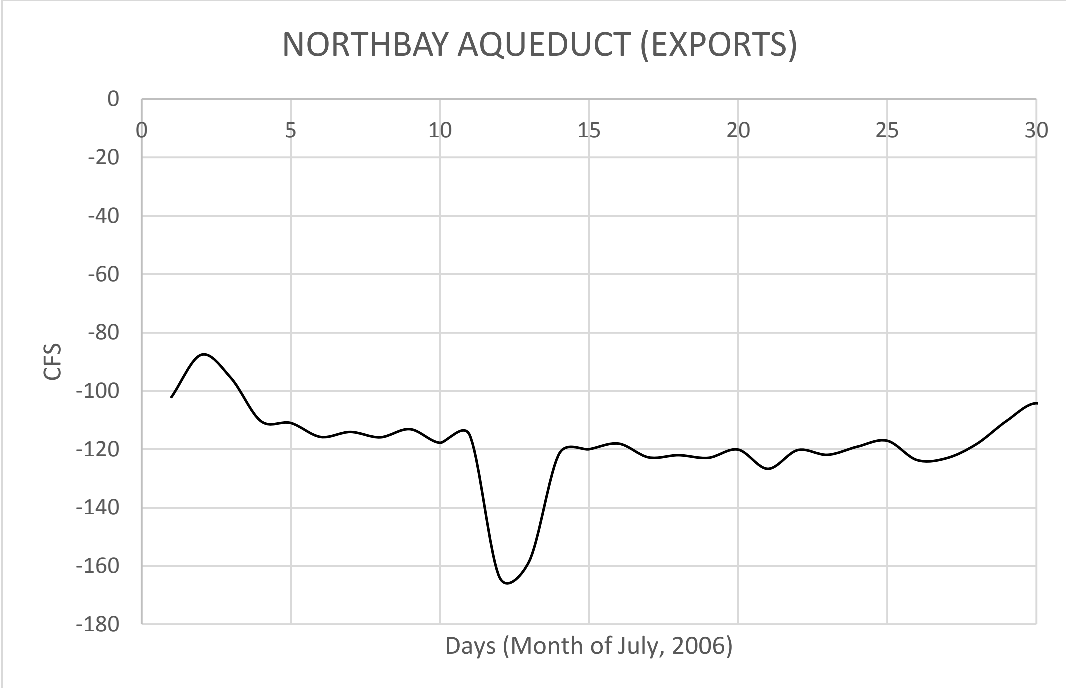

Figure A-9: Northbay Aqueduct

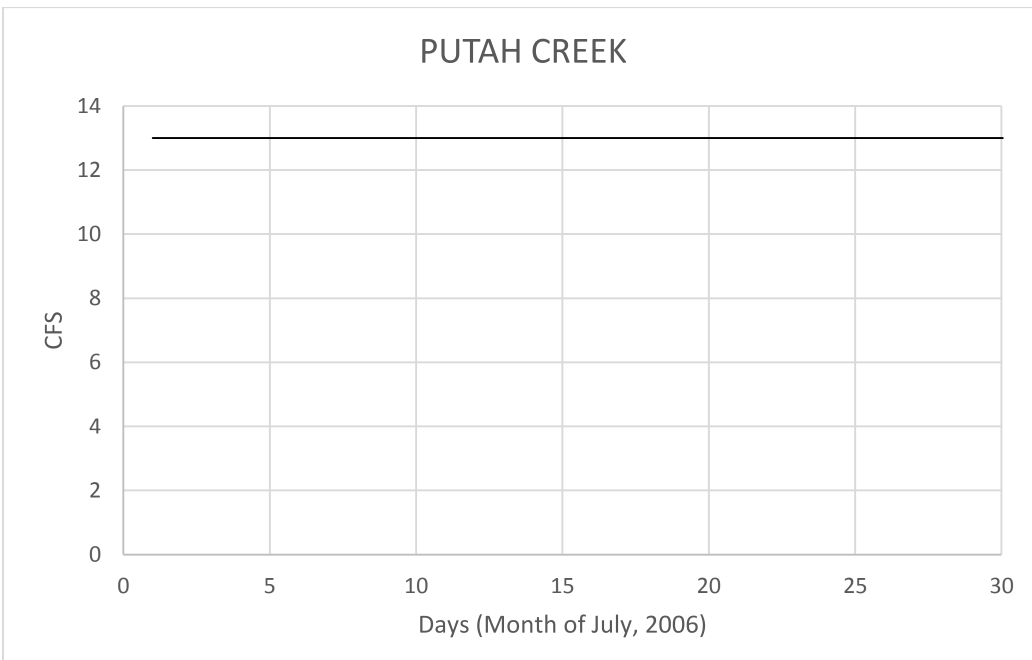

Figure A-10: Putah Creek

Table A-1: Boundary Conditions used from cbec eco engineering

DATE	CACHE CREEK SETTLING BASIN (CFS)	CACHE SLOUGH (CFS)	CALHOUN CUT (CFS)	CAMPBELL LAKE (CFS)	DELTA CROSS CHANNEL + GEORGIANA SL. (EXPORTS) (CFS)	FEATHER RIVER (CFS)	HAAS SLOUGH (CFS)	KNIGHTS LANDING RIDGE CUT (CFS)	NATOMAS CROSS CANAL (CFS)	NORTHBAY AQUEDUCT (EXPORTS) (CFS)	PUTAH CREEK (CFS)	RIOVISTA BRIDGE (FT)
7/1/06	58.6	-233.3	217.3	-54.9	-6884.6	4928.4	-233.3	381.6	163.6	-102.1	13.0	4.5
7/2/06	70.9	-231.7	216.7	-54.8	-7112.9	4473.9	-231.7	409.7	226.3	-87.6	13.0	4.5
7/3/06	70.2	-230.0	216.1	-54.6	-7148.8	4501.9	-230.0	428.3	149.5	-95.6	13.0	4.3
7/4/06	62.6	-228.4	215.5	-54.5	-7169.2	4344.0	-228.4	451.0	55.9	-110.4	13.0	4.3
7/5/06	71.2	-226.7	214.9	-54.3	-7179.6	4205.7	-226.7	404.1	136.3	-111.0	13.0	4.4
7/6/06	76.6	-225.0	214.3	-54.1	-7151.3	4230.7	-225.0	336.8	133.3	-115.8	13.0	4.5
7/7/06	64.1	-223.3	213.6	-53.9	-7082.9	4222.4	-223.3	377.1	134.9	-114.1	13.0	4.5
7/8/06	53.8	-221.5	212.9	-53.6	-7060.8	4158.8	-221.5	304.3	138.8	-115.9	13.0	4.7
7/9/06	66.8	-219.8	212.2	-53.3	-7069.6	4198.2	-219.8	356.6	93.0	-113.1	13.0	5.0
7/10/06	75.4	-218.0	211.5	-53.0	-6983.8	4267.1	-218.0	375.3	46.9	-117.8	13.0	5.2
7/11/06	73.2	-216.2	210.8	-52.7	-6941.7	4079.3	-216.2	351.1	131.3	-115.1	13.0	5.2
7/12/06	67.5	-214.4	210.1	-52.4	-6997.5	4043.2	-214.4	374.0	111.0	-163.9	13.0	5.0
7/13/06	65.2	-212.6	209.3	-52.0	-7028.8	4019.0	-212.6	371.2	51.5	-158.3	13.0	4.7
7/14/06	57.6	-210.8	208.6	-51.6	-7077.9	3985.4	-210.8	372.0	105.5	-121.6	13.0	4.8
7/15/06	61.6	-209.0	207.8	-51.1	-7233.3	4562.8	-209.0	368.2	107.0	-120.0	13.0	4.7
7/16/06	76.7	-207.1	207.0	-50.7	-7326.3	4806.5	-207.1	380.5	115.6	-118.1	13.0	4.5
7/17/06	65.1	-205.3	206.2	-50.2	-7349.2	4628.2	-205.3	336.9	158.2	-122.8	13.0	4.4
7/18/06	51.2	-203.4	205.4	-49.8	-7340.4	4823.2	-203.4	370.5	117.8	-122.0	13.0	4.7
7/19/06	54.6	-201.5	204.6	-49.3	-7368.8	5053.4	-201.5	335.6	76.7	-123.0	13.0	4.8
7/20/06	50.4	-199.7	203.9	-48.9	-7427.5	5332.3	-199.7	391.5	93.2	-120.1	13.0	4.9
7/21/06	46.3	-197.8	203.1	-48.4	-7525.8	5201.2	-197.8	434.3	94.0	-126.7	13.0	4.9
7/22/06	49.7	-195.9	202.4	-48.0	-7645.0	5024.4	-195.9	411.1	94.0	-120.3	13.0	4.9
7/23/06	55.5	-194.0	201.7	-47.5	-7774.6	5167.5	-194.0	405.2	95.9	-121.9	13.0	5.0
7/24/06	56.0	-192.1	200.9	-47.1	-7971.7	5635.9	-192.1	432.8	96.0	-119.1	13.0	5.2
7/25/06	41.1	-190.2	200.2	-46.6	-8171.7	5889.8	-190.2	370.8	138.2	-117.1	13.0	5.3
7/26/06	30.6	-188.2	199.5	-46.2	-8132.1	5887.5	-188.2	429.3	109.3	-123.7	13.0	5.3
7/27/06	39.4	-186.3	198.9	-45.7	-8062.9	5919.6	-186.3	465.5	98.4	-123.0	13.0	5.3
7/28/06	48.4	-184.4	198.2	-45.3	-7964.2	5685.3	-184.4	514.9	92.3	-118.2	13.0	5.2
7/29/06	52.7	-182.5	197.5	-44.8	-7768.3	5258.1	-182.5	486.3	32.6	-110.3	13.0	5.2
7/30/06	70.5	-180.5	196.9	-44.4	-7539.6	4964.0	-180.5	398.8	116.3	-104.3	13.0	5.0
7/31/06	84.9	-178.6	196.3	-43.9	-7395.8	5049.8	-178.6	346.1	75.0	-109.8	13.0	4.9

B. Appendix B

Table B-1: Gauge Information

Station ID	WLK	**Elevation**	30' ft
River Basin	SACRAMENTO R	**County**	SUTTER
Hydrologic Area	SACRAMENTO RIVER	**Nearby City**	YUBA CITY
Latitude	39.009895°N	**Longitude**	-121.824692°W
Operator	US Geological Survey	**Data Collection**	
Station ID	KNL	**Elevation**	30' ft
River Basin	SACRAMENTO R	**County**	SUTTER
Hydrologic Area	SACRAMENTO RIVER	**Nearby City**	KNIGHT'S LANDING
Latitude	38.803349°N	**Longitude**	-121.716393°W
Operator	CA Dept of Water Resources	**Data Collection**	
Station ID	FRE	**Elevation**	40' ft
River Basin	SACRAMENTO R	**County**	YOLO
Hydrologic Area	SACRAMENTO RIVER	**Nearby City**	WOODLAND
Latitude	38.759258°N	**Longitude**	-121.667274°W
Operator	CA Dept of Water Resources/NCRO	**Data Collection**	
Station ID	VON	**Elevation**	43' ft
River Basin	SACRAMENTO R	**County**	SUTTER
Hydrologic Area	SACRAMENTO RIVER	**Nearby City**	VERONA
Latitude	38.774155°N	**Longitude**	-121.598068°W
Operator	USGS and DWR	**Data Collection**	
Station ID	GES	**Elevation**	0' ft
River Basin	SACRAMENTO R	**County**	SACRAMENTO
Hydrologic Area	SACRAMENTO RIVER	**Nearby City**	WALNUT GROVE
Latitude	38.238900°N	**Longitude**	-121.523400°W
Operator	US Geological Survey	**Data Collection**	
Station ID	FPT	**Elevation**	0' ft
River Basin	SACRAMENTO R	**County**	SACRAMENTO
Hydrologic Area	SACRAMENTO RIVER	**Nearby City**	FREEPORT
Latitude	38.450000°N	**Longitude**	-121.500000°W
Operator	US Geological Survey	**Data Collection**	
Station ID	LIY	**Elevation**	0' ft
River Basin	SACRAMENTO R	**County**	SOLANO
Hydrologic Area	SACRAMENTO RIVER	**Nearby City**	SACRAMENTO
Latitude	38.329277°N	**Longitude**	-121.693977°W
Operator	CA Dept of Water Resources	**Data Collection**	
Station ID	LIS	Elevation	0' ft
River Basin	SACRAMENTO R	County	YOLO
Hydrologic Area	SACRAMENTO RIVER	Nearby City	FREEPORT
Latitude	38.474781°N	Longitude	-121.588226°W
Operator	CA Dept of Water Resources	Data Collection	

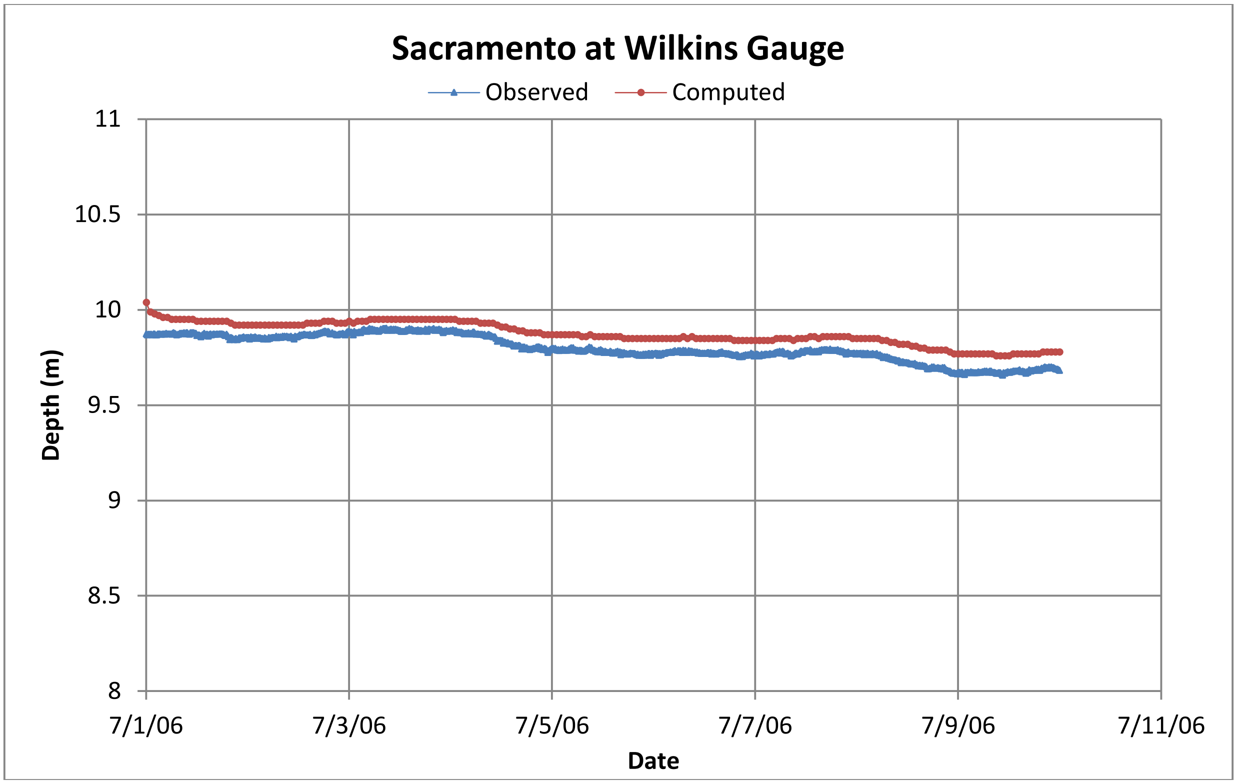

Figure B-1: Observed and Computed Stage at Wilkins

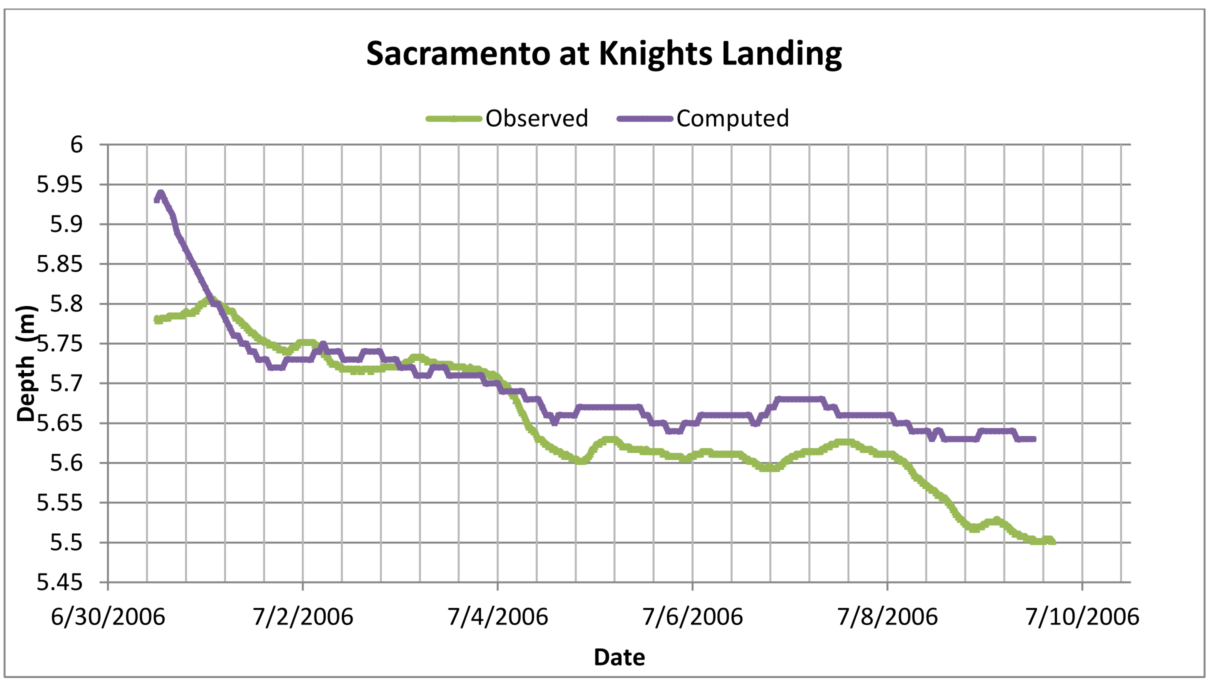

\

Figure B-2: Observed and Computed Stage at Knight's Landing

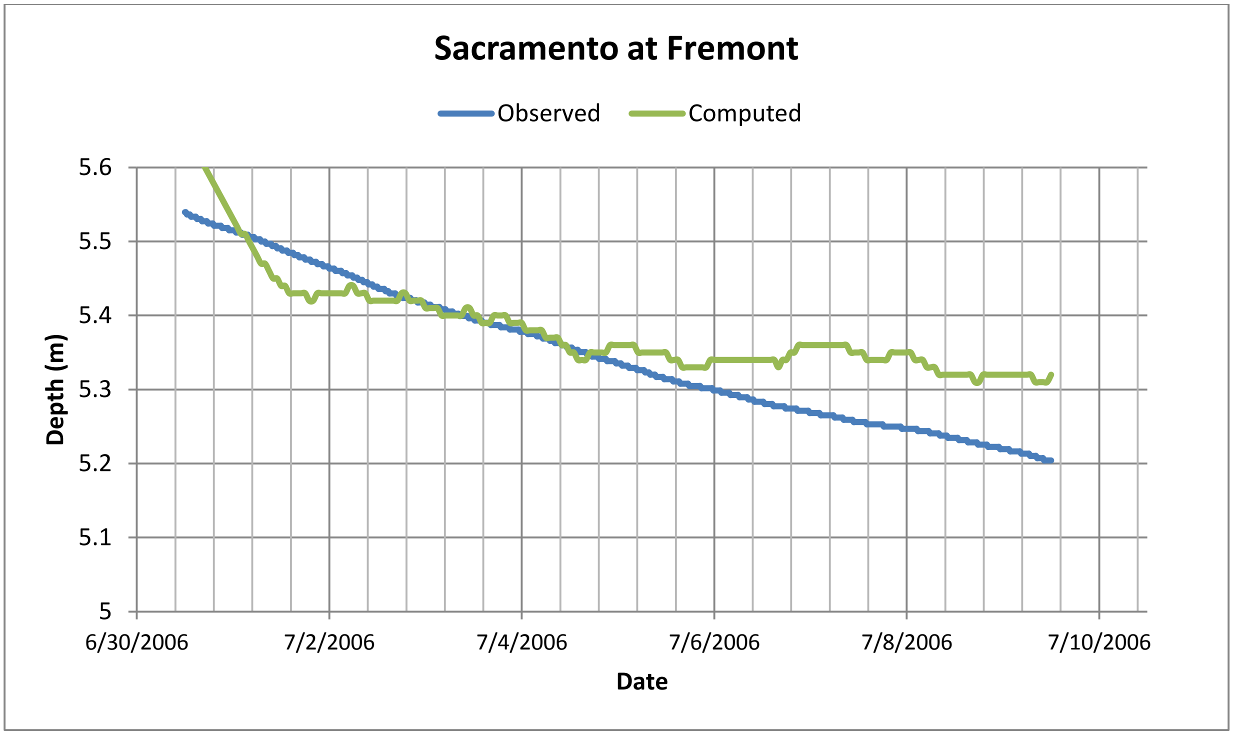

\

Figure B-3: Observed and Computed Stage at Fremont (Western end)

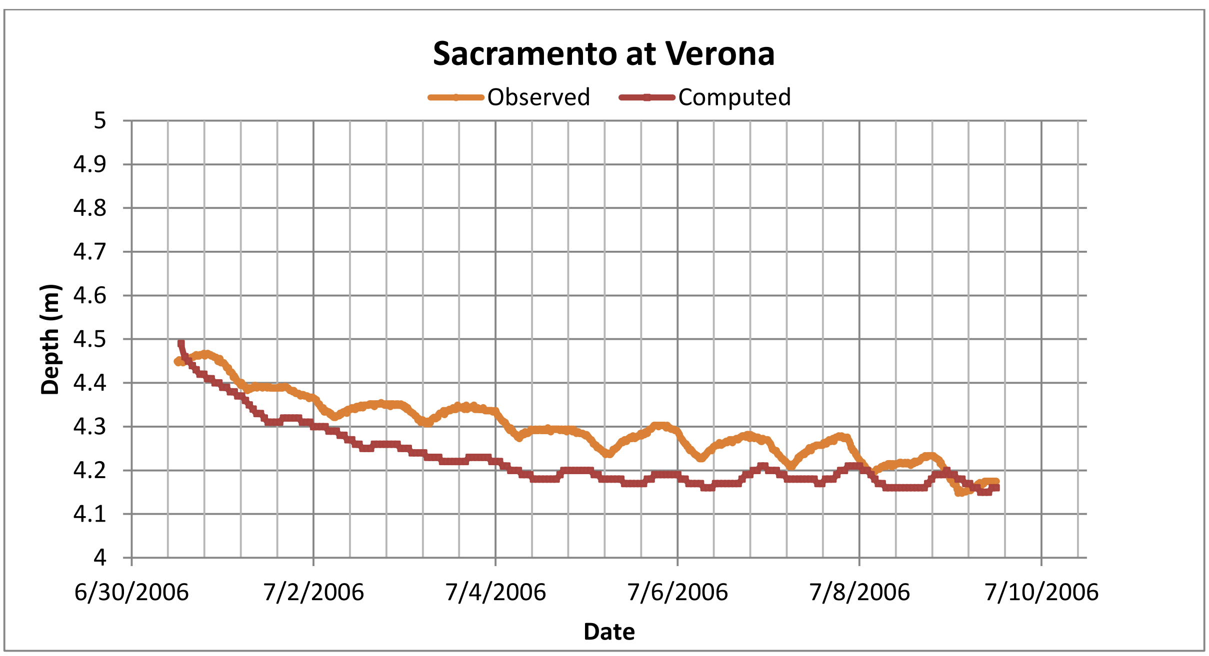

Figure B-4: Observed and Computed Stage of Sacramento River at Verona

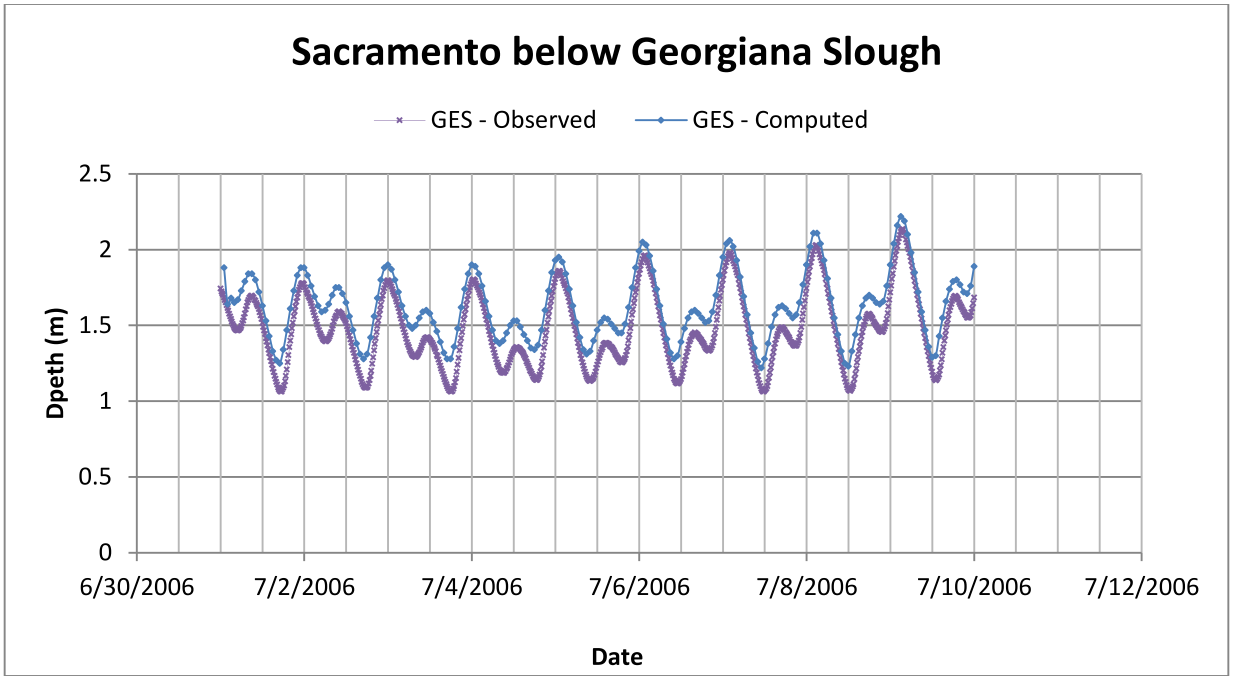

Figure B-5: Observed and Computed Stage of Sacramento River below Georgiana Slough

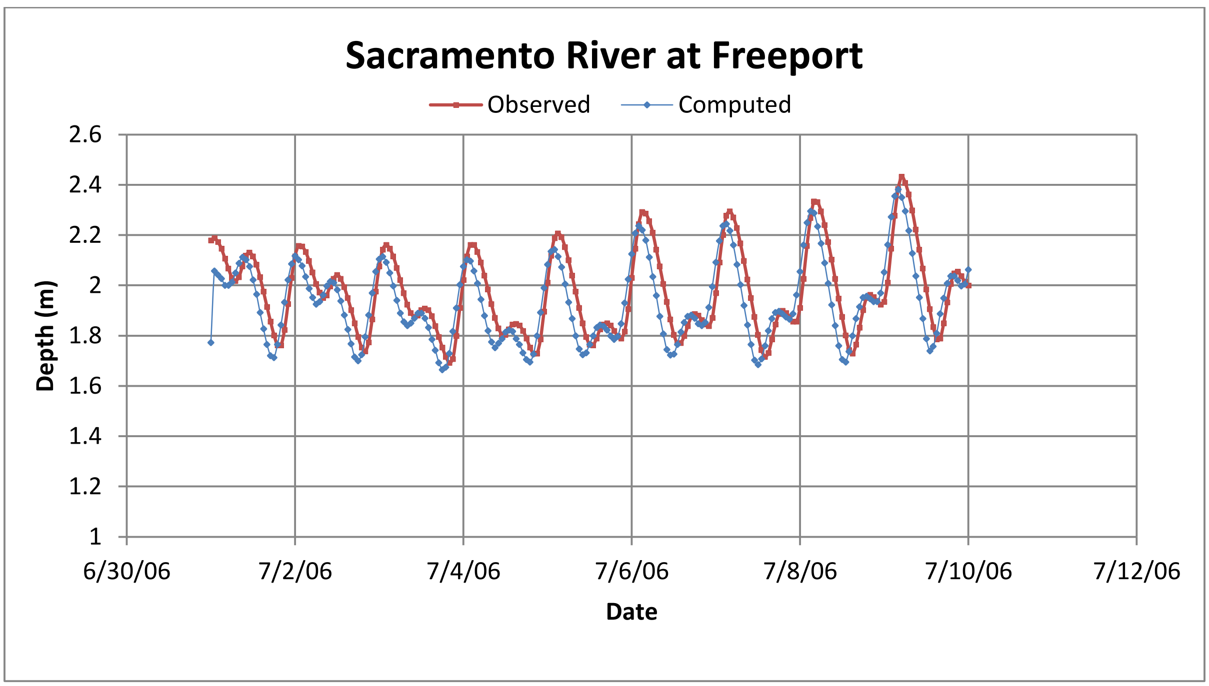

Figure B-6: Observed and Computed Stage of Sacramento River at Freeport

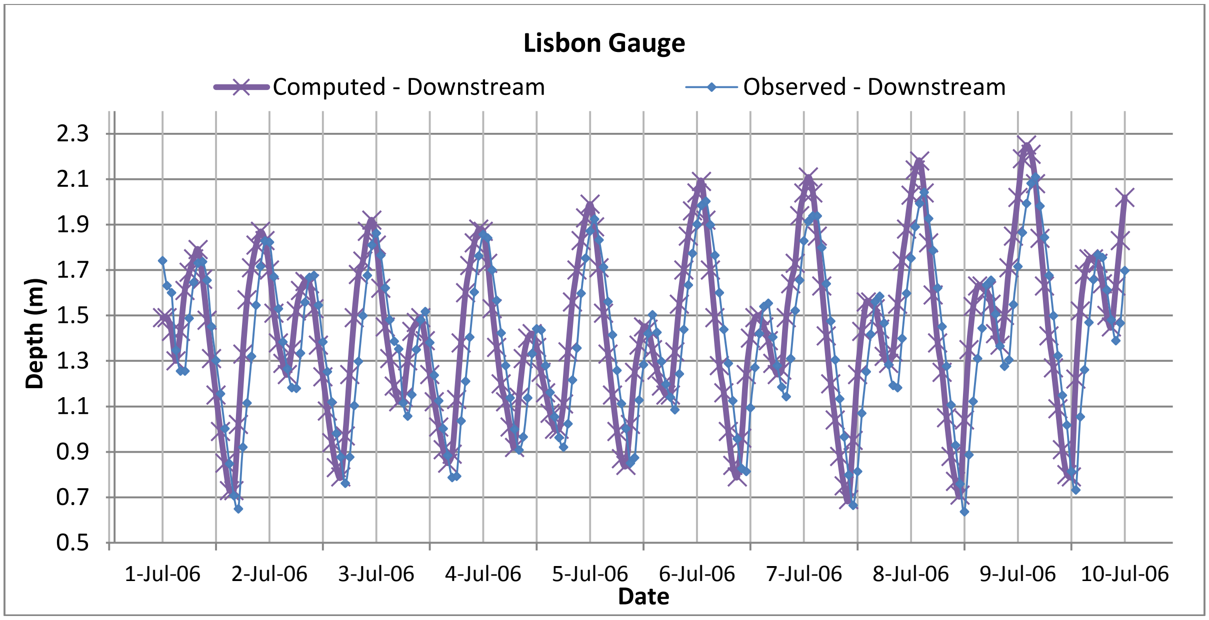

Figure B-7: Lisbon Gauge Tidal Boundary

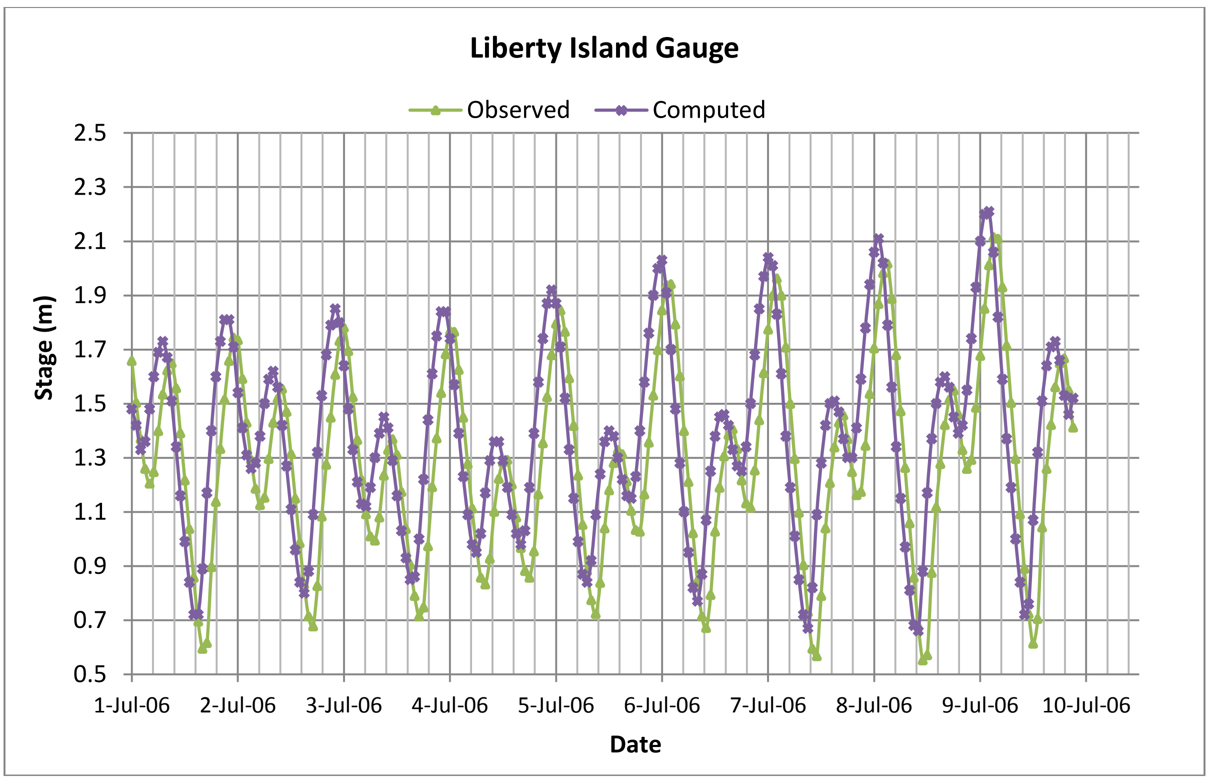

Figure B-8: Liberty Island Upstream and Downstream Tidal Boundary

C. Appendix C

Table C-1 and C-2 show the water surface elevations and average channel velocities along the Toe Drain using two different solution schemes.

Table C-1: Water Surface Elevations and Channel velocity in the Toe Drain, for 2,4 and 6 K (Diffusive Wave)

Channel Distance	Channel Elevation	2,000 cfs		4,000 cfs		6,000 cfs	
		W.S. Elev	Vel Chnl	W.S. Elev	Vel Chnl	W.S. Elev	Vel Chnl
(m)	(m)	(m)	(m/s)	(m)	(m/s)	(m)	(m/s)
59229.6	2.9	6.21	0.44	6.81	0.69	7.16	0.92
59191.5	2.9	6.2	0.44	6.8	0.7	7.14	0.93
59097.6	2.9	6.2	0.41	6.79	0.65	7.14	0.87
58995.7	2.87	6.17	0.5	6.75	0.77	7.08	1.01
58357.8	2.8	6.08	0.4	6.65	0.51	6.94	0.63
58307.4	2.79	6.08	0.46	6.64	0.55	6.93	0.66
58233.8	2.77	6.07	0.47	6.63	0.59	6.92	0.72
57318.2	2.71	5.98	0.34	6.57	0.26	6.85	0.41
57255.8	2.68	5.97	0.42	6.56	0.28	6.85	0.44
57196.7	2.65	5.97	0.31	6.56	0.22	6.85	0.39
56762.1	2.59	5.95	0.28	6.56	0.19	6.87	0.36
56092.3	2.38	5.9	0.39	6.52	0.44	6.82	0.53
55353.6	2.35	5.82	0.51	6.45	0.51	6.75	0.55
55245.5	2.32	5.81	0.48	6.44	0.47	6.74	0.49
53682.4	2.32	5.48	0.74	6.2	0.74	6.53	0.7
53455.0	2.3	5.38	0.87	6.13	0.85	6.46	0.85
53307.4	2.29	5.34	0.56	6.09	0.71	6.41	0.76
52051.9	2.23	5.13	0.49	5.69	0.81	5.94	0.95
51925.5	2.23	5.12	0.42	5.66	0.68	5.91	0.79
51735.7	2.23	5.11	0.32	5.64	0.53	5.89	0.62
51054.7	2.13	5.01	0.63	5.47	0.93	5.7	1.01
50945.7	2.13	5	0.46	5.44	0.74	5.66	0.82
50907.5	1.89	4.99	0.47	5.43	0.76	5.65	0.86
50689.5	2.1	4.98	0.39	5.41	0.54	5.63	0.59
50260.9	2.07	4.96	0.19	5.39	0.26	5.61	0.29
50221.7	2.07	4.96	0.19	5.39	0.26	5.61	0.29
50057.2	2.07	4.95	0.18	5.38	0.26	5.6	0.28
50022.5	2.04	4.95	0.21	5.38	0.29	5.6	0.31
49816.5	2.01	4.95	0.17	5.37	0.25	5.59	0.27
49277.0	1.98	4.93	0.28	5.34	0.42	5.55	0.46
48927.3	1.95	4.91	0.34	5.3	0.52	5.51	0.57
48630.8	1.94	4.89	0.32	5.27	0.46	5.48	0.5
47979.5	1.92	4.86	0.25	5.25	0.22	5.46	0.22
47939.4	1.89	4.86	0.29	5.25	0.25	5.46	0.25
47898.3	1.86	4.86	0.26	5.25	0.23	5.46	0.22
47539.1	1.83	4.84	0.36	5.23	0.32	5.44	0.32
47003.8	1.68	4.77	0.45	5.19	0.4	5.41	0.4
46290.3	1.48	4.61	0.65	5.05	0.68	5.25	0.78
45814.8	1.34	4.46	0.59	4.94	0.61	5.13	0.64
45279.6	1.19	4.36	0.48	4.85	0.49	5.04	0.52
44804.1	1.05	4.3	0.42	4.8	0.44	4.99	0.46
42069.4	0.27	4.02	0.4	4.57	0.39	4.75	0.4
41460.1	0.24	3.96	0.4	4.53	0.39	4.71	0.4
41408.8	0.21	3.96	0.28	4.53	0.27	4.71	0.28
41338.7	0.18	3.95	0.42	4.52	0.43	4.7	0.46
41275.0	0.15	3.94	0.49	4.51	0.51	4.69	0.54
39214.4	-0.15	3.22	0.99	3.94	1.16	4.2	1.18
39087.9	-0.15	3.21	0.56	3.94	0.59	4.21	0.59
39027.1	-0.15	3.21	0.45	3.94	0.55	4.2	0.56
38920.5	-0.15	3.2	0.45	3.93	0.47	4.19	0.47
36551.6	-0.3	2.99	0.35	3.73	0.39	4.01	0.38
36524.9	-0.34	2.98	0.4	3.73	0.45	4.01	0.43
36487.7	-0.4	2.98	0.44	3.73	0.49	4.01	0.47
35716.5	-0.7	2.93	0.41	3.68	0.47	3.97	0.44
35327.4	-1.01	2.91	0.34	3.66	0.39	3.95	0.36
34902.9	-1.13	2.89	0.39	3.64	0.46	3.93	0.44
28242.0	-1.39	2.52	0.43	3.08	0.58	3.41	0.45
28181.4	-1.39	2.52	0.43	3.07	0.58	3.41	0.44

28120.8	-1.4	2.1	0.49	3.02	0.59	3.4	0.44
28060.3	-1.4	2.1	0.49	3.01	0.59	3.39	0.44
27939.2	-1.4	2.08	0.48	3	0.59	3.39	0.44
27883.9	-1.4	2.08	0.55	2.99	0.66	3.38	0.49
27775.5	-1.4	2.07	0.48	2.98	0.59	3.38	0.44
27667.2	-1.4	2.06	0.47	2.97	0.58	3.37	0.43
27415.4	-1.4	2.04	0.43	2.95	0.53	3.37	0.39
22399.1	-2.14	1.66	0.46	2.37	0.76	2.87	0.86
22382.2	-2.16	1.65	0.47	2.36	0.78	2.87	0.88
22362.1	-2.35	1.65	0.48	2.36	0.8	2.86	0.9
22084.8	-2.38	1.64	0.39	2.33	0.65	2.83	0.73
22058.6	-2.41	1.64	0.35	2.33	0.58	2.84	0.66
21958.7	-2.44	1.63	0.35	2.32	0.6	2.82	0.69
21855.0	-2.53	1.63	0.37	2.31	0.63	2.81	0.72
21484.1	-2.53	1.62	0.3	2.29	0.52	2.79	0.59
21439.5	-2.56	1.62	0.28	2.29	0.47	2.78	0.54
21358.8	-2.59	1.62	0.24	2.28	0.41	2.78	0.47
21299.6	-2.56	1.61	0.33	2.27	0.55	2.77	0.62
21232.7	-2.58	1.61	0.35	2.26	0.6	2.76	0.69
20986.2	-2.59	1.6	0.35	2.24	0.61	2.73	0.7
20959.8	-2.61	1.6	0.37	2.24	0.63	2.73	0.72
20927.0	-2.62	1.59	0.39	2.23	0.67	2.72	0.76
19178.6	-2.93	1.52	0.28	2.06	0.52	2.52	0.61
19117.8	-2.8	1.52	0.28	2.05	0.53	2.52	0.62
18917.1	-3.05	1.52	0.26	2.04	0.49	2.5	0.58
13782.4	-3.66	1.43	0.28	1.74	0.6	2.08	0.79
13678.0	-3.66	1.42	0.29	1.74	0.61	2.07	0.81
13250.1	-3.69	1.42	0.26	1.71	0.57	2.03	0.75
13056.2	-3.69	1.41	0.27	1.7	0.58	2.01	0.77
12960.0	-3.69	1.41	0.2	1.7	0.43	2.01	0.57
12870.4	-3.72	1.41	0.24	1.69	0.53	2	0.7
12794.1	-3.72	1.41	0.25	1.69	0.55	1.99	0.73
12605.4	-3.75	1.4	0.28	1.67	0.62	1.96	0.83
11940.0	-3.78	1.39	0.3	1.6	0.66	1.85	0.89
11701.0	-3.79	1.38	0.28	1.58	0.65	1.81	0.88
11416.5	-3.81	1.38	0.28	1.55	0.64	1.77	0.87
7422.7	-4.63	1.34	0.15	1.37	0.37	1.42	0.54
6355.3	-3.57	1.33	0.17	1.33	0.44	1.34	0.65
6270.5	-3.99	1.33	0.17	1.33	0.45	1.33	0.66
6119.4	-7.25	1.33	0.09	1.34	0.22	1.34	0.33
5959.3	-6	1.33	0.12	1.33	0.32	1.33	0.47
5617.5	-7.25	1.33	0.05	1.33	0.14	1.34	0.21
5511.8	-7.16	1.33	0.03	1.33	0.07	1.34	0.1
4490.6	-6.28	1.33	0.04	1.33	0.09	1.34	0.14
4356.4	-5.91	1.33	0.05	1.33	0.12	1.34	0.18
3410.0	-5.76	1.32	0.03	1.33	0.07	1.33	0.1
2881.8	-6.86	1.32	0.03	1.33	0.08	1.33	0.11
2251.2	-8.41	1.32	0.03	1.32	0.09	1.33	0.14
2148.8	-8.12	1.32	0.03	1.32	0.09	1.33	0.14
1842.2	-11.25	1.32	0.02	1.32	0.05	1.33	0.08
1747.5	-10.27	1.32	0.02	1.32	0.05	1.33	0.08
1489.6	-11.25	1.32	0.02	1.32	0.06	1.33	0.1
1199.7	-11.25	1.32	0.01	1.32	0.04	1.33	0.06
855.9	-11.25	1.32	0.01	1.32	0.03	1.33	0.04
609.9	-11.25	1.32	0	1.32	0.02	1.33	0.02
561.7	-11.25	1.32	0.01	1.32	0.02	1.33	0.03
57.4	-11.58	1.32	0.01	1.32	0.04	1.32	0.06

Table C-2: Water Surface Elevations and Channel velocity in the Toe Drain, for 2, 4 and 6 K (Dynamic Wave)

Channel Distance	Channel Elevation	2,000 cfs		4,000 cfs		6,000 cfs	
		W.S. Elev	Vel Chnl	W.S. Elev	Vel Chnl	W.S. Elev	Vel Chnl
(m)	(m)	(m)	(m/s)	(m)	(m/s)	(m)	(m/s)
59229.6	2.9	6.23	0.44	6.8	0.69	7.23	0.89
59191.5	2.9	6.22	0.44	6.79	0.69	7.22	0.89
59097.6	2.9	6.22	0.41	6.79	0.65	7.21	0.83
58995.7	2.87	6.19	0.49	6.75	0.77	7.16	0.96
58357.8	2.8	6.11	0.38	6.71	0.33	7.11	0.37
58307.4	2.79	6.1	0.43	6.75	0.23	7.2	0.19
58233.8	2.77	6.09	0.45	6.72	0.69	7.05	0.91
57318.2	2.71	6.01	0.32	6.59	0.25	6.86	0.32
57255.8	2.68	6	0.39	6.59	0.26	6.86	0.32
57196.7	2.65	6	0.28	6.59	0.21	6.86	0.27
56762.1	2.59	5.98	0.25	6.58	0.17	6.86	0.24
56092.3	2.38	5.94	0.35	6.55	0.38	6.82	0.42
55353.6	2.35	5.86	0.48	6.48	0.46	6.76	0.48
55245.5	2.32	5.85	0.46	6.47	0.43	6.75	0.45
53682.4	2.32	5.5	0.71	6.25	0.65	6.55	0.62
53455.0	2.3	5.39	0.85	6.17	0.77	6.48	0.76
53307.4	2.29	5.36	0.56	6.12	0.68	6.43	0.72
52051.9	2.23	5.14	0.49	5.71	0.8	5.95	0.91
51925.5	2.23	5.13	0.41	5.69	0.66	5.93	0.75
51735.7	2.23	5.11	0.32	5.66	0.53	5.9	0.6
51054.7	2.13	5.02	0.62	5.49	0.87	5.72	0.93
50945.7	2.13	5	0.44	5.46	0.7	5.68	0.77
50907.5	1.89	5	0.46	5.45	0.73	5.67	0.81
50689.5	2.1	4.98	0.39	5.43	0.52	5.65	0.56
50260.9	2.07	4.96	0.18	5.4	0.24	5.62	0.26
50221.7	2.07	4.96	0.18	5.4	0.25	5.62	0.27
50057.2	2.07	4.95	0.18	5.4	0.25	5.62	0.27
50022.5	2.04	4.95	0.2	5.39	0.27	5.61	0.28
49816.5	2.01	4.95	0.17	5.39	0.24	5.61	0.26
49277.0	1.98	4.93	0.28	5.35	0.41	5.57	0.44
48927.3	1.95	4.91	0.33	5.31	0.49	5.53	0.53
48630.8	1.94	4.89	0.32	5.28	0.44	5.49	0.47
47979.5	1.92	4.86	0.25	5.26	0.21	5.47	0.21
47939.4	1.89	4.86	0.28	5.26	0.24	5.47	0.24
47898.3	1.86	4.86	0.25	5.26	0.22	5.47	0.22
47539.1	1.83	4.83	0.35	5.24	0.31	5.46	0.31
47003.8	1.68	4.77	0.45	5.2	0.38	5.42	0.39
46290.3	1.48	4.6	0.64	5.07	0.65	5.26	0.74
45814.8	1.34	4.46	0.58	4.96	0.57	5.15	0.58
45279.6	1.19	4.36	0.47	4.88	0.46	5.07	0.48
44804.1	1.05	4.3	0.41	4.83	0.4	5.03	0.42
42069.4	0.27	4.01	0.39	4.57	0.35	4.75	0.35
41460.1	0.24	3.96	0.4	4.52	0.36	4.7	0.36
41408.8	0.21	3.96	0.27	4.52	0.26	4.7	0.26
41338.7	0.18	3.95	0.41	4.51	0.41	4.69	0.42
41275.0	0.15	3.94	0.45	4.5	0.46	4.69	0.48
39214.4	-0.15	3.24	0.97	3.98	1.13	4.24	1.14
39087.9	-0.15	3.23	0.53	3.98	0.52	4.25	0.5
39027.1	-0.15	3.22	0.43	3.97	0.5	4.24	0.51
38920.5	-0.15	3.21	0.43	3.96	0.44	4.23	0.43
36551.6	-0.3	3.01	0.35	3.78	0.38	4.06	0.36
36524.9	-0.34	3.01	0.39	3.78	0.42	4.06	0.39
36487.7	-0.4	3	0.42	3.77	0.43	4.06	0.4
35716.5	-0.7	2.95	0.4	3.72	0.43	4.02	0.39
35327.4	-1.01	2.93	0.33	3.7	0.36	4.01	0.32
34902.9	-1.13	2.91	0.38	3.68	0.42	3.99	0.38
28242.0	-1.39	2.52	0.42	3.1	0.53	3.45	0.39
28181.4	-1.39	2.52	0.42	3.09	0.53	3.44	0.37
28120.8	-1.4	2.1	0.48	3.05	0.54	3.44	0.37
28060.3	-1.4	2.1	0.49	3.05	0.54	3.44	0.38
27939.2	-1.4	2.08	0.49	3.03	0.54	3.43	0.38
27883.9	-1.4	2.07	0.54	3.02	0.59	3.43	0.4
27775.5	-1.4	2.06	0.48	3.02	0.54	3.42	0.37

27667.2	-1.4	2.05	0.47	3	0.54	3.41	0.38
27415.4	-1.4	2.04	0.43	2.99	0.49	3.41	0.34
22399.1	-2.14	1.65	0.45	2.4	0.74	2.91	0.82
22382.2	-2.16	1.65	0.47	2.39	0.77	2.91	0.85
22362.1	-2.35	1.65	0.48	2.39	0.78	2.9	0.85
22084.8	-2.38	1.64	0.38	2.36	0.63	2.86	0.68
22058.6	-2.41	1.64	0.34	2.36	0.56	2.86	0.62
21958.7	-2.44	1.63	0.35	2.35	0.59	2.85	0.65
21855.0	-2.53	1.63	0.36	2.34	0.61	2.83	0.68
21484.1	-2.53	1.62	0.3	2.31	0.5	2.81	0.56
21439.5	-2.56	1.62	0.27	2.31	0.46	2.81	0.52
21358.8	-2.59	1.61	0.24	2.31	0.41	2.8	0.46
21299.6	-2.56	1.61	0.32	2.3	0.54	2.79	0.6
21232.7	-2.58	1.61	0.34	2.29	0.59	2.78	0.66
20986.2	-2.59	1.6	0.34	2.27	0.59	2.75	0.67
20959.8	-2.61	1.6	0.36	2.26	0.62	2.75	0.69
20927.0	-2.62	1.59	0.38	2.26	0.65	2.74	0.73
19178.6	-2.93	1.52	0.28	2.07	0.51	2.53	0.59
19117.8	-2.8	1.52	0.28	2.07	0.52	2.52	0.6
18917.1	-3.05	1.52	0.26	2.06	0.48	2.51	0.56
13782.4	-3.66	1.42	0.28	1.74	0.59	2.06	0.77
13678.0	-3.66	1.42	0.29	1.74	0.6	2.05	0.78
13250.1	-3.69	1.42	0.26	1.71	0.56	2.01	0.74
13056.2	-3.69	1.41	0.27	1.7	0.58	1.99	0.76
12960.0	-3.69	1.41	0.2	1.7	0.42	1.99	0.56
12870.4	-3.72	1.41	0.24	1.69	0.52	1.98	0.67
12794.1	-3.72	1.41	0.25	1.68	0.55	1.97	0.72
12605.4	-3.75	1.4	0.28	1.67	0.62	1.94	0.81
11940.0	-3.78	1.39	0.29	1.6	0.66	1.84	0.87
11701.0	-3.79	1.38	0.28	1.58	0.65	1.8	0.86
11416.5	-3.81	1.38	0.27	1.55	0.64	1.75	0.86
7422.7	-4.63	1.34	0.15	1.37	0.37	1.41	0.53
6355.3	-3.57	1.33	0.17	1.33	0.44	1.34	0.63
6270.5	-3.99	1.33	0.17	1.33	0.44	1.33	0.65
6119.4	-7.25	1.33	0.09	1.33	0.22	1.34	0.32
5959.3	-6	1.33	0.12	1.33	0.32	1.33	0.46
5617.5	-7.25	1.33	0.05	1.33	0.14	1.34	0.2
5511.8	-7.16	1.33	0.03	1.33	0.07	1.34	0.1
4490.6	-6.28	1.33	0.04	1.33	0.09	1.34	0.14
4356.4	-5.91	1.33	0.05	1.33	0.12	1.33	0.18
3410.0	-5.76	1.32	0.03	1.33	0.07	1.33	0.1
2881.8	-6.86	1.32	0.03	1.33	0.07	1.33	0.11
2251.2	-8.41	1.32	0.03	1.32	0.09	1.33	0.14
2148.8	-8.12	1.32	0.03	1.32	0.09	1.33	0.14
1842.2	-11.25	1.32	0.02	1.32	0.05	1.33	0.07
1747.5	-10.27	1.32	0.02	1.32	0.05	1.33	0.08
1489.6	-11.25	1.32	0.02	1.32	0.06	1.33	0.09
1199.7	-11.25	1.32	0.01	1.32	0.04	1.32	0.06
855.9	-11.25	1.32	0.01	1.32	0.03	1.32	0.04
609.9	-11.25	1.32	0	1.32	0.02	1.32	0.02
561.7	-11.25	1.32	0.01	1.32	0.02	1.32	0.03
57.4	-11.58	1.32	0.01	1.32	0.04	1.32	0.06

Figure C-1, C-2 and C-3 show the flooding extents and depths based on the classification scheme set by Suddeth (2014)

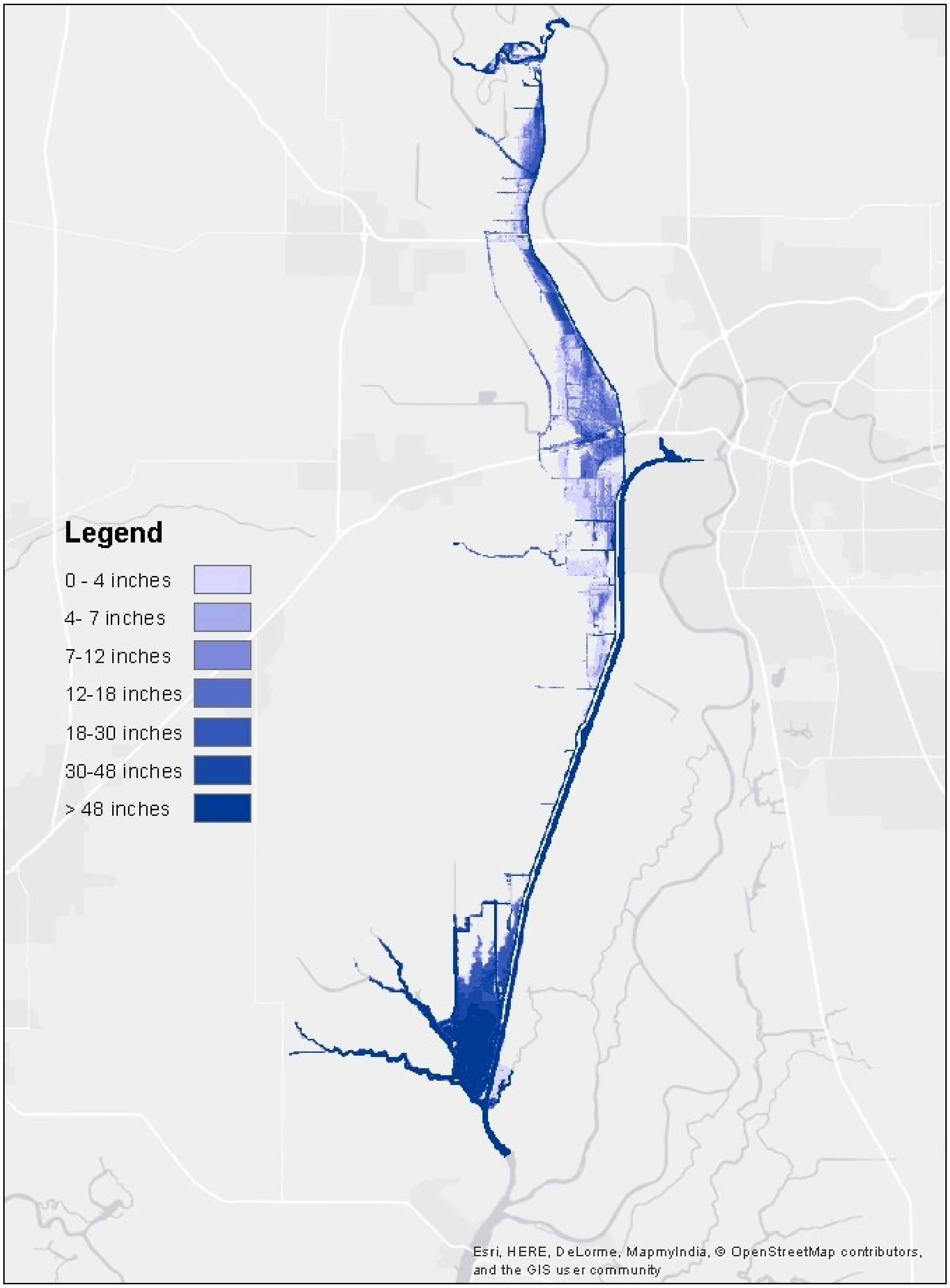

Figure C-1: Flooding extents for 2000 cfs

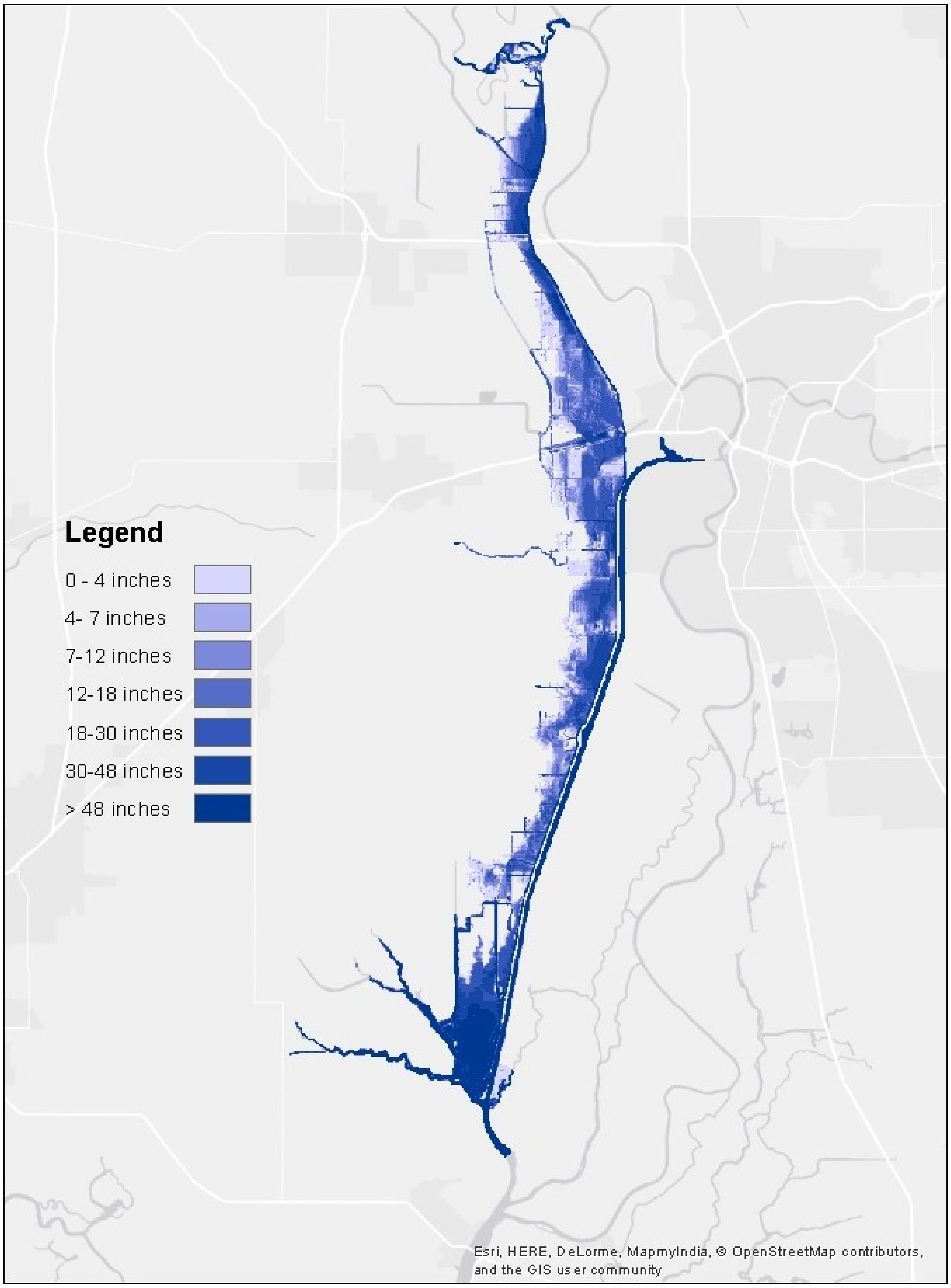

Figure C-2: Flooding extents for 4000 cfs

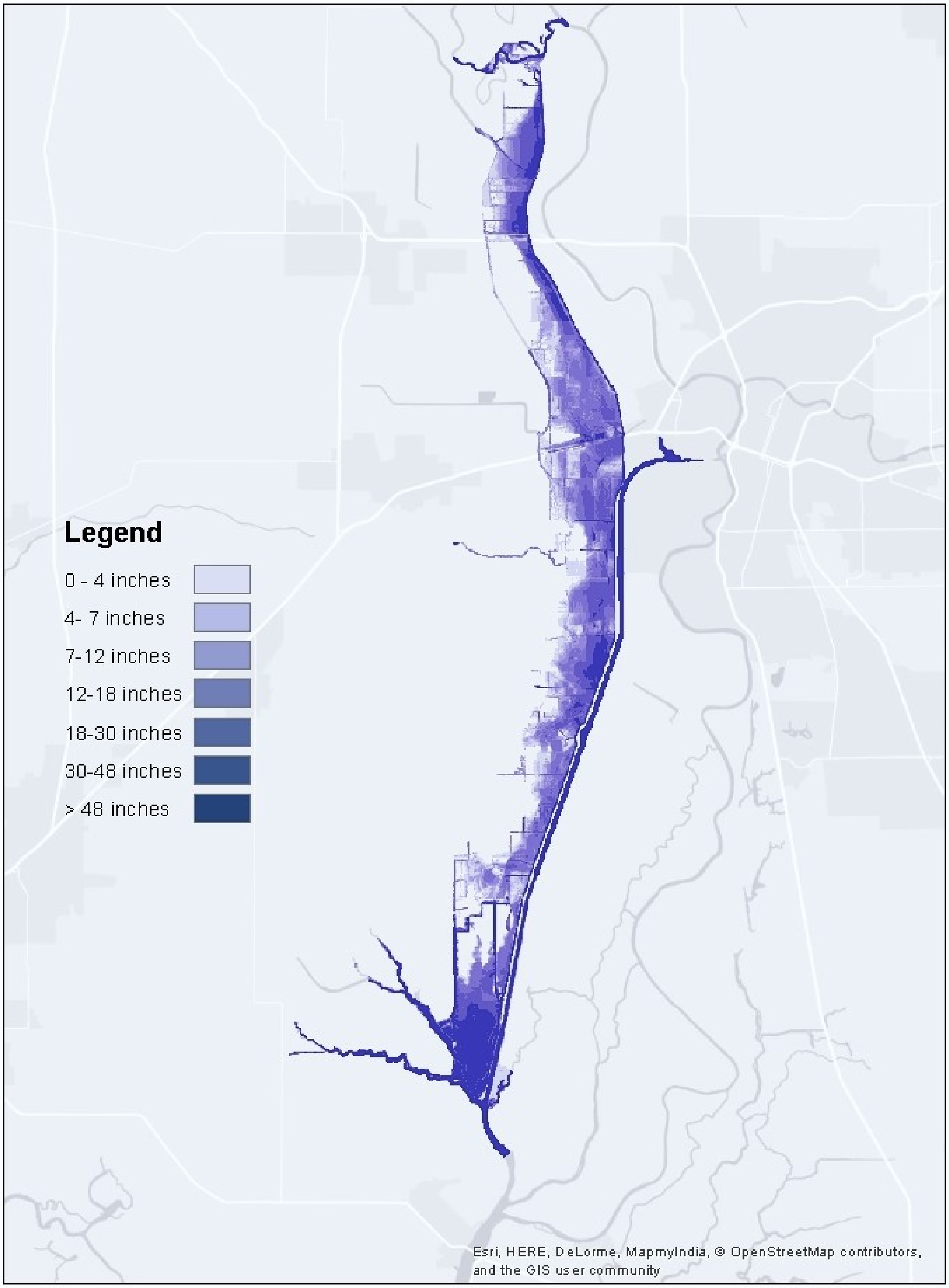

Figure C-3: Flooding extents for 6000 cfs

D. Appendix D

Table D-1, D-2 and D-3 show the flooding footprint for each agro-ecological zone.

Table D-1:Detailed Inundation footprint for 2000 cfs by zones

Depths	Zone 1	Zone 2	Zone 3	Zone 4	Zone 5	Zone 6	Zone 7
0-4 inches	112.6	64.57	316.24	302.89	511.25	445.57	2.9
>4-7 inches	91.6	67.32	279.29	138.64	335.55	250.5	1.3
>7-12 inches	187.2	102.22	427.41	248.39	328.06	253.8	3.2
>12-18 inches	191.0	64.62	451.27	202.25	251.47	303.1	4.8
>18-30 inches	242.4	29.58	399.45	73.06	158.01	244.9	8.9
>30-48 inches	90.0	11.15	219.95	7.54	49.28	91.8	3.2
>48 inches	122.5	11.35	50.00	0.53	214.58	143.5	2.6
All	1037.5	350.80	2,143.62	973.30	1,848.19	1733.1	27.0

Table D-2: Detailed Inundation footprint for 4000 cfs by zones

Depths	Zone 1	Zone 2	Zone 3	Zone 4	Zone 5	Zone 6	Zone 7
0-4 inches	56.8	145.9	107.1	325.1	513.1	784.3	2.9
>4-7 inches	42.8	105.3	118.8	230.2	445.5	510.4	1.3
>7-12 inches	83.3	136.9	332.9	300.9	814.7	775.5	3.2
>12-18 inches	153.7	94.8	526.4	318.0	920.4	780.9	4.8
>18-30 inches	367.7	187.6	807.1	460.4	1837.2	1104.6	8.9
>30-48 inches	634.0	210.3	445.9	70.8	1177.3	285.9	3.2
>48 inches	261.9	64.1	162.9	3.5	326.8	194.6	2.6
All	1600.3	944.8	2501.2	1709.0	6035.0	4436.2	27.0

Table D-3: Detailed Inundation footprint for 6000 cfs by zones

Depth	Zone 1	Zone 2	Zone 3	Zone 4	Zone 5	Zone 6	Zone 7
0-4 inches	20.8	242.0	0.5	276.4	316.4	888.0	2.9
>4-7 inches	20.9	158.9	52.7	243.3	266.6	629.5	1.3
>7-12 inches	60.9	210.3	156.1	415.7	548.0	906.3	3.2
>12-18 inches	88.5	213.6	366.0	377.1	766.4	1042.5	4.8
>18-30 inches	265.7	219.8	932.8	601.7	1994.2	1673.2	8.9
>30-48 inches	634.3	297.3	707.5	301.8	2220.3	846.3	3.2
>48 inches	583.1	148.5	337.4	10.1	954.1	269.6	2.6
All	1674.2	1490.3	2552.9	2226.1	7066.0	6255.4	27.0

Figure D-1, D-2, D-3 and D-4 show the flooding footprint using berms and dams, as defined by the different options.

Figure D-1: Base Case (left) and Option 1 (right), only top view

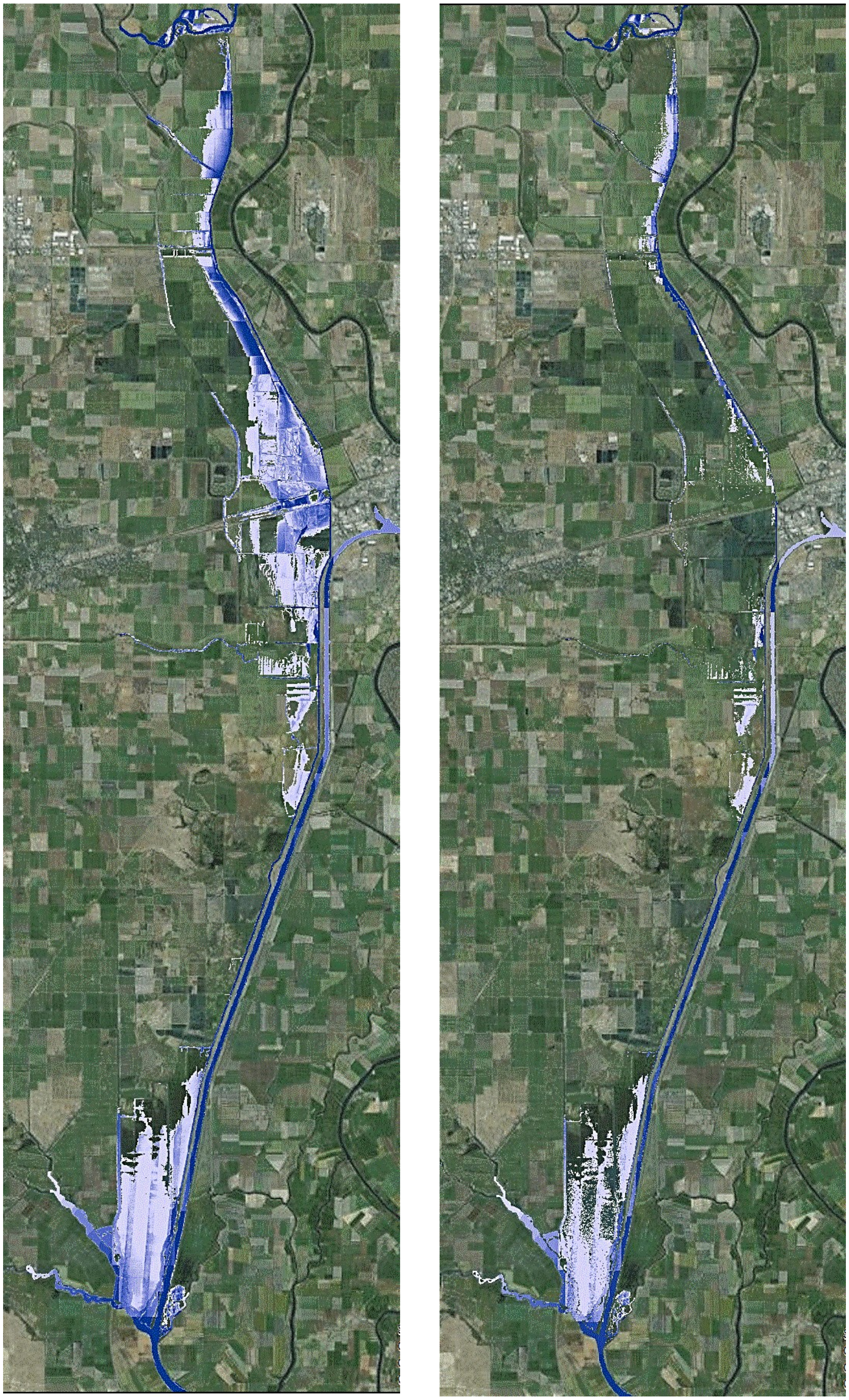

Figure D-2: Base case (right) and Option 2 (left)

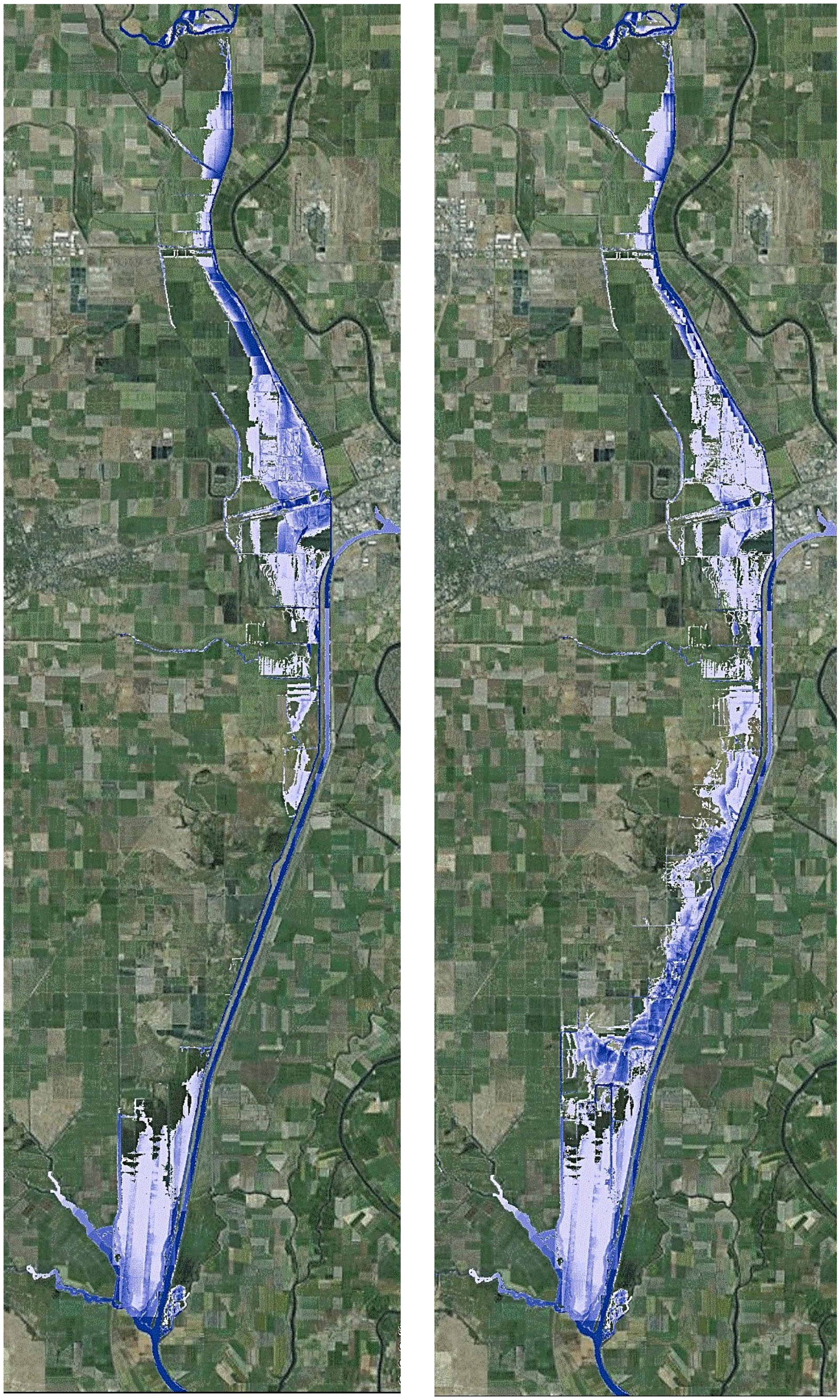

Figure D-3: Base case (left) and Option 3(right)

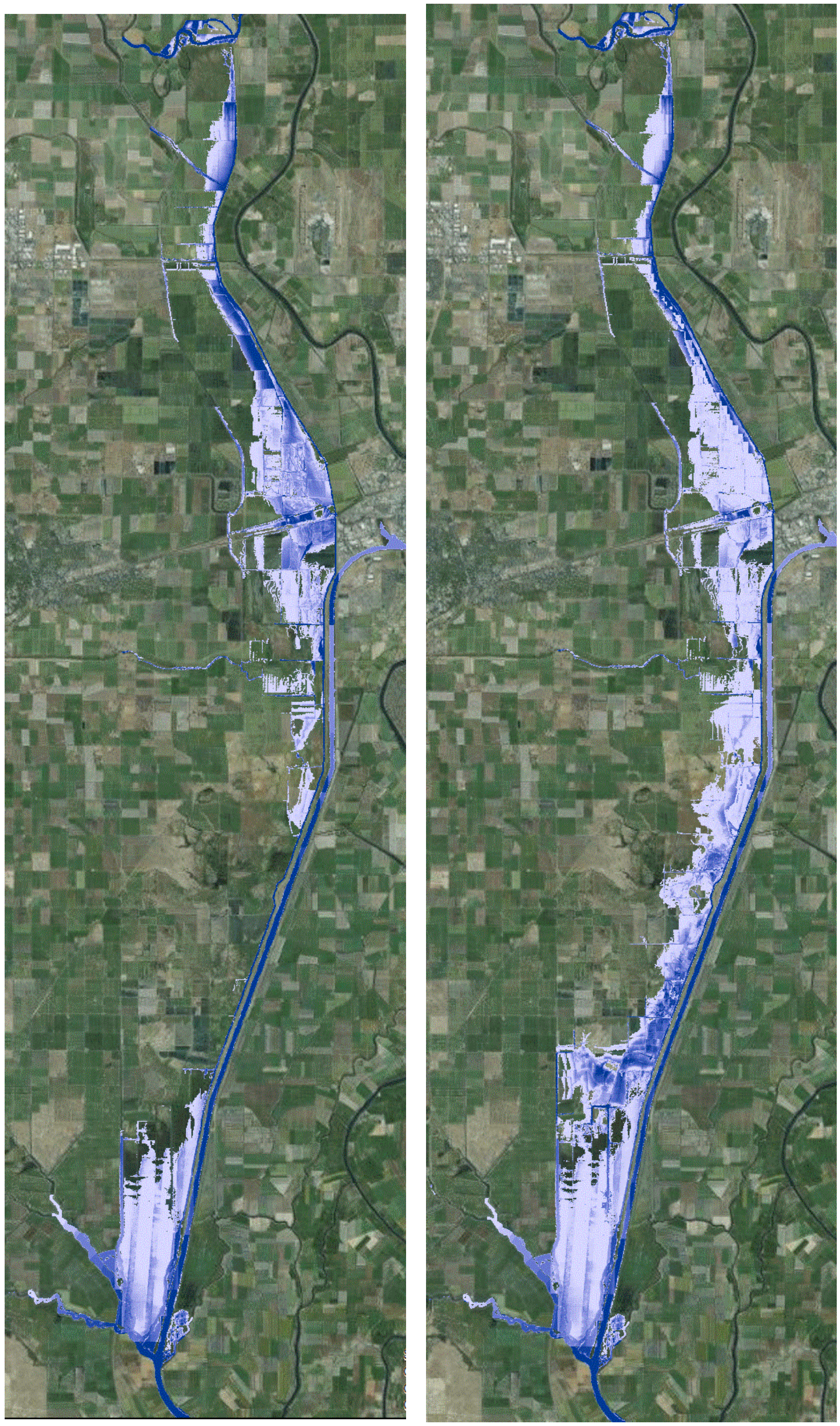

Figure D-4: Base case (left) and Option 4(right)